Snow Cover on the Arctic Sea Ice:
Model Validation, Sensitivity, and 21st Century Projections

by

Benjamin Andrew Blazey

B.A, University of California, Berkeley 2006
M.S., University of Colorado, 2011

A thesis submitted to the
Faculty of the Graduate School of the
University of Colorado in partial fulfillment
of the requirement for the degree of
Doctor of Philosophy
Department of Atmospheric and Oceanic Science
2012

This thesis entitled:
Snow Cover on the Arctic Sea Ice:
Model Validation, Sensitivity, and 21st Century Projections
written by Benjamin Andrew Blazey
has been approved for the Department of Atmospheric and Oceanic Science

____

(James A. Maslanik)

____

(Baylor Fox-Kemper)

Date_______________

The final copy of this thesis has been examined by the signatories, and we
Find that both the content and the form meet acceptable presentation standards
Of scholarly work in the above mentioned discipline.

Abstract

Blazey, Benjamin Andrew (PhD, Department of Atmospheric and Oceanic Science)

Snow Cover on the Arctic Sea Ice: Model Validation, Sensitivity, and 21st Century Projections

Thesis Directed by Research Professor James A. Maslanik and Associate Professor John J. Cassano

The role of snow cover in controlling Arctic Ocean sea ice thickness and extent is assessed with a series of models. Investigations with the stand alone Community Ice CodE (CICE) show, first, a reduction in snow depth triggers a decrease in ice volume and area, and, second, that the impact of increased snow is heavily dependent on ice and atmospheric conditions. Hindcast snow depths on the Arctic ice, simulated by the fully coupled Community Climate System Model (CCSM) are validated with 20th century *in situ* snow depth measurements. The snow depths in CCSM are found to be deeper than observed, likely due to excessive precipitation produced by the component atmosphere model. The sensitivity of the ice to the thermal barrier imposed by the biased snow depth is assessed. The removal of the thermodynamic impact of the exaggerated snow depth increases ice area and volume. The initial increases in ice due to enhanced conductive flux triggers feedback mechanisms with the atmosphere and ocean, reinforcing the increase in ice. Finally, the 21st century projections of decreased Arctic Ocean snow depth in CCSM are reported and diagnosed. The changes in snow are dominated by reduced accumulation due to the lack of autumn ice cover. Without this platform, much of the early snowfall is lost directly to the ocean. While this decrease in

snow results in enhanced conductive flux through the ice as in the validation sensitivity experiment, the decreased summer albedo is found to dominate, as in the CICE stand alone sensitivity experiment. As such, the decrease in snow projected by CCSM in the 21st century presents a mechanism to continued ice loss. These negative (ice growth due decreased insulation) and positive (ice melt due to decreased albedo) feedback mechanisms highlight the need for an accurate representation snow cover on the ice in order to accurately simulate the evolution of Arctic Ocean sea ice.

Acknowledgements

Support for this research comes from National Science Foundation grant ARC-0712950 and National Aeronautics and Space Administration grant NNX07AR21G. In addition, computing time was supplied by the National Atmospheric Research Center through a one-time graduate student grant. Support was also supplied by the Department of Atmospheric and Oceanic Sciences via funding through teaching assistantships.

I would like to thank my advisors Dr. James Maslanik and Dr. John Cassano for guidance with regards both to the research contained in this dissertation and for guidance throughout my graduate studies. I would also like to acknowledge Dr. Marika Holland, who has guided me in the design, execution, and writing of the research comprising this dissertation.

I also acknowledge the support of my two other committee members. Dr. Mark Serreze has provided valued input, and helped steer me towards valuable contributions to the scientific community. I thank Dr. Baylor Fox-Kemper for completing my committee and providing useful input on relatively short notice.

I have received much valued support from other members of the Polar Climate Working Group. In addition to computing resources of the PCWG, I received patient guidance from Dr. Elizabeth Hunke of Los Alamos National Laboratory and Dr. David Bailey of the National Center For Atmospheric Research.

Lastly, I thank the rest of the students in the ATOC department and the Graduate Assistant Laurie Conway. I also thank my family, especially Dr. Gerald Blazey, who provided much needed and appreciated editing, comments, and encouragement.

Table of Contents

Chapter

List of Tables

List of Figures

Chapter 1.

I. Introduction

Due to high albedo and low thermal conductivity, snow cover acts in two distinct and often competing ways on any overlain surface. While the high albedo of snow serves to reduce the absorption of short wave solar radiation, the low thermal conductivity results in a reduction of energy flow from the substrate to the atmosphere. In the case of Arctic Ocean ice cover, the enhanced albedo is expected to reduce summertime ice melt, while the reduced conductive flux impedes transfer of heat from the basal ice forming regions, and hence reduces the formation of additional ice in the winter months. These effects cause snow to influence the ice cover, and hence make the snow cover on the Arctic sea ice a fruitful avenue for investigation.

Climate change in the Arctic has been observed in many elements of the Earth system (ACIA 2005). The Arctic is considered a bellwether for global climate change, with the highest sensitivity to climatic change of any region (IPCC 2007). The enhancement of global temperature anomalies in the Arctic has been observed to correspond to sea ice conditions (Johannessen et al 2004).

The focus of this dissertation is the Arctic sea ice, which continues to decrease in extent (Stroeve et at al 2011, Stroeve et al 2007), particularly in September, for which a rate exceeding 10% per decade is reported (Comiso et al 2012). As this occurs, the remaining ice becomes progressively younger (Maslanik et al 2011). These changes have become more acute, as the summer ice minima for the four years from 2007 to 2010 were the lowest on record (Perovich et al 2010), with 2011 continuing this trend (Perovich et al 2011). Considering the projected decrease in 21st century Arctic sea ice (Vavrus et al

2011) the current trends in ice area are expected to continue. Due to the ice-ocean albedo feedback (Curry et al 1995) and atmospheric response to Arctic ice conditions (Holland et al 2006a, Porter et al 2012), changes in this component of the Arctic climate system potentially trigger feedback mechanisms which serve to further enhance the Arctic ice loss, pushing the Arctic progressively closer to an ice free summer state (Holland et al 2006b).

Moreover, changes in the Arctic ice cover impact the climate system both in the Arctic region and globally. In general, the areal extent of ice cover affects the degree of summertime shortwave radiation absorbed by the ocean and the wintertime surface heat flux to the atmosphere (Alexander et al 2004, Screen and Simmons 2010). This is expected to trigger increased surface temperatures as well as precipitation and increased low level cloudiness (Schweiger et al 2008). In addition to interaction with the atmosphere, changes in the ice cover are expected to have a wide range of impacts. For one, the North Atlantic meridional overturning region of the thermohaline circulation (Mauritzen and Hakkinen, 1997) may be influenced. Similar freshening of the Arctic Ocean has been implicated in the rapid climatic shifts that occurred following the most recent glacial maximum (Peltier et al 2006). Decreases in ice cover are expected to lead to increases in the length of the open water season that, in turn, trigger enhanced primary biological production (Arrigo et al 2008). However, for purposes of indigenous food security, reduced ice area has a negative effect (Ford 2009). In addition, the coastal regions of the Arctic Ocean erode easily and are sensitive to ice loss (Mars and Houseknech, 2007; Jones et al 2009). Degradation of the terrestrial Arctic permafrost is also sensitive to ice loss, with the loss of sea ice negatively impacting permafrost as much as 1500 km inland (Lawrence et al 2008).

The changing Arctic climate affects the precipitation, and in turn has the potential to contribute to changes in the snowfall and accumulation. Of particular relevance to this study is the increase in precipitation projected to occur over the 21st century, approximately 20% in a survey of IPCC model simulations (Cassano et al 2007*)*. This precipitation increase may be focused during the autumn months of October and November, which are projected to have a 50%-70% increase in precipitation (Vavrus et al 2011). Changes in precipitation have already been observed, with a 7% increase in river runoff observed in the Eurasian and Arctic river basins from 1936 to 1999 (Peterson et al 2002). However, reductions in ice area may lead to decreases in cyclogenesis (Screen et al 2011).

Given the impact of ice cover on both the Arctic and general climate, modeling of ice cover is a well-established field in which the role of snow cover has long been considered (Untersteiner 1964, Maykut and Untersteiner 1971). Despite the long history of modeling efforts addressing both sea ice and the role of snow, there is still a lack of consensus with regards to the strength and importance of the mechanisms by which the snow cover affects the ice. Many past modeling studies have found that snow played a secondary role in determining wintertime ice growth Ledley (1991), Holland et al (1993), Ebert and Curry (1993). These studies generally made use of relatively thick ice, with mean ice thicknesses from 2 meters to greater than 3 meters (Maykut and Untersteiner 1971). Such thick ice presents a large thermal barrier, and understandably reduces the impact of the overlying snow. However, these studies also concluded that the summertime impact of increased snow was to increase ice thickness by delaying the onset of melt due to increased albedo.

While these earlier sensitivity studies appeared to often conclude the snow was less important than other elements of the ice system, this finding has not been confirmed in the subsequent literature. While Ebert and Curry (1993) concluded that increased snow fall resulted in increased ice thickness due to delayed melt, Wu et al (1999) concluded that for thick ice either removal of the snow cover or doubling of snow both triggered a decrease in ice volume. More striking, Brown and Cote (1992) found that snow explained nearly all of the variance in observed ice thickness. While focused on the Southern Ocean, Fichefet et al (2000) found the ice to be 'remarkably sensitive to changes in snow conductivity'. More recently, Powell et al (2005) found that initially ice volume decreases with increasing snow due to insulation, but once the increased mass depresses the ice surface below sea level, flooding of the snow-ice interface occurs, which easily freezes, leading to increased ice mass. Powell et al 2005 concluded that snow-ice formation and the insulating effects of snow were intertwined. When snow accumulation was increased by 50%, volume increased by 10%. Reducing the thermal conductivity from 0.31 W m^{-1} K^{-1} to 0.12 W m^{-1} K^{-1} decreased ice volume by 7%.

Due to the large variability in measured values of snow characteristics, modeling approaches are potentially neglecting a source of variability. Field observations (Sturm et al., 1997, 1998) have suggested that the thermal conductivity of snow used by the Community Ice CodE (CICE) (0.3 W m^{-1} K^{-1}) may be too high by a factor of two. In addition, the fixed conductivity used by CICE neglects snow metamorphosis, which leads to snow conductivities ranging from 0.1 $Wm^{-1}K^{-1}$ to 0.6 $Wm^{-1}K^{-1}$. Regardless, these conductivities are an order of magnitude less than the 2.0 W m^{-1} K^{-1} thermal conductivity of ice used by CICE. Pointedly, observations of lake ice have concluded that ice thickness is anti-correlated with snow depth on the ice (Sturm and Liston, 2003).Because the lake ice regime is much less dynamic than the se ice, this presents a rather idealized situation. Focused snow conductivity sensitivity studies have found a 10%-20% change in ice thickness when snow conductivity is halved from the typical ~0.3 $Wm^{-1}K^{-1}$ to a more physical 0.15 $Wm^{-1}K^{-1}$ (Sturm et al 2002, Wu et al 1999, Fichefet 2000). While more recent studies have explored the introduction of additional thermodynamic complexity to the treatment of snow (Lecomte 2011, Cheng 2008), these studies have focused on one-dimensional modeling and validation.

As previously mentioned, albedo is also an important component when considering the effect of snow on sea ice. This is due to the lower albedo of bare ice (1^{st} year) than frozen white ice (multiyear) with albedos of 0.52 vs. 0.70 or snow, which has an albedo of 0.81 to 0.87 when not altered by melt, depending on wind alteration (Perovich 1998). Ledley et al 1991 identified the magnitude of this feedback in summer ice melt. While the treatment of snow conductivity has remained relatively constant in CICE, snow and ice albedo have been updated to a Delta-Eddington multiple scattering parameterization, providing a seasonal evolution not represented in snow conductivity (Briegleb and Light 2007).

The goal of this dissertation is to improve our understanding of the effects of snow on ice, and to assert that accurate representation of snow on ice in general circulation models (GCMs) is a key element of accurate ice simulation, and therefore of the Arctic and global climate. Due to the range of responses sea ice has to snow depth, it is clear that the configuration of the models has significant impact. As a result, over the last several decades, studies trying to assess the effect of snow on sea ice have failed to produce a consistent picture. Considering the publication history and the changing environment of the Arctic, fully determining the effect of snow on the ice cover is a detailed task. While the literature indicates that models react differently to snow conditions, likely due to different thermodynamic treatments, the models do frequently show significant sensitivity to the snow conditions. As such, this thesis will assess how the ice cover in a particular model: CICE within the Community Climate System Model (CCSM) responds to different snow cover conditions.

While previous studies have indicated that snow is an important element of the sea ice system, there is a multitude of ways in which this problem could be addressed. For instance, a key question of this thesis regards the relative strengths of decreased snow cover leading to enhanced wintertime ice formation and summer time melt and conversely increased snow cover leading to inhibited wintertime ice formation and summer time melt. Simplified models allow the ready alteration of snow depth, testing how depth affects the ice mass balance budget. This thesis begins with an exploration of ice sensitivity to snow depth in a reanalysis driven stand alone configuration of CICE. This thesis continues by validating the snow depths produced by CCSM, which are expected to be too high given the known high biases in Arctic precipitation in this model (de Boer et al. 2011). Following the diagnosis of snow depth biases in CCSM, the thesis proceeds to investigate the impact of these biases; for instance, the differences in ice state that would occur if the atmospheric model was producing the correct precipitation and hence the correct snow depth are assessed. Due to the projected 21st century increases in precipitation this thesis also seeks to determine whether a corresponding increase in snow depth on the ice occurs. This leads to a second main hypothesis and conclusion: Increased temperatures and the lack of perennial ice could result in lower average 21st century sea ice snow depths.

CCSM and the component ice model, CICE present a novel simulation environment in which to ask these questions. Many of the previous investigations of the sensitivity of ice to snow were performed in relatively simple model environments. However, CCSM is able to reproduce the Arctic climate with fairly high fidelity, including both the atmosphere (de Boer et al. 2011) and ice cover Jahn et al. (2011). CCSM is used in a variety of configurations, and in-depth discussions of CCSM and CICE are reserved for later chapters.

The research comprising this dissertation is expected to contribute the field in several ways. First, as a whole, this work determines how the ice production simulated by CICE is sensitive to snow conditions under a fixed atmosphere. The identified sensitivity motivates additional diagnostic assessments of the accuracy of the on-ice snow depth in CCSM. In turn, we find that the ice produced in CICE is highly sensitive to the snow provided by the atmospheric component of CCSM, and that a decreased snow depth results in lower ice area and volume. The validation of on-ice snow depths and identified sensitivity is intended to motivate adjustments to the Community Atmosphere Model (CAM) component of CCSM to compensate for existing precipitation biases. In addition, the limited *in situ* measurements of snow on the Arctic ice indicate the need for additional measurements of snow depth. Finally, by examining the 21st century projections of on-ice snow cover, we are able to identify additional feedback mechanisms between the ice cover and overlying snow. The identification and timing of these mechanisms is potentially inaccurate due to biases in the 20th century snow depths, which we suspect may lead to timing changes in the projected ice loss during the 21st century. Overall, these studies will coalesce around the competing roles of snow cover fraction on shortwave absorption and snow depth on conductive flux through the ice. With this in mind, we hope to determine whether 21st century changes in snow cover present potential feedback mechanisms to continued Arctic ice loss and whether the sum effect of these mechanism is positive of negative. The implications of the hindcast snow validation reflect upon the changes in 21st century projections of snow depth, with the initial sensitivity anchoring these investigations.

However, the implications of the findings herein should not be relegated to CCSM and CICE alone. While this study does focus on CCSM and its component ice model, the identification of ice sensitivity to snow depth, potential feedback mechanisms, and implications for 21st century ice projections are relevant to any modern GCM used for climate projections. In fact, inter-model variability in snow depth is one potential source of variability in ice state, and in turn the climate as a whole.

The remainder of this dissertation is organized as follows. Chapter 2 compares the sensitivity of ice to overlying snow cover in the reanalysis driven CICE environment. The sensitivity of the ice cover to snow is assessed under different atmospheric conditions given different initial ice states. Note that in Chapter 2, an earlier iteration of CCSM is used, so the sea ice module used in Chapter 2 is the Community Sea Ice Model (CSIM), which is largely equivalent to the previous version of CICE. In Chapter 3, the snow depth accumulated on CICE under both a reanalysis atmosphere and coupled to

CCSM is validated against *in situ* measurements. The sensitivity of the ice to the changes in thermal conductivity due to the identified biases is also addressed in this chapter. Chapter 3 is currently in the final stages of preparation for publication. In Chapter 4, the 21^{st} century projected snow depths are identified, the causal mechanisms are investigated, and potential feedback mechanisms are surveyed. Chapter 4 is also in preparation for publication. Finally, Chapter 5 contains a review of the findings of this thesis, with a discussion of overarching conclusions and the direction of possible future work on this topic.

Chapter 2

II. Sea Ice Sensitivity to Precipitation, Atmospheric Forcing, and Initial Conditions

Abstract: The sensitivity of Arctic Ocean sea ice extent and volume is explored and examined using a dynamic-thermodynamic ice model, under different atmospheric conditions, precipitation regimes, and initial ice thickness states. The Community Sea Ice Model (CSIM), the "active ice-only model", component of the Community Climate System Model (CCSM) is used for multiyear integrations. Atmospheric conditions are found to quickly dominate ice area, but initial ice conditions continue to influence total volume of the Arctic sea ice throughout the modeling period. Decreased precipitation is found to significantly decrease the amount of sea ice in the Arctic. Under most scenarios, increased precipitation produces a nominal increase in sea ice area and volume. However, under a scenario most comparable to current and projected conditions in the Arctic, an increase in precipitation is found to serve as a potential mechanism for arresting Arctic sea ice loss, resulting in increased ice. This increase is due in part to the conversion of snow cover to ice. This process occurs when the ice surface is depressed below sea level by snow accumulation, resulting in surface flooding and rapid ice formation at the expense of the snow cover.

II.1. Introduction

Changing conditions in the Arctic have been highlighted by a dramatic decrease in September minimum sea ice extent (Serreze et al 2007a). Recent extreme minimums exceed a linear trend of -0.7 million km^2 per decade observed since the beginning of the satellite record. Coupled models project continued sea ice loss throughout the 21^{st} century (Holland 2008; Zhang and Walsh 2006; Gerdes and Koberle 2007; Arzel et al. 2006). However, these models have underestimated ice loss (Stroeve 2007). A seasonally near ice free Arctic has been predicted to occur near mid 21^{st} century (Holland 2006, Arctic Climate Impact Assessment 2005). A shift in the Arctic pack from ice that has survived multiple melt seasons and deformation events to younger, less dynamically altered ice has been observed (Nghiem et al. 2007). Ice surviving five or more melt seasons has largely disappeared (Maslanik et al 2007, Maslanik et al 2011). These shifts in the Arctic sea ice are just a few of the changes observed in the Arctic (Overland et al. 2004, Serreze et al. 2000). As discussed below, a number of environmental conditions impact the Arctic ice pack.

The shift from old, rough, multiyear ice to smooth, young ice may result in a positive feedback mechanism in a warming climate. First, new ice has a lower albedo than older ice. During melt, the surface overlain by 1^{st} year ice drops from an albedo of 0.52 to 0.06 (Perovich 1998) as the ice cover is replaced by open ocean. This occurs more easily when the ice is thinner and easily melted. Additionally, bare (1^{st} year) ice is observed to have a significantly lower albedo than frozen white ice (multiyear) (0.52 vs. 0.70). Note that both of these have a higher albedo than surface melt ponds (0.15-0.29).

Additionally, the presence of snow on ice has a significant effect on albedo; snow which is not experiencing melt has albedo 0.81 to 0.87 depending on wind alteration. The role of snow albedo therefore has a significant effect on ice melt (Ledley et al. 1991).

Snow affects ice in additional ways, including the formation of ice via the flooding of the snow pack at the snow/ice interface, and the addition of insulation that reduces thermal conductivity through the ice/snow column, reducing basal ice growth. During the summer months, the ice formed via these processes serves to delay complete melt of the sea ice. During the winter, however, flooding and insulation compete by promoting or inhibiting the formation of ice, respectively.

Thermal conductivity of snow can vary from 0.1 to 0.6 W m^{-2} K^{-1} as a result of snow characteristics and metamorphosis (Sturm et al., 1997, 1998). Throughout this range, the thermal conductivity of snow is significantly less than the thermal conductivity of ice (~2 W m^{-1} K^{-1}). Thus, snow is more insulative than the ice into which it can be converted.

The interdependence of these effects has been documented to cause thinner or thicker ice depending on environmental conditions (Saloranta 2000; Makysym & Markus, 2008). Thus, the interaction of these processes may yield either a positive or negative feedback in the Arctic ice conditions and climate as the precipitation is modified by the changing climate.

Observed decreases in mean ice thickness will correspondingly reduce the amount of snow necessary to initiate snow-to-ice conversion. Additionally, changes in total precipitation and precipitation patterns projected for the Arctic may lead to an increase in snow and hence increase both snow ice formation and insulation.

Runoff in the Eurasian and Arctic river basins was observed to increase 7% from 1936 to 1999 (Peterson et al 2002). General Circulation Models (GCMs) predict changes in precipitation patterns and net precipitation in the Arctic Ocean. An ensemble of ten models participating in the IPCC AR4 scenario all experienced an increase in precipitation, evaporation, and net precipitation (P-E) over the Arctic Ocean from the period 1940-1949 to 2040-2049 (Holland et al 2007). Significant variability was observed in precipitation increases with a mean increase of 11% in net precipitation. Another study examining an ensemble of 17 models observed increases in precipitation ranging from 16% to 57% by 2080-2099, with a mean of 33% (Kattsov et al 2007). These increases were much higher than the global mean increase in precipitation of 4.5%. Cassano et al (2007) examined changes in synoptic forcing and associated precipitation changes observed in 15 GCMs, with particular focus on the four GCMs capable of reliably producing current precipitation patterns. Net precipitation increases of 20% were observed over the Arctic over the 21st century. Significant spatial variability in these changes was documented in this study as a confirmation of previous studies (Meehl et al. 2005). These studies generally report increases in both evaporation and precipitation, with precipitation dominating, resulting in the reported increases in net precipitation. However, in Chapter 4 it is apparent that the increase in precipitation strongly favors rain over snow.

Several previous studies have examined the sensitivity of sea ice to changes in precipitation, with varying conclusions. As part of a detailed sensitivity study investigating the sensitivity of the sea ice model component of a coupled numerical GCM, Holland et al (1993) found that increasing snow depth resulted in an increase in summer ice thickness and extent. Significant thickness changes were observed with snowfall greater than 80cm/year. Fichefet and Maqueda (1997) found greater sensitivity to the removal of snow in the Antarctic sea ice than Arctic ice. In a later study Fichefet et al (2000) found a 10% reduction in ice thickness and alterations in extent when snow thermal conductivity was reduced by half.

As the previous discussion indicates, the relationships between sea ice and a host of variables are not fully understood. The mean ice state, timing of precipitation, and initialization state may all play an important role in how the ice responds to snow cover. This work examines the importance of precipitation and snow depth to Arctic Ocean sea ice area and thickness and examines the influence of changes in precipitation, bulk forcing, and the initial condition of the sea ice on the modeled ice thickness and area. Due to the range of responses in previous studies, this work is important because the response in recent generations of CCSM has not been sufficiently investigated. The Community Sea Ice Model (CSIM) component of CCSM version 3.5 (CCSM3.5) is briefly described in Section II.2, followed by a description of the simulation configurations used. Section II.3 discusses the results of the model simulations. Finally, in Section II.4, the conclusions of this work and potential future work are discussed.

II.2. Model and Simulation Description: Community Climate System Model 3.5 and Community Sea Ice Model 5

II.2.a. Model Description

This study uses only the active ice component (CSIM5) of CCSM 3.5. CSIM is a detailed thermodynamic dynamic model, a detailed description of the processes included in CSIM 5 is readily available (Briegleb et al 2004). For purposes of this work, we note several characteristics of the model. CSIM includes five sub grid scale ice categories, which we use as a proxy for ice age. While not directly correlated to age, this allows better quantification of the effects of forcing and precipitation on ice of different ages and, in the physical system, correspondingly different thermal conductivity and albedo. Especially important to this study is the inclusion of snow to ice conversion due to surface flooding, discussed in the introduction of this paper. This allows changes in precipitation to influence ice growth both thermodynamically and dynamically through snow to ice conversion.

These simulations use the Slab Ocean Model (SOM) rather than the full Parallel Ocean Program (POP2) in large part due to the lower computational costs. The lower computational costs are due both to the simplified model and the faster equilibration of the model to adjustments. For example, a doubling of CO_2 equilibrates in 20 years, while in a fully coupled simulation the ocean is still adjusting after 900 years (Danabasoglu and Gent 2009). Danabsoglu and Gent (2009) also found that the results of the SOM and fully coupled simulations were similar under control conditions, with differences under a perturbed climate focused in the Southern Ocean. This is unsurprising; The Community Climate System Model component Slab Ocean Model (CCSM-SOM) aims to reproduce the results of the fully coupled climate model, rather than reproduce the observed climate. This version of the SOM is intended for use specifically with the active configuration of the ice model (CICE). Equation 1, reproduced from Bailey et al (2012) is solved for the mixed layer temperature, T_{mix}. F_{net} is the net surface heat flux including the ice ocean heat exchange, and Q_{flx} is the implied horizontal and vertical flux of heat where the local mixed layer column is considered. h_{mix} is the mixed layer depth, r is the density, and c_p is the specific heat. Unlike previous iterations of the SOM, Q_{flx} is calculated using h_{mix}, T_{mix}, and F_{net} from a fully coupled simulation instead of observations (Bailey et al 2012).

$$\rho c_p h_{mix} \frac{dT_{mix}}{dt} = F_{net} - Q_{flx} \qquad (1)$$

II.2.b. Simulation Design

For this modeling study, there are two series of simulations. The first series was run for three years, and varies the initial ice condition and atmospheric forcing. The second series was run for two years, and in addition to initial conditions and atmospheric forcing, varies the precipitation north of 70 degrees latitude.

The ice conditions in S. Yeager's g3_5_19.11 run (Yeager 2009) are used to select initial ice conditions and forcing. This simulation used CSIM (version 3.5 beta19) and Parallel Ocean Program (POP) components of CCSM. G3_5_19.11 is run for two cycles from 1948 to 2006, yielding 116 years, with an additional cycle ending with a year run with 2007 forcing conditions. Since the simulations in this study are active-ice only, the CSIM/POP simulation is an appropriate comparison because the same atmospheric conditions, which are discussed in the following passage, are used. A visual inspection of the July, August, and September ice extent from g3_5_19.11 determines the selection of initial ice conditions and global forcing for both series of simulations.

In both of the model series in this study, there are two sets of simulations with different initial ice conditions used. Initial conditions at the end of 2006 and 1978 serve as representatives of a thin ice and thick ice regime, respectively. See Fig. 1 for ice

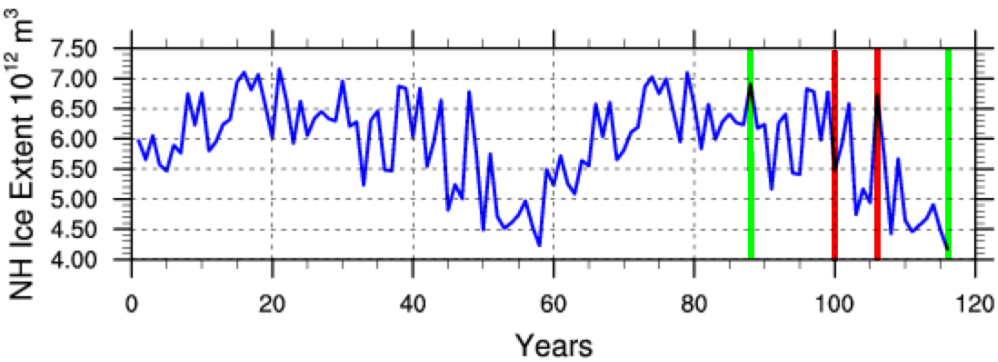

Figure 2. July August, and September mean ice extent from g3_4_19.11, red vertical lines (inner two) represent forcing years (1990,1996). Green vertical lines(outer most two) represent ice conditions in the year prior to integration (1978,2006) (Yeager 2009).

extent from g3_5_19.11, where ice conditions from the second cycle of forcing are selected. The green horizontal lines at model year 89 and 116 correspond to 1978 and 2006. Initialization of the simulations use ice conditions for January of the next model year. The year 1979 is selected as a year with ice extent representative of historic ice extent. 2007 is the thin ice year. The physical ice conditions at the end of 2006 preceded the record September ice minimums for 2007, significantly reduced from 2006 (Stroeve 2008).

Additionally, in both model series, simulations with two distinct atmospheric forcing conditions are created, one with atmospheric conditions conducive to ice loss and one conducive to ice growth. These simulations use the interannually varying climatology dataset, the COREv2. This product is comprised of fluxes assembled by Large and Yeager (2004). While various observations and reanalyses were used as starting points for the atmospheric characteristics, attempts were made to reduce the biases through comparison to more reliable observations which were too restrictive either in temporal or spatial coverage to be used for the entire globe or duration of the COREv2 forcing dataset.

For example, the International Satellite Cloud Climatology Project-C1 input data (ISCCP-FC) is used as a starting point for the radiative budget (Large and Yeager 2009). As part of the process of producing the COREv2 forcing, the radiative flux is compared to a variety of other measurements appropriate at different latitudes, resulting in latitude dependent adjustments to the radiative fluxes. The adjustment relevant to the Arctic is a 5W/m^2 reduction in the downwelling longwave radiation poleward of 70N. This is linearly blended to 60N, and is based on *in situ* observations made during the Surface Heat Budget of the Arctic (SHEBA) campaign. The solar insolation is not adjusted in the high latitudes. These adjustments are reasonable, considering a comparison of ISCCP-FD to the Baseline Surface Radiation Network (BSRN) Downwelling radiation found the radiation budget poleward of 65N to have biases of <0.01W/m^2 for downwelling shortwave and 7.2 W/m^2 for downwelling long wave radiation (Zhang et al 2004).

Much of the atmospheric state is based on the NCEP reanalysis, for which biases have previously been identified (Smith et al 2001). As such, modifications are made here as well. In the case of SST poleward of 70N, the annual mean is similar to the Polar Exchange at the Sea Surface (POLES) sea surface temperature (Rigor et al 2000). However, monthly adjustments on the order of 1 ^{o}C are made (Large and Yeager 2009).

NCEP wind vectors were also validated using data from the Quick SCATterometer satellite (QSCAT) by Large and Yeager (2009). Comparison of the wind direction showed good agreement in the high latitudes, with significant biases occurring in lower latitudes. However, wind speed biases in excess of a factor of 2 were observed and corrected in the high latitude regions.

As with initial ice conditions, selection of atmospheric data from the interannually varying COREv2 data is based on a visual inspection of the July, August, and September mean ice extent in g3_5_19.11. 1990 forcing serves for conditions conducive to ice loss, and 1996 as conducive to ice gain. The red horizontal lines in Fig 1 indicate model year 100 and 106, corresponding to 1990 and 1996, respectively. Note the significant ice loss between year 99 and 100, and the significant gain between year 105 and 106.

The second series of simulations investigates the sensitivity of sea ice to changes in precipitation. As no single precipitation dataset is applicable globally, CSIM uses a combination of several precipitation data products. Unfortunately, the precipitation dataset used for the Arctic does not provide inter-annual variability. This “Serreze” monthly Arctic dataset combines the climatology from Serreze & Hurst (2000) with gauge corrected (Yang 1999) monthly precipitation acquired from Russian north-pole drifting stations and coastal stations (Large & Yeager 2004 technote). This dataset is blended with other products between 65N and 70N, and serves as the only precipitation data from 70N poleward. Due to the lack of inter-annual variability in precipitation poleward of 70N, all previous forcing and initial condition runs are simulated with precipitation both increased and decreased by a factor of two in Series 2. This method is used because all years have the same precipitation, so a high and low precipitation year cannot be selected. As these runs do not use the POP component of CCSM, the influences of additional freshwater flux to the ocean and changes to the total water budget are not of concern.

II.3. Simulation Results

For CCSM model results, grid point values provided by model output are used to derive metrics. The study area is restricted to 70N pole ward. This limitation is due partially to a desire to alter precipitation only for the "Serreze" monthly Arctic dataset. Additionally, this region comprises the majority of the Arctic Ocean, see map in Fig 2.

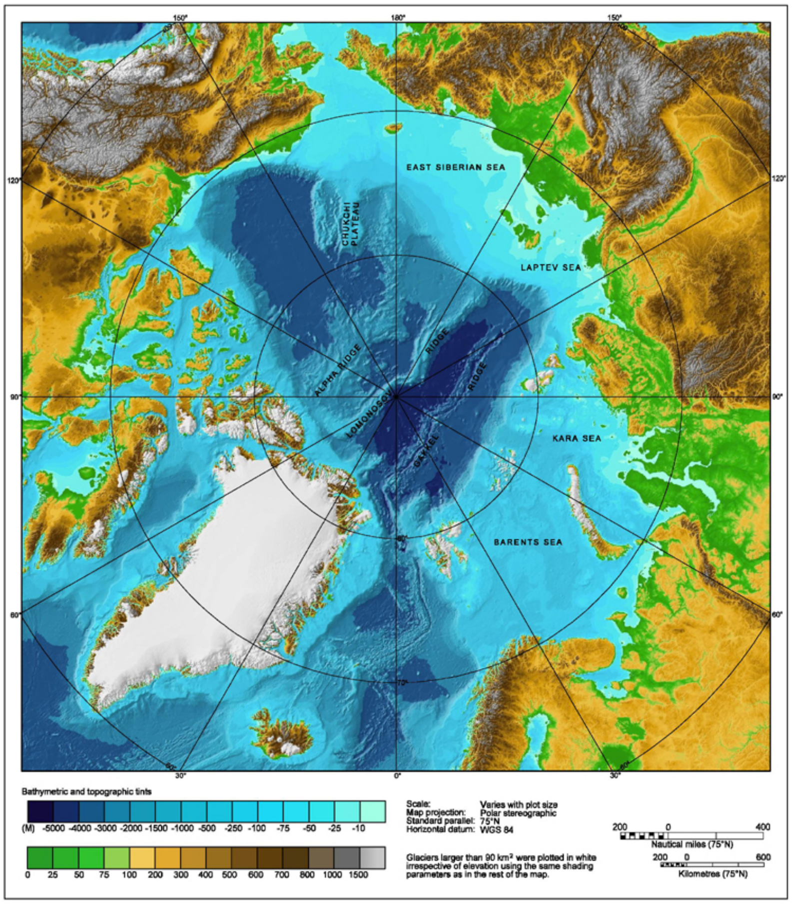

Figure 2. Arctic Ocean, with 10 degree latitude delineation.

Significance is determined through the use of paired t-tests between these values for all run combinations. Paired t-tests are used for full year means, as well as September means, corresponding to the ice minimum. All run pairings are significant to $P<0.05$.

Four metrics describe the ice state for all runs of both series: total ice extent, total ice volume, ice extent with thickness less than 1.39m (ice in the 1st and 2nd sub grid scale categories), and ice extent with thickness more than 1.39m (ice in the 3rd, 4th, and 5th sub grid scale categories). Additionally, for those runs when precipitation sensitivity is investigated, two additional metrics are included: the volume of ice being generated by snow to ice formation and the accumulated ice volume generated by snow to ice conversion since model initialization. Much of the analysis focuses on the area and volumes in September, corresponding to the ice minimum. The analysis begins with the Series 1 simulations and continues to the series 2 simulations.

II.3.a. Results of Series 1

Figure 3 contains the results of Series 1 simulations, where sensitivity of sea

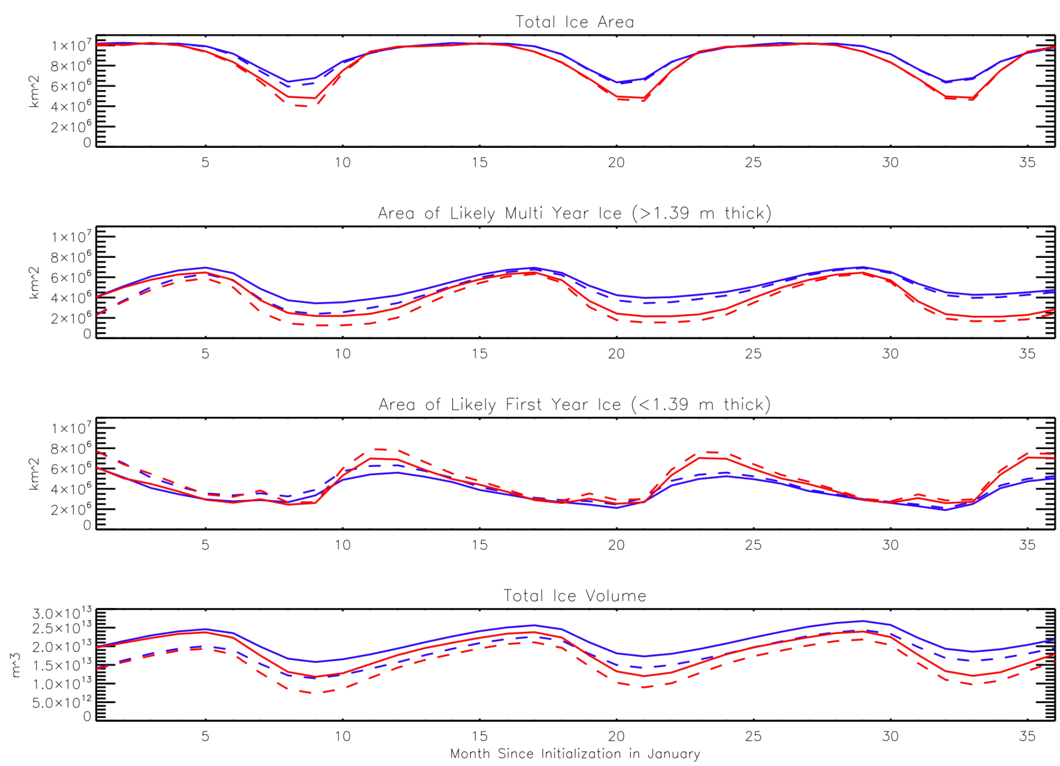

Figure 3. Results of series 1 model runs. Dashed lines indicate 2007 initial ice conditions (Thin ice). Solid lines indicate 1979 initial ice conditions (Thick ice). Red indicates 1990 forcing (Conducive to ice loss). Blue indicates 1996 forcing (Conducive to ice gain).

ice to initial ice state and forcing conditions is compared. Tables 1.a and 1.b give September values for total area and total volume. Note that all runs achieve near

	Year 1	Year 2	Year 3
1979 Ice, 1990 Forcing	4.80×10^6 km^2	4.83×10^6 km^2	4.84×10^6 km^2
1979 Ice, 1996 Forcing	6.79×10^6 km^2	6.71×10^6 km^2	6.79×10^6 km^2
2007 Ice, 1990 Forcing	3.95×10^6 km^2	4.53×10^6 km^2	4.63×10^6 km^2
2007 Ice, 1996 Forcing	6.29×10^6 km^2	6.54×10^6 km^2	6.69×10^6 km^2

Table 1.a September areal ice area for series 1 runs

	Year 1	Year 2	Year 3
1979 Ice, 1990 Forcing	1.18×10^{13} m^3	1.20×10^{13} m^3	1.21×10^{13} m^3
1979 Ice, 1996 Forcing	1.58×10^{13} m^3	1.73×10^{13} m^3	1.85×10^{13} m^3
2007 Ice, 1990 Forcing	0.73×10^{13} m^3	0.87×10^{13} m^3	0.97×10^{13} m^3
2007 Ice, 1996 Forcing	1.14×10^{13} m^3	1.41×10^{13} m^3	1.60×10^{13} m^3

Table 1.b September total ice volume from series 1 runs

100% coverage of the study area during winter months, see Fig 3. While this study does not establish whether these simulations reach true equilibrium for the forcing conditions applied, simulations of different initial ice conditions reach a relative equilibrium in ice area fairly rapidly. Relative equilibrium is defined here as the area of 2007 (thin) ice with 1990 (warm) forcing and 1979 (thick) ice with 1996 (cold) forcing. As such, relative equilibrium is the ice state relative to the simulation where initial ice state is expected to require the least adjustment to reach quasi-equilibration given the atmospheric state. Hence thin initial state with a warm atmosphere and thick initial state with a cold atmosphere represent the relative equilibriums. Note that warm/cold are not necessarily representative of the temperature, but the overall atmospheric effect on the ice. These simulations could be regarded as controls, but we avoid the use of this language due to the nature of the Series 2 simulations below. The ice area reaches relative equilibrium within the period of model integration. September ice area from 2007 (thin) initial ice conditions exposed to 1996 (cold) forcing reaches 93%, 98%, and 99% of relative equilibrium over 3 years of model integration. Similarly, 1979 (thick) ice exposed to 1990 (warm) forcing reaches 122%, 107%, and 105%. As such, by the conclusion of the three-year simulation, the initial conditions have been largely dominated by the repeated application of a given atmospheric forcing regime when ice area is considered.

Relative equilibration of total ice volume occurs more slowly. 2007 ice exposed to 1996 forcing reaches 72%, 82%, and 87% of relative equilibrium over the model integration. Note that at model initialization, 2007 ice contains 72% of 1979 ice volume. Correspondingly, 1979 ice contains 142% of 2007 ice volume. Equilibration of 1979 ice exposed to 1990 forcing also occurs slowly, initially not occurring at all with 161% of relative equilibrated volume produced in the first September of integration. In the second and third years of model integration, total volume of 1979 ice exposed to 1990 forcing begins to equilibrate, with 133% and 124% of relative equilibrium ice volume. Figure 3 also reveals the slower equilibration of ice area when ice of similar thicknesses are compared, whereby the >1.39m and <1.39m ice areas remain unequilibrated for longer than the total area. In general, the initial ice state is dominated by atmospheric conditions within a handful of years, with ice area equilibrating faster than total volume, and initially thick ice taking longer to thin than initially thin ice takes to gain volume. It is unsurprising that low ice conditions will equilibrate in area most quickly, as the open water will produce new ice rapidly. This suggests that as ice thins, it may become increasingly difficult to predict future ice states, as the atmospheric conditions will be an increasingly dominant factor.

II.3.b. Results of Series 2 – Increased Ice Scenario (1996 Atmosphere)

Figure 4 reports the series 2 CSIM response to changes in precipitation under 1996 forcing conditions. September area and total volume are reported in Tables 2.a and 2.b. As with series 1, the analysis considers relative equilibrium. For the Series 2, 1996 forcing runs, those runs initialized with 1979 (thick) ice conditions define relative equilibrium.

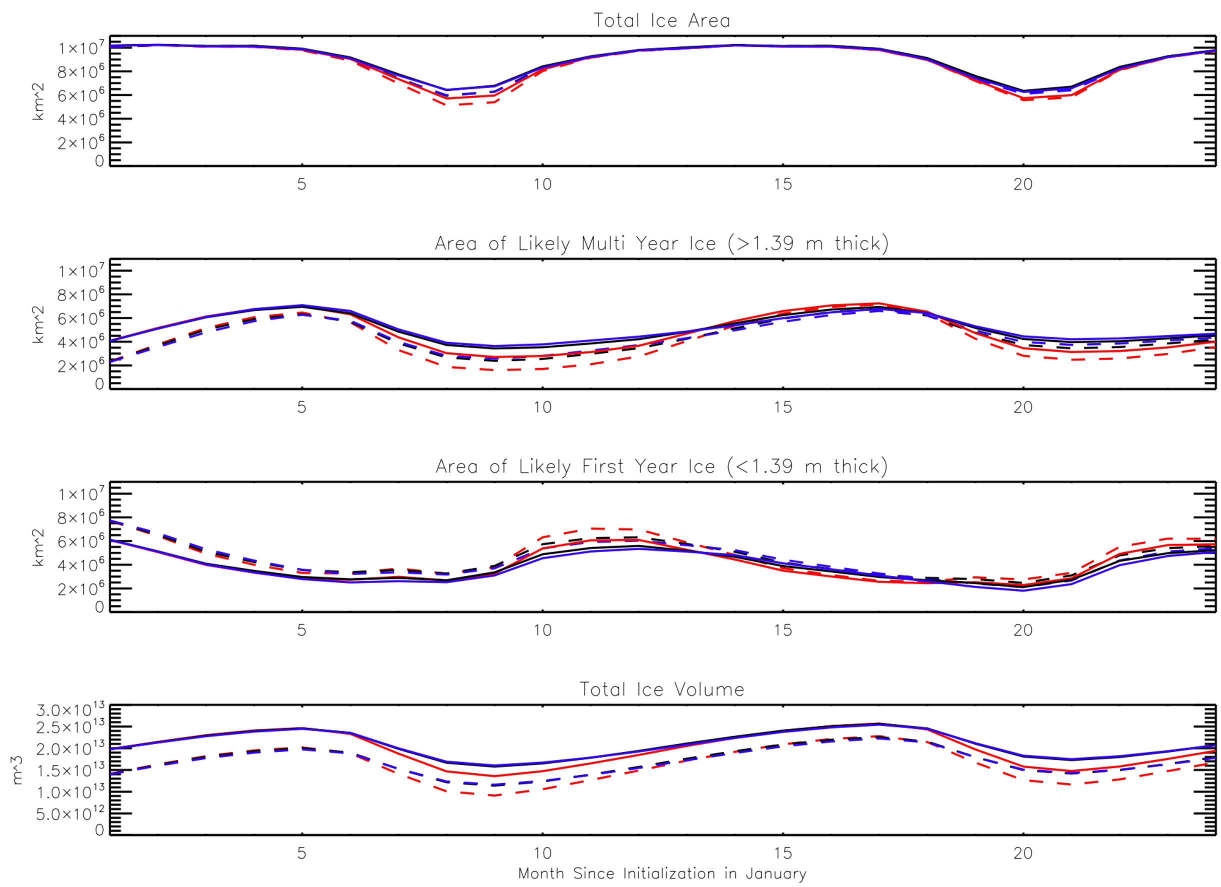

Figure 4. Results of series 2, 1996 atmospheric forcing. Dashed lines indicate 2007 initial ice solid lines indicate 1979 initial ice . Red indicates 50% climatology precipitation, black indicates climatology precipitation, and blue 200% precipitation.

	Year 1	Year 2
1979 Ice, 50% Precip	5.96×10^6 km^2	6.00×10^6 km^2
1979 Ice, Climate Precip	6.79×10^6 km^2	6.71×10^6 km^2
1979 Ice, 200% Precip	6.73×10^6 km^2	6.58×10^6 km^2
2007 Ice, 50% Precip	5.39×10^6 km^2	5.81×10^6 km^2
2007 Ice, Climate Precip	6.29×10^6 km^2	6.54×10^6 km^2
2007 Ice, 200% Precip	6.27×10^6 km^2	6.40×10^6 km^2

Table 2.a September ice area for series 1 and series 2 1996 forcing

	Year 1	Year 2
1979 Ice, 50% Precip	1.36×10^{13} m^3	1.48×10^{13} m^3
1979 Ice, Climate Precip	1.58×10^{13} m^3	1.73×10^{13} m^3
1979 Ice, 200% Precip	1.60×10^{13} m^3	1.75×10^{13} m^3
2007 Ice, 50% Precip	$.91 \times 10^{13}$ m^3	1.17×10^{13} m^3
2007 Ice, Climate Precip	1.14×10^{13} m^3	1.41×10^{13} m^3
2007 Ice, 200% Precip	1.16×10^{13} m^3	1.43×10^{13} m^3

Table 2.b September total volume for series 1 and series 2 1996 forcing

However, for relative equilibrium, the precipitation is matched between the fully experimental and relative equilibrium run. As such, we include additional relative equilibrium comparisons to disentangle the role of precipitation, initial conditions, and atmospheric forcing. For purposes of clarity, each of these equilibrium relationships is defined in Table 3, which indicates that each relative equilibrium is effectively a control

	Relative Equilibrium	Relative Climatology Equilibrium	Relative Initial Equilibrium
Initial Cond.	Control	Control	Experimental
Atmosphere	Control	Control	Control
Snow	Experimental	Control	Control

Table 3. Relative Equilibriums definitions, clarifies which of the three varied conditions are control and experimental.

simulation. However, relative equilibrium uses the experimental snow depths, where applicable. This equilibrium is a measure of sensitivity of the ice cover to snow given different initial conditions. For a complete control simulation, where snow is set to climatology and atmospheric conditions and ice initial states match as in series 1, the 'relative climatology equilibrium' is added. For completeness, the 'relative initial equilibrium' is included, which contains the climatology snow depth and the atmospheric forcing of interest with the exception of initial state. This is only included for one of the two initial states (when the 1996 atmosphere is discussed, the relative initial equilibrium is only included for 2007 initialized runs). This equilibrium highlights the effect of precipitation changes given matching initial conditions and atmospheric state.

As such, these additional relative equilibriums were not included for the earlier series 1 simulations, which investigated only the effects of initial ice state and atmospheric conditions. Instead, these additional relative equilibriums are included only for the following series 2 runs, which mirror the series 1 simulations in investigating the role of initial ice state and atmospheric conditions, but introduce the additional effect of changes in precipitation to this sensitivity study.

These three relative equilibriums are provided in Tables 4.a and 4.b. for the 1996 atmospheric conditions. As an example, the simulation with 2007 initial ice, 1996

	Relative Equilibrium	Rel. Climate Equil.	Rel Initial Equil.
1979 Ice, 50% Precip	N/A	88%, 89%	88%, 89%
1979 Ice, 200% Precip	N/A	99%, 98%	99%, 98%
2007 Ice, 50% Precip	90%,97%	79%, 87%	86%,89%
2007 Ice, Clim. Precip	93%,98%	93%, 98%	N/A
2007 Ice, 200% Precip	93%, 97%	92%, 95%	100%, 98%

Table 4.a Relative equilibrium of September icea area for series 2 1996 forcing

	Relative Equilibrium	Rel. Climate Equil.	Rel Initial Equil.
1979 Ice, 50% Precip	N/A	86%,85%	86%,85%
1979 Ice, 200% Precip	N/A	101%,101%	101%,101%
2007 Ice, 50% Precip	67%,79%	58%,67%	80%,82%
2007 Ice, Clim. Precip	72%,82%	72%,82%	N/A
2007 Ice, 200% Precip	72%,82%	73%,82%	102%,101%

Table 4.b Relative equilibrium of September volume for series 2 1996 forcing

forcing, and 200% climatology precipitation is normalized to the simulation with 1979 ice, 1996 forcing, and 200% precipitation for its relative equilibrium, the simulation with 1979 ice, 1996 forcing, and climatology precipitation for its relative climatology equilibrium, and 2007 ice, 1996 forcing, and climatology precipitation simulation for relative initial equilibrium. While this may appear overly complex, the use of multiple relative equilibriums allows for easy comparison of the relative importance of initial conditions, atmospheric forcing, and precipitation.

Upon initial examination of these tables, it is apparent that under 1996 (conducive to ice gain) forcing an increase in precipitation does not serve to dramatically change either ice area or total volume of the ice relative to climatology precipitation. In fact, relative to climate equilibrium, an increase in precipitation produces marginally less ice area than the climatology precipitation simulation. The shifts in volume are a relatively modest 1-2% when compared to relative initial equilibrium. Under this forcing regime, a reduction in precipitation significantly decreases both area and volume relative to both climate and initial equilibriums. When comparing to relative initial equilibriums decreases in excess of 10% in both ice area and volume occur. This is potentially due to enhanced summer melt due to reduced summer albedo.

II.3.c. Results of Series 2 – Decreased Ice Scenario (1990 Atmosphere)

The second set of simulations in series 2 investigates sensitivity to the same precipitation modifications as the previous simulations, but provided with 1990 (conducive to ice loss) atmospheric conditions. For these 1990 forcing simulations, 2007 (thin) ice conditions are the “relative equilibrium”. The results of these runs and metrics are presented in Fig. 5, and Tables 5. and 6. Here a reduction to 50% precipitation results

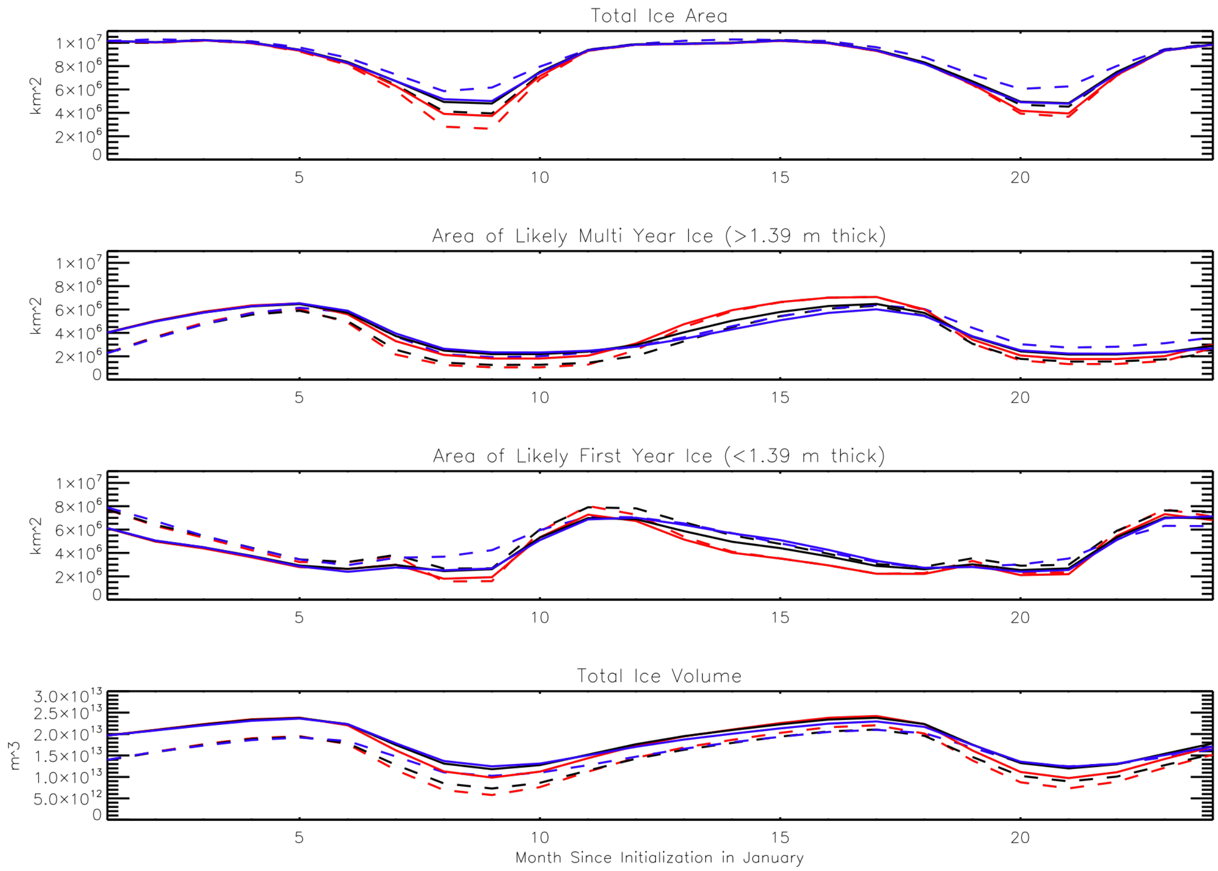

Figure 5. Results of series 2, 1990 atmospheric forcing. Dashed lines indicate 2007 initial ice and solid lines indicate 1979 initial ice . Red indicates 50% climatology precipitation, black indicates climatology precipitation, and Blue 200% precipitation.

	Year 1	Year 2
1979 Ice, 50% Precip.	3.74×10^6 km^2	3.95×10^6 km^2
1979 Ice, Climate Precip.	4.80×10^6 km^2	4.83×10^6 km^2
1979 Ice, 200% Precip.	5.01×10^6 km^2	4.78×10^6 km^2
2007 Ice, 50% Precip.	3.95×10^6 km^2	4.53×10^6 km^2
2007 Ice, Climate Precip.	2.64×10^6 km^2	2.66×10^6 km^2
2007 Ice, 200% Precip	6.16×10^6 km^2	6.26×10^6 km^2

Table 5.a. September ice area for series 2 1990 forcing

	Year 1	Year 2
1979 Ice, 50% Precip.	$.99 \times 10^{13}$ m^3	$.97 \times 10^{13}$ m^3
1979 Ice, Climate Precip.	1.18×10^{13} m^3	1.20×10^{13} m^3
1979 Ice, 200% Precip.	1.25×10^{13} m^3	1.24×10^{13} m^3
2007 Ice, 50% Precip.	$.58 \times 10^{13}$ m^3	$.73 \times 10^{13}$ m^3
2007 Ice, Climate Precip.	0.73×10^{13} m^3	0.87×10^{13} m^3
2007 Ice, 200% Precip.	1.03×10^{13} m^3	1.25×10^{13} m^3

Table 5.b. September total volume for series 2 1990 forcing

	Relative Equilibrium	Rel. Climate Equil.	Rel Initial Equil.
1979 Ice, 50% Precip.	141%,108%	95%,87%	78%,82%
1979 Ice, Clim. Precip.	122%,107%	122%,107%	N/A
1979 Ice, 200% Precip	81%,76%	127%,105%	104%,99%
2007 Ice, 50% Precip.	N/A	67%,81%	67%,81%
2007 Ice, 200% Precip	N/A	156%,138%	156%,140%

Table 6.a. Relative equilibrium of September ice area for series 2 1990 forcing

	Relative Equilibrium	Rel. Climate Equil.	Rel Initial Equil.
1979 Ice, 50% Precip	171%,132%	135%,108%	83%,81%
1979 Ice, Clim. Precip	162%,134%	162%,134%	N/A
1979 Ice, 200% Precip	121%,99%	171%,138%	106%,103%
2007 Ice, 50% Precip	N/A	79%,82%	79%,82%
2007 Ice, 200% Precip	N/A	141%,139%	141%,139%

Table 6.b. Relative equilibrium of September volume for series 2 1990 forcing. The response of the initially thin ice to an increase in precipitation is highlighted.

in significantly decreased ice area and total ice volume. Both the initially thick ice and initially thin ice simulated less than 90% of the ice area of the relative climate equilibrium. In addition, both of these simulations result in a nearly 20% reduction in ice area when compared to the respective initial condition simulation (relative initial equilibrium). As with the series 1 model simulations, changes in volume significantly trail changes in area.

Under these atmospheric forcing conditions, an increase in precipitation produces different effects for the two initial ice states. For 1979 initial conditions, 200% precipitation results in nearly the same areal extent as climatology precipitation, with only minor increases to total volume. However, when compared to the relative equilibrium (200% precipitation over 2007), the 1979 initial conditions with 200% precipitation actually result in a lower area, a shortfall in excess of 20% by the second year of simulation. This is due to the high sensitivity of 2007 initial conditions to an increase in precipitation under this atmospheric regime.

2007 initial conditions provided with 200% precipitation under this regime produce approximately 40% increases in both ice area and total volume by the second year of integration. 1979 initial conditions also result in high volume and extent in this scenario, although both volume and area are lost from the 1st year of simulation to the second year. Moreover, the 2007 initial ice with 200% precipitation actually results in a greater total area than the 1979 initial ice, in excess of 20% (relative equilibrium). Due to the strikingly different reaction to precipitation under different atmospheric conditions, process other than direct growth and melt must be at play. In this case, we find that due to the low initial ice volume in the 2007 initiation state, this ice is more susceptible to snow to ice conversion.

II.3.d. Results of Series 2 – Snow to Ice Conversion

Ice volume produced by snow to ice conversion via surface flooding also deserves discussion. Figure 6 shows the monthly volume of ice generated by snow to ice conversion. Table 7.a reports the total ice volume produced by snow to ice conversion by the second year of integration. Those simulations receiving 200% climatology precipitation generate 2.91×10^{12} m^3 to 3.75×10^{12} m^3 more ice volume via this process than simulations with the same initial conditions but climatology precipitation. Tables 7.b and 7.c compare the inter-simulation difference between snow ice conversion volume to the total ice volume difference for different precipitation regimes.

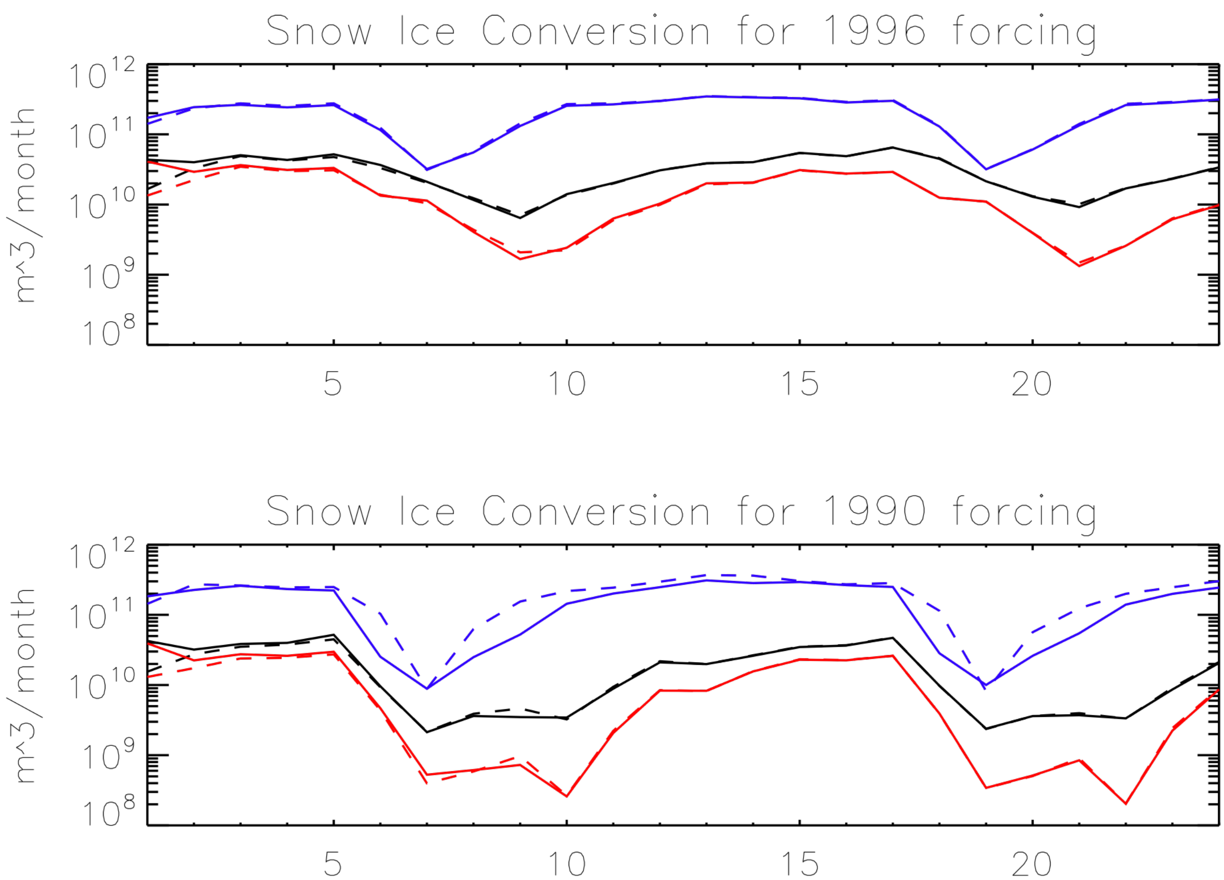

Figure 6. Volume of ice generated monthly by snow-to-ice conversion. Solid lines are 1979 initial ice conditions, dotted lines are 2007 initial ice conditions. Red corresponds to 50% of climatology precipitation, black to climatalogy precipitation, and blue to 200% climatology precipitation.

	50% Clim. Precip.	Clim. Precip.	200% Clim Precip.
1979 ice 1996 forcing	3.78×10^{11} m^3	7.05×10^{11} m^3	42.89×10^{11} m^3
1979 ice 1990 forcing	2.63×10^{11} m^3	4.41×10^{11} m^3	33.51×10^{11} m^3
2007 ice 1996 forcing	3.36×10^{11} m^3	6.63×10^{11} m^3	43.66×10^{11} m^3
2007 ice 1990 forcing	2.25×10^{11} m^3	4.01×10^{11} m^3	41.54×10^{11} m^3

Table 7.a. Volume of ice generated by snow-to-ice conversion for all runs prior to the total volumes reported for September of the second year of integration.

	Snow ice Volume Difference	Total Volume Difference
1979 ice 1996 forcing	-3.28×10^{11} m^3	-25.24×10^{11} m^3
1979 ice 1990 forcing	-1.77×10^{11} m^3	-22.72×10^{11} m^3
2007 ice 1996 forcing	-3.27×10^{11} m^3	-25.24×10^{11} m^3
2007 ice 1990 forcing	-0.65×10^{11} m^3	-16.43×10^{11} m^3

Table 7.b. Difference in ice volume from snow-to-ice conversion and total ice volume at September of the second year of model integration for 50% precipitation and climatology precipitation.

	Snow ice Volume Difference	Total Volume Difference
1979 ice 1996 forcing	35.83×10^{11} m^3	2.22×10^{11} m^3
1979 ice 1990 forcing	29.20×10^{11} m^3	3.87×10^{11} m^3
2007 ice 1996 forcing	37.03×10^{11} m^3	1.30×10^{11} m^3
2007 ice 1990 forcing	**37.53×10^{11} m^3**	**35.01×10^{11} m^3**

Table 7.c. Difference in ice volume from snow-to-ice conversion and total ice volume at September of the second year of model integration between 200% precipitation and climatology precipitation.

For those runs where precipitation is reduced to 50% of climatology, the total volume was reduced by an order of magnitude more than the reduction in snow to ice conversion. For example 1979 initial conditions under a 1996 atmosphere produced 3.28×10^{11} m^3 less volume via snow to ice conversion than the climatology precipitation simulation, while the total volume was 2.52×10^{12} m^3 less than the same climatology precipitation simulation. This indicates significant losses of ice volume to thermodynamic processes, likely surface melt in the summer months considering the restricted nature of the CSIM stand alone simulations.

The simulations where precipitation is increased to 200% of climatology produce an order of magnitude more ice via snow to ice conversion than the differences in total volume observed relative to climatology precipitation. For example, 2007 precipitation under 1996 atmospheric conditions with 200% snow produced 3.7×10^{12} m^3 additional volume via snow to ice conversion with respect to climatology precipitation. However, this same simulation experienced a modest 1.30×10^{11} m^3 total volume difference. This suggests that the increased formation of ice at the surface is largely offset by a decrease in basal ice formation due to the insulative properties of additional snow. However, for 2007 (thin) ice exposed to 1990 (ice loss) forcing with 200% climatology precipitation the amount of ice produced by snow to ice conversion is only slightly greater than the total volume difference from climatology precipitation. When extensive snow to ice conversion occurs this source of ice volume generally serves to expedite the equilibration to a new volume, but often triggers more modest changes in total ice volume.

II.4. Conclusion

This investigation of CSIM sensitivity to the initial ice state, atmospheric forcing, and precipitation yields several results. Series 1 simulations experienced quick adjustment in the September ice area of the ice pack to a change in forcing conditions, nearly reaching quasi-equilibrium during model integration. However, total volume was significantly slower to adjust to a new forcing regime. This slower adjustment was also observed when ice area was divided into ice thickness <1.39m and >1.39m. One potential explanation is that volume of initially thick ice exposed to conditions conducive to ice loss does not quickly equilibrate due to the difficulty in melting very thick ice. In the case of initially thin ice, the insulative properties of the newly formed ice delay continued equilibration. Total ice volume to is expected to eventually equilibrate to a new forcing regime, but any subsequent changes in atmospheric forcing will once again quickly affect ice area. The differing responses as a function of initial ice thickness contribute to explaining the variation in the results of previous modeling investigations of the role of snow cover. To fully explore the variation between previous investigations, it would be necessary to examine the changes in summer melt and winter growth, including processes such as snow to ice conversion in differing model environments. Such an undertaking is beyond the scope of this investigation, but suggests an avenue of future work.

Series 2 simulations, investigating sensitivity to changes in precipitation, generally found greater sensitivity to a decrease in precipitation than an increase, with one notable exception. In this reanalysis forced environment, sensitivity to decreased snow depth indicates that for thin snow cover the change in the role snow plays in the summer as a barrier to melt outweighs the change in role it plays in the winter as a barrier to thermal conduction, and hence basal ice formation. Physically, the snow and ice simply melt more quickly in the summer when the snow is thinned. The importance of this effect may be modified throughout the 21st century as the ice thins and the precipitation regime changes. The strength of this effect is addressed in Chapter 4.

However, it is important to note these observations occur under a fixed atmosphere. In this situation, the surface conditions have no effect on the atmosphere. There are no feedback mechanisms to delay melt once the radiative budget and surface temperatures trigger melt. In a fully coupled environment, it is possible that the sensitivity of the ice cover to precipitation would be considerably different. For example, surface feedback mechanisms may delay summer snow melt under all conditions, while changes in winter conductive flux due to modified snow cover will also impact the surface temperature and other atmospheric conditions.

However, in general there was less sensitivity to precipitation changes when the model was forced with 1996 forcing (conducive to ice gain) than 1990 (conducive to ice loss) forcing. Considering the higher sensitivity of the ice to precipitation under an atmosphere conducive to loss, understanding this sensitivity becomes more important as Arctic climate conditions become less favorable for perennial sea ice.

The most notable simulation in series 2 was initialized with 2007 (thin) ice conditions, was forced with 1990 (conducive to ice loss) atmospheric conditions, and received 200% of climatology precipitation. This simulation was anomalous among runs provided with 200% precipitation in its pronounced increases in both ice area and total ice volume. Increases were sufficient to provide the greatest September areal extent for simulation forced with 1990 atmospheric conditions for both years of the model integration, and the greatest September total volume by the second September. September ice area for this run was more in line with ice area observed for runs forced with 1996 (conducive to ice gain) atmospheric conditions. This significant increase in sea ice serves as a potential negative feedback mechanism, whereby predicted increases in precipitation may also serve to increase total ice extent. However, as indicated in Chapter 4, 21st century increases in precipitation may not result in increased snow depth.

While the ice produced by snow to ice conversion under the thin ice regime (2007 initialization) is similar for both sets of atmospheric forcing, the insulative role of additional snow varies depending on forcing conditions. When the ice is already thin, the apparent importance of insulation in the winter is outweighed by protection from ice melt in the summer only when forcing is conducive to ice loss (1990 forcing). When forcing is conducive to ice gain (1996 forcing) the apparent reduction in basal ice formation in the winter roughly balances both ice produced by snow to ice conversion and protection from surface melt provided by the additional snow. This seems to also be the case for runs initialized with 1979 ice, whatever forcing is applied. While not included in this study, CSIM model output allows for the directly investigation of the sensitivity of basal formation, surface melt, and other thermodynamic (and dynamic) processes to changes in snow cover. While this investigation is included in Chapter 3, a more ambitious analysis of the response in diverse ice modeling environments would also benefit the community understanding with regards to response of ice models to changes in snow conditions.

This study has addressed some initial questions regarding the relative importance of initial ice conditions, atmospheric state, and the importance of snow on the Arctic sea ice. This study has identified the role of snow on the Arctic sea ice in CSIM/CCSM as a fruitful avenue of research. Atmospheric forcing conditions dominate initial ice conditions with regards to areal ice extent in an uncoupled model environment. When the same initial state and atmospheric conditions are used, a decrease in snow results in a decrease in sea ice. A more complex reaction to an increase in precipitation occurs, including a possible significant increase in ice extent as a result of increases in precipitation. Considering the projected 21st century increases in Arctic precipitation it is important to fully understand this complex reaction to an increase in precipitation. Regardless, at this point it is not clear that the projected increases in precipitation over the 21st century will occur as snow, or that additional accumulation on the ice cover will occur. The question of precipitation partitioning and accumulation in the 21st century is addressed in Chapter 4.

The results of this study indicate snow on the Arctic ice plays an important role in modulating ice growth. However, this study is limited due to the reanalysis atmosphere, which does not interact with changes in the ice cover. This is important due to the tenuous nature of the snow cover under an atmosphere that does not react to the melt of the snow cover or ice. Potentially, future work would investigate the role of feedback mechanisms not present in CSIM configured in this way, which would surface in CCSM. Moreover, the sensitivity of ice cover to snow depth warrants the validation of CCSM and CSIM snow depths to observations. Finally, considering increasing Arctic precipitation in the 21st century, it is important to determine whether the increases in precipitation translate to increased snow depths, and to determine how 21st century snow depths are likely to influence the ice cover.

Chapter 3

III. Arctic Ocean Sea Ice Snow Depth Validation and Bias Sensitivity in CCSM and CICE

Abstract: In this study, we assess the capability of hindcast driven ice-ocean coupled and fully coupled hindcast simulations of the Community Climate System Model (CCSM) to reproduce observed snow depths and densities overlying the Arctic Ocean ice. The model is validated against *in situ* measurements provided by historic Russian polar drift stations. Following the identification of seasonal biases in both the depth and density produced in these hindcast simulations the thermodynamic transfer through the snow - ice column is perturbed to determine model sensitivity to these biases in the seasonally changing snow conditions. This study concludes that thermodynamic perturbations on the order of observed biases result in modification of the annual mean conductive flux of $0.5 W/m^2$ relative to an unmodified simulation. In addition, the results suggest that the ice has a complex response to snow characteristics, with ice of different thicknesses producing distinct reactions. Consequently, we suggest that the inclusion of additional snow evolution such as densification and seasonal changes in snow conductivity in CICE would increase the fidelity of the model with respect to the physical system. Moreover, improvements to the precipitation generated by CCSM over the ice cover would be an important step in improving the treatment of ice cover in CICE.

III.1 Introduction

The decline of Arctic Sea ice extent over recent decades is well documented (Parkinson et al 1999, Meier et al 2007). Major shifts in the character and age of the ice are indicative of a persistent shift in the state of the Arctic ice cover (Maslanik 2007, 2011). This decline continues unabated, with the period 2007-2010 including the four lowest summer ice extents on record. (Perovich 2010). The high sensitivity to climate change in the Arctic (Holland et al 2006) combined with anticipated feedback mechanisms, such as the ice albedo feedback (Curry et al 1995), warrants a continuing focus on successfully reproducing the Arctic system with high fidelity. In addition, the transition from a perennial to a seasonal ice pack is occurring more quickly than general circulation models are capable of generally reproducing (Stroeve 2007). This shortfall highlights the need to examine the thermodynamic processes controlling the evolution and state of the Arctic ice pack.

Previous iterations of the Community Climate System Model (CCSM) have been utilized for a variety of climatic studies. Following important participation in the Coupled Model Intercomparison Project (CMIP3), a 2006 *Journal of Climate* special collection included several papers on the performance and projections of CCSM3. More recently, a series of related papers in a second CCSM special collection of the J*ournal of Climate* highlighted the 20th century climatology and 21st century projections of CCSM4 under the RCP 8.5 scenario (Vavrus et al 2012; de Boer et al 2012; Jahn et al 2012).

As with previous versions of the CCSM, the most recent iteration, the Community Climate System Model version 4 (CCSM4), includes a component model, the Community Ice CodE (CICE), to simulate ice conditions. CICE is designed to be computationally efficient while including a thermodynamic model, a model of ice dynamics, a transport model that describes advection, ridging parameterization, and a sub-gridscale ice thickness distribution. Following these computations, the computed ice ocean and ice atmosphere fluxes are passed to other climate model components through an external "flux coupler". For a more detailed discussion of CICE, see Hunke and Lipscomb 2004.

While CICE continues to be developed, the treatment of snow cover on the Arctic ice lags behind other ice characteristics. While the albedo of snow cover does experience a seasonal evolution within CICE due to temperature changes (Brigeleb and Light 2007) and the inclusion of absorption by black carbon (Holland et al 2011), the density and thermal conductivity of snow in CICE are fixed. As a result, the treatment of CICE snow is more rudimentary than the treatment of snow in the Community Land Model (CLM) (Lawrence et al 2011, Olsen et al 2010). However, the advection of ice cover presents a distinct challenge for snow treatment by CICE in comparison to CLM. Moreover, the actual snow depths produced in simulations including CICE have not been validated. Because the thermal snow conductivity is nearly an order of magnitude less than the thermal conductivity of the ice it covers, the snow depth is an important component of the thermal transfer through the ice column despite its relatively tenuous nature.

This study focuses on the modulating role of snow cover on the Arctic sea ice. In historic sensitivity studies, the importance of snow depth to ice seasonality varies. For example, Holland et al 1993 found snow to be of secondary importance to ice characteristics, while Brown & Cote 1992 found ice thermodynamics including ice growth to be highly sensitive to snow cover. While the study discussed here focuses on the Arctic region, a previous study focusing on the Southern Ocean found the ice cover to be "remarkably sensitive to the accumulation rate of snow" (Fichefet and Maqueda 1999). While this study did find a high sensitivity to snow depth, the Southern Ocean is dominated by thinner ice than the Arctic Ocean, where historically thicker ice, surviving multiple melt seasons dominates. In the thinner ice of the Southern Ocean, the snow represents a greater fraction of the barrier to thermal conductivity. The role of snow cover in modulating ice growth has been verified in the field, where the heterogeneity of snow distribution has been observed to produce corresponding heterogeneous growth in underlying lake ice. (Sturm and Liston 2003)

More specifically, focused snow conductivity sensitivity studies have found a 10%-20% change in ice thickness when snow conductivity is halved from the typical ~0.3W/m/K to a more physical 0.15W/m/K (Sturm et al 2002, Wu et al 1999, Fichefet 2000). While more recent studies have explored the introduction of additional thermodynamic complexity to the treatment of snow (Lecomte 2011, Cheng 2008), these studies have focused on one-dimensional modeling and validation.

This study validates the snow depth and density over sea ice as simulated both in CCSM fully coupled runs (denoted as CCSM) and in CICE stand-alone hindcast runs forced with historical reanalysis atmospheric data (denoted as CICE-reanalysis. After an initial discussion of the models and validation data used, the validation results for the CCSM model are discussed. Using the validation, this study determines the biases generated across the model domain by inaccurate snow depth and density. This is followed by an assessment of the sensitivity of the CCSM generated ice state to a seasonal evolution of conductivity specifically derived from the observed density and depth biases. This seasonal evolution is computationally efficient and does not depend on additional physical calculations. Following the discussion of the bias and sensitivity of CCSM runs, we will discuss the biases produced by CICE-reanalysis runs, and compare the bias sensitivity between CCSM and CICE-reanalysis.

Section III.2 describes the General Circulation Model (GCM) utilized: CCSM4 and its component ice model, CICE. Section III.3 describes the *in situ* measurements and validation method. Section III.4 discusses validation of the CCSM model and the design and results of the CCSM bias sensitivity experiment. Finally, Section III.5 is similar to Section III.4, and covers the validation of the CICE-reanalysis model. In addition, Section III.5 discusses the effects of the CICE-reanalysis biases on the CCSM ice conditions. Section III.6 begins with a discussion of the implications of our results with regards to the CICE and the CCSM results as a whole. We conclude with a discussion of future directions for this work.

III.2 Model

This study makes use of CCSM in multiple configurations. For the validation in this study, the release version of the CCSM4 is used with all components, including CICE, active. Following the description of the models, we refer to this simply as CCSM due to full coupling to the other components. In addition, this study make use of the stand-alone version of CICE in combination with a Slab Ocean Model (SOM) with the other components either turned off, or replaced by inter-annually varying re-analyses. Consequently, we refer to this as the CICE-Reanalysis simulation.

III.2.a. CCSM4

CCSM4 derives from CCSM3, and was released in spring 2010 with improvements to all component models. CCSM4 includes coupled component models for the atmosphere, ocean, ice, and land surface and is mass and energy conserving. Here we focus on the improvements to CCSM most important to the Arctic Ocean. A more comprehensive discussion of the improvements in CCSM4 is available in Gent et al (2011). Below we discuss the component models: The Community Atmosphere Model (CAM), the Community Land Model (CLM), the Parallel Ocean Program (POP), and most importantly for this study, the Community ice CodE (CICE).

The atmospheric component model, the Community Atmospheric Model version 4 (CAM4), includes 26 vertical layers with a resolution of 1.25 degrees by 0.9 degrees. CAM4 uses a Lin-Rood dynamical core (Lin, 2004). For a more detailed description of CAM4, see Neale et al (in preparation). In the Arctic, the inclusion of a freeze dry modification serves to reduce the winter low-level clouds in the Arctic (Vavrus & Waliser 2008). For a detailed discussion of CAM4 in coupled simulations, see *Gent et al 2011*.

The land model, the Community Land Model version 4 (CLM4) uses the same grid as CAM4, and includes improvements to hydrology. CLM4 makes use of the Snow and Ice Aerosol Radiation model (SNICAR), and includes grain size dependent snow aging, aerosol deposition, and vertically resolved snowpack heating. For full documentation, see Lawrence et al 2011 and Oleson et al 2010.

The Parallel Ocean Program version 2 (POP2) handles ocean dynamics and thermodynamics. POP2 uses a 1-degree grid with the North Pole displaced into

Greenland. POP2 uses 60 vertical levels, with a surface layer thickness of 10 m, increasing with depth (Smith et al 2010). Improvements to POP2 include mixing parameterizations allowing improved simulation of North Atlantic dense water transport (Briegleb 2010, Danabasoglu 2010). In the sensitivity experiments described in Sections 4 and 5, to save computation time, the fully active POP2 is replaced with a SOM. The SOM serves as a heat reservoir, computes an upper ocean temperature, and specifies an ocean heat transport based on coupled model output (Bitz et al 2012). These simulations use the Slab Ocean Model (SOM) rather than the full Parallel Ocean Program (POP2) in large part due to the lower computational costs. The lower computational costs are due both to the simplified model and the faster equilibration of the model to adjustments. For example, a doubling of CO_2 equilibrates in 20 years, while in a fully coupled simulation the ocean is still adjusting after 900 years (Danabasoglu and Gent 2009). Danabsoglu and Gent (2009) also found that the results of the SOM and fully coupled simulations were similar under control conditions, with differences under a perturbed climate focused in the Southern Ocean. This is unsurprising; The Community Climate System Model component Slab Ocean Model (CCSM-SOM) aims to reproduce the results of the fully coupled climate model, rather than reproduce the observed climate. This version of the SOM is intended for use specifically with the active configuration of the ice model (CICE). Equation 1, reproduced from Bailey et al (2012) is solved for the mixed layer

$$\rho c_p h_{mix} \frac{dT_{mix}}{dt} = F_{net} - Q_{flx} \tag{2}$$

temperature, T_{mix}. F_{net} is the net surface heat flux including the ice ocean heat exchange, and Q_{flx} is the implied horizontal and vertical flux of heat where the local mixed layer column is considered. h_{mix} is the mixed layer depth, r is the density, and c_p is the specific heat. Unlike previous iterations of the SOM, Q_{flx} is calculated using h_{mix}, T_{mix}, and F_{net} from a fully coupled simulation instead of observations (Bailey et al 2012). The required input for the SOM is the oceanic heat flux, and a climatology field is produced.

The SOM should be sufficiently complex for sensitivity experiments due to the relatively long time scales on which deep ocean circulation occurs. However, use of the SOM omits changes in the dynamic interaction between the ocean and atmosphere as a result of a changed ice state.

While CAM4 or an atmospheric reanalysis supplies the precipitation, the snow cover accumulated in the Community Ice CodE (CICE) version 4 is the focus of this study (Hunke & Lipscomb 2010). CICE is a dynamic-thermodynamic ice model, which includes a sub-gridscale ice thickness distribution (Thorndike et al 1975). CICE includes elastic-viscous-plastic dynamics (Hunke and Dukowiz 2002) and is energy conserving (Bitz and Lipscomb 1999). In the configurations used in this study, the sub grid-cell ice thickness includes five prescribed thickness categories. Each category includes a discrete thermodynamic treatment. Ice is transferred between categories by means of a one-dimensional linear remapping (Lipscomb 2001) and includes deformation, dynamical advection, and thermodynamic thickness change as pathways. Spatial advection occurs by means of a two dimensional linear remapping (Lipscomb and Hunke 2004).

CICE v4 also includes improvements to the snow cover, such as the removal of 50% of snow cover to the ocean model during deformation events. In addition, the inclusion of a new Delta-Eddington multiple scattering treatment of snow and ice, which uses internal snow properties to determine albedo, sets CICE ahead in relation to most GCMs (Brigeleb and Light 2007). The effects of this parameterization are reported in Holland et al 2011. In addition, CICE now includes melt ponds, aerosol deposition, and a non-zero heat capacity for the snow cover. Comprehensive documentation of CICE is available in Hunke and Lipscomb 2010.

The validation hereafter referred to as CCSM makes use of a six-member ensemble of fully coupled 20th century simulations (Gent et al, 2011). Each ensemble member is simulated over the period 1850-2005 and includes anthropogenic effects for this period. The general performance of CCSM4 in this ensemble is available in Gent et al 2011. More specifically, discussions of the Arctic region performance for this ensemble are available in the CCSM special collection of the *Journal of Climate* (de Boer et al 2011, Jahn et al 2011).

III.2.b. CICE Stand Alone (CICE-Reanalysis)

CCSM includes the capability to run individual model components with other components inactive. In the configuration we use in this study, CICE remains active, while other components are deactivated, replaced with historic reanalysis (either long term monthly mean or interannually varying), or replaced with significantly simplified versions. In addition to the fully coupled ensemble, we include a stand-alone CICE integration for the period 1950-2007. In general, in this study this is referred to as CICE-Reanalysis.

In the CICE-Reanalysis portion of this study CLM is completely inactive. CAM is replaced with corrected inter-annually varying reanalysis forcing fields (Large and Yeager 2009). The corrected National Center for Environmental Prediction / National

Center for Atmospheric Research (NCEP/NCAR) reanalysis (Kalnay et al 1996) is used for the majority of fields with the following exceptions. The radiative budget, including shortwave and longwave fluxes, is based on the Goddard Institute for Space Sciences (GISS) International Satellite Cloud Climatology Project (ISCCP) climatology (Zhang et al 2004) (Rossow and Zhang 1995). Finally, the precipitation budget, which determines the snow and rain flux to the ice cover, is a blend of several data products (Large and Yeager 2004, Serreze and Hurst 2000). The need for combination of data products is used due to the scarcity of high quality precipitation data in the Arctic. Of special note to this study is the lack of inter-annually varying precipitation in the Arctic Ocean. However, the reanalysis hybrid does provide monthly varying precipitation climatologies. While not ideal, this limitation is somewhat mitigated by the inter-annually varying radiation and surface flux budgets. However, as described later, the considerable uncertainty in these atmospheric fields over the Arctic is potentially one important source of the biases identified by this study (Drobot, unpublished). Finally, as mentioned in the preceding Section, POP2 is replaced by a SOM in the CICE stand alone simulations.

III.3. Snow Depth Validation Data and Design

III.3.a Validation Data

The validation compares *in situ* snow measurements to the output of both the CCSM and CICE-Reanalysis experiments. This Section describes the *in situ* data used for the body of this work, and mention additional *in situ* data disqualified for this study.

The primary source of *in situ* snow measurements is the Russian drift stations (Arctic Climatology Project, 2000). These stations were located on multiyear ice and at least one station was in operation from the period 1954-1991. Snow depth measurements were made two ways. First, an (ideally) daily observation occurred at a snow stake adjacent to the ice camp. Second, once to thrice monthly, a 500 m to 1000 m transect ("snow line") was made at least 500 m from the camp. Snow depth was measured every 10 m along this transect. In addition to depth, snow density was measured using a cylinder massing technique. Transects were made when snow depth exceeded 0.05 m and covered at least 50% of the transect length. Subsequent transects would occur in the same direction but offset several meters. When making use of transect snow measurements, we consider the mean of a transect value (depth or density) to constitute a single measurement. While it would be natural to assume the snow stake measurement could be contaminated by snow alteration due to proximity to the ice camp, Warren et al (1999) did not find this to be the case. However, Warren et al (1999) did favor using the transect snow depths when generating a snow climatology. While climatology reported in Warren et al (1999) could be used for validation, this study makes direct use of the in situ measurements. This method generates sufficient comparisons for statistical purposes without needlessly introducing complexity and potential errors due to the interpolation and extrapolation used by the Warren et al (1999) climatology. Nonetheless, this study does make use of this snow climatology when comparing the geographic distribution of snow depth.

The Cold Regions Research and Engineering Laboratory (CRREL) managed Ice Mass Balance (IMB) buoys were considered as an additional source of *in situ* snow depth data (Perovich et al 2009). However, the buoys' advection paths along the Eastern coast of Greenland were found to cause difficulty matching the buoys to appropriate model grid cells. A more in depth discussion of this issue is included in Appendix A.

III.3.b. Validation method

In principle, combining the ice station and buoy readings, depth validation can be performed for the period 1954-2007. Rejection of the IMB buoy data restricts the validation period to 1954-1993. In both of the model configurations, monthly mean model states are saved. As such, *in situ* measurements discussed in the previous Section are matched to a single monthly output file. The matched CICE locations are restricted to grid cells above 70N, which eliminates the seas along the margin of the Arctic.

Each i*n situ* measurement is matched to two model grid cells. The first is the nearest grid cell, pole-ward of 70N, with at least 15% ice cover, hereafter referred to as the 'all ice' snow thickness, as all ice cover is considered. This definition of ice cover corresponds to commonly used ice cover definitions (ex: Meier et al 2006). However, 15% ice cover does not correspond well with the ice conditions in which the *in situ* measurements were made since the stations were located in areas of high concentration, multiyear ice. To better match the thicker multiyear ice conditions of the Russian stations, this matching process is repeated with the selection restricted to the nearest grid cell, north 70N, with at least 50% of the cell covered with ice greater than 1.5m thickness. We refer to this snow depth as the 'thick ice' depth. 1.5m is used because it is the maximum thickness of the second of five thickness categories. In general, using ice that remains thick throughout the summer was found to produce higher autumn and early winter snow depths, but the exact choice of thickness does not effect the snow depth at other times of the year.

Density validation is performed for the period 1954-1993. As mentioned in Section III.3.a the *in situ* density data is exclusively from the Russian drift stations.

III.4 CCSM Snow Depth Validation and Bias Sensitivity

III.4.a CCSM Validation Results

This Section describes the comparison of the CCSM ensemble to the *in situ* measurements taken at the Russian drift stations. Both depth and density are compared as a function of season. This Section also reports the distribution of snow depths in the simulations and *in situ* data.

Unsurprisingly considering the excessive precipitation produced by CAM in the Arctic (De Boer et al 2012), the validation results indicate significant depth and density differences between the CCSM ensemble and the *in situ* measurements. Figure 7 shows the model snow depths in relation to the *in situ* measurements. At a qualitative level, CCSM 4 snow depths are generally too thick relative to the *in situ* measurements.

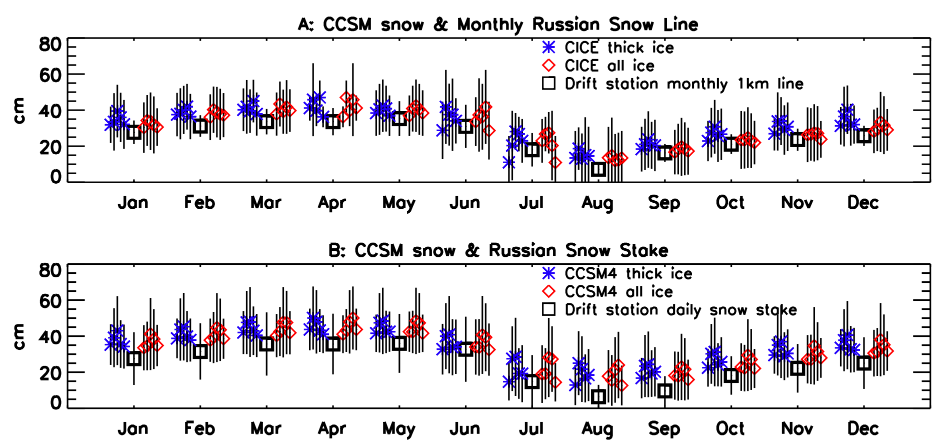

Figure 7. Panels A&B: CCSM Arctic Ocean snow depths for the period 1954-1993 validated against Russian drift station measurements. Panel A reports the Russian snow line as the *in situ* validation data, panel b reports the Russian snow stake as the *in situ* data. Each ensemble member is reported separately. Black squares indicate the *in situ* values for the period, red diamonds indicate the snow depth overlaying the nearest ice of any thickness, blue asterisks indicate the snow depth overlaying the nearest ice with greater than 1.49m thickness.

CCSM snow depths are 20% in excess of Russian drift station transects on all ice; 30% in excess on thick ice. These excesses are much higher by mid summer, and in August reach 80% and 105% respectively. The average mean annual biases in absolute terms are 4.7cm and 6.4cm, while the August values are actually higher, 6.9cm and 7.7cm, for thin and thick ice, respectively. As such, the high biases in late summer snow are due both to an increase in absolute bias and the lower mean snow depths by which the biases are divided. The differences between the CCSM snow depths (for both all ice and thick ice) of the individual ensemble members in Fig. 7 are not necessarily statistically significant ($p<=0.05$) in comparison to the Russian *in situ* data. When considering individual ensemble members, the most likely months to lack statistically significant differences in snow depths are June, July, and August. This is likely due to a low number of *in situ* samples for the summer period. However, taken as an ensemble, the differences for the CCSM snow depth differences (both all ice and thick ice) are statistically significant for all months except July when validated against the Russian drift station transect data.

In addition, the Russian drift station transect data has a lower standard deviation in snow depth than the model, a mean of 30% of the total snow thickness, in comparison to 54% and 49% for the all ice and thick ice CCSM snow thickness. It is unsurprising that the all ice comparison produces the largest variance, as ice of highly variable thickness is selected. As a result, thin ice that has accumulated little snow is included in this population. In addition, the snow transect snow depths have a lower variability in part due to the averaging of the snow depths across the transect. This is consistent with the higher average 64% standard deviation of the Russian snow stake measurements. In this case, each value is a single measurement, rather than a mean of many measurements. This compares more favorably with the 51% and 48% mean standard deviations for the CCSM all ice and thick ice snow depths, as detailed below. Because the CCSM snow depths are averaged over a grid cell, rather than the point measurements of the snow stake *in situ* measurements, the lower standard deviations for these snow depths are unsurprising.

CCSM snow depth biases are slightly higher in relation to the Russian drift station snow stake measurements. The all ice snow depth excess is greater than 20%, and the thick ice snow depth excess is greater than 50%. As with the snow line, the snow stake validation biases are very high in the summer, exceeding 80% and 195% in August. The significance of these comparisons is very similar to the transect comparisons, with July failing our significance test ($P<0.05$)

Next, the geographical distribution of the thickness bias is examined, as shown in Fig. 8. In general, it appears that the CCSM ensemble produces a snow depth excess of the order 20 cm near the Canadian Archipelago when compared to the Warren et al (1999) climatology. This excess is most pronounced in the winter and summer (as

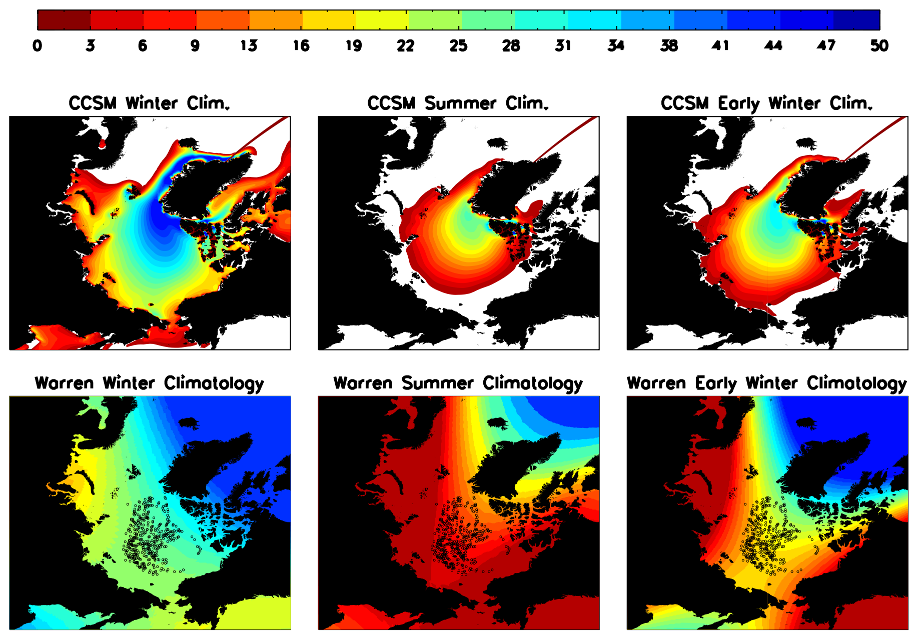

Figure 8. Geographical distribution of modeled snow depth and *in situ* measurements. As defined by the color bar, red corresponds to low snow depth and blue to high snow depth. From left to right: winter (Jan, Feb, March), summer (June, July, Aug), and freeze-up (Oct). The top row is the CCSM ensemble snow depth climatology in cm. The second row overlays the position of the Russian drift station locations over a snow depth climatology derived from the i*n situ* measurements taken at these stations (Warren et al 1999).

opposed to the fall freeze-up) when CCSM produces snow greater than 50cm thick, while the *in situ* snow climatology is ~30cm thick in this region. However, the edge effects along the Atlantic caused by the lack of Russian drift stations used by Warren et al (1999) in this region of the Arctic, as shown by the symbols in Fig. 8. However, the snow climatology reproduced in the bottom row of Fig. 8 suggests the thickest snow was observed on this side of the Arctic. While CCSM is producing too much snow depth overall, the highest biases are in the area where the thickest snow depths are expected.

Figure 9 presents a histogram of the frequency of snow depths modeled by CCSM and observed at the location of the *in situ* validation measurements. The significant excessive mean snow depth observed for CCSM in relation to the drift stations is confirmed by the offset in the snow depth distribution in Fig9a and Fig9b.

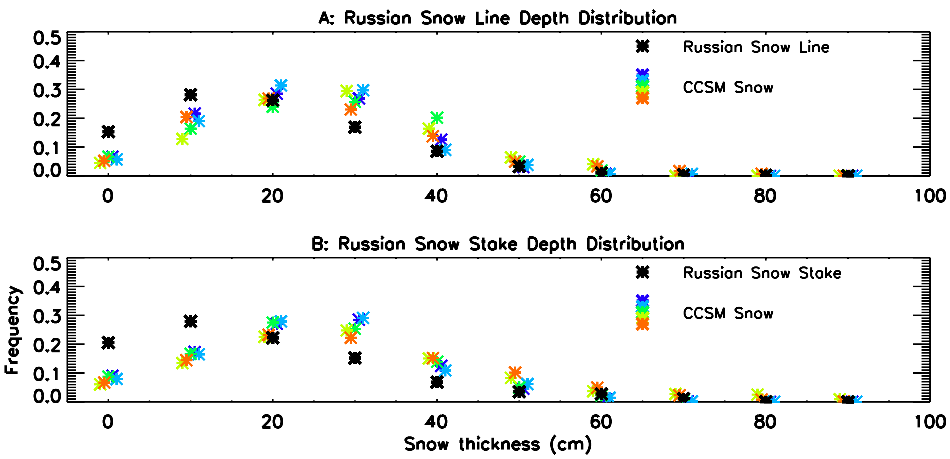

Figure 9. Histogram frequency of snow depth (cm) for CCSM model output and *in situ* observations. Panel A: Russian drift station transects. B: Russian drift station daily snow stake.

Finally, Fig. 10 reports a density bias between the density measurements made as part of the Russian snow depth transect and the CICE default snow density of 330kg/m^3 (Hunke and Lipscomb 2010). Note that no snow density measurements were made in July and August. The most apparent difference results from the omission of snow densification by the invariant snow density in CICE. As a result, the snow density is approximately 30% too great in the early autumn, but is approximately correct by the onset of melt. This implies that the excess in snow mass, or snow water equivalent is larger in the fall than the depth validation would imply.

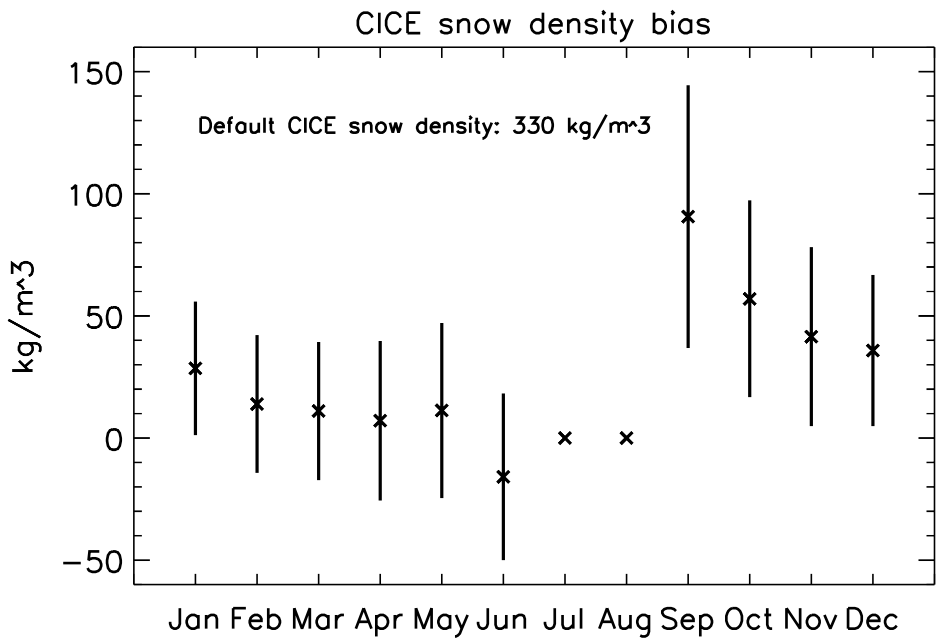

Figure 10. Snow density bias: CICE model default less *in situ* measurements.

Overall, we find that the CCSM ensemble produces year-round excesses in snow depth, for both of the *in situ* measurements (stake and transect) used for validation. This excess is especially pronounced in the summer months. In addition to depth biases, the model produces snow that is too dense in the fall, but is much nearer the *in situ* measurements by the onset of the spring and summer melt.

III.4.b. CCSM Bias Sensitivity Simulation Design

The sensitivity portion of this study seeks to determine the effects of snow depth and density biases on ice characteristics and the controlling thermodynamics. The general method is intended to assess the effects of snow depth changes of a magnitude equal to the bias we reported in Section III.4.a on the Arctic ice cover and climate.

The sensitivity experiments are integrated over a period of 60 years. As the results indicate, this is sufficient to allow the CCSM and CICE to come to quasi-equilibrated states. Because the timescale for ocean circulation is much greater and to decrease computational time by removing the simulation of the ocean as a fluid, we remove the POP ocean component, and replace it with the SOM, allowing the transfer of heat between the active components and a heat reservoir representing the upper ocean. By leaving CAM and CLM active, the Arctic atmosphere and adjacent landmass are allowed to respond to changes in the ice cover.

As outlined earlier in this paper, CICE currently has a fairly advanced treatment of snow albedo. This investigation of snow sensitivity does not require modification of the snow or ice albedo, as the current treatment results in a seasonal evolution. In addition, the validation focused on depth and density, rather than snow cover extent. Specifically, the focus is on the effects of the snow density and snow thickness bias on thermal transfer through the snow-ice column. Nonetheless, it is noted that under the Delta-Eddington multiple scattering parameterization of short wave absorption, snow depth does affect the shortwave absorption when the snow cover is thin.

While altering density and snow thickness directly would be the most straightforward method to explore biases in these quantities, such alternations pose difficulties surrounding mass and energy conservation. More specifically, reducing the precipitation mass at the coupling interface between CAM and CICE would result in the removal of precipitation mass and the thermal energy present in the mass from the model environment. This would create instabilities in the model environment, and as a result is not a viable solution. Instead, we manipulate the snow thermal conductivity. This method allows alterations, which are used to investigate the thermodynamic role of snow in the thermal transmittance through the snow ice column. Thermal transmittance is the rate at which energy is transferred through a barrier of a given thickness, whereas the thermal conductivity is the rate of transfer through a barrier per unit thickness. To clarify thermal transmittance, U_{tot}, as a function of the snow and ice thermal conductivities k_{snow}, k_{ice}, and thickness, h_{snow}, h_{ice}.

$$U_{total} = \frac{1}{\frac{h_{ice}}{k_{ice}} + \frac{h_{snow}}{k_{snow}}} \qquad (3)$$

In addition, these adjustments remain independent of other processes including snow ice formation and the internal snow energy budget.

An average of the monthly bias derived from the snow stake bias and snow line bias is used to calculate the biases tested in this Section. This is a simpler method than that used by Warren et al (1999) in the development of their climatology, but will serve to determine whether the biases are relevant to the state of the Arctic ice.

In addition, rather than consider the direct effect of snow density on conductivity as determined by Sturm et al 1997, the bias correction instead compensates for the excessive snow density early in the season by mimicking a thicker snow pack, which would contain the same snow mass per unit area while having a lower density. We consider a linear relationship between excessive snow density and the total thermal resistance presented by the snow cover. This is likely a lesser effect on snow conductivity than the more complex relationship between density and conductivity. However, our results still reflect the role of a more complex relationship between an evolving snow density and conductive flux through the snow-ice column. To clarify, the method used effectively reduces the thickness of the snow pack without changing mass by mimicking a thicker snow pack. However, it is important to note that because method does not change the snow mass, the thermal diffusivity is not altered. As a result, the perturbation introduced is a lesser effect than a fully bias corrected snow depth would trigger. To clarify, without the mass altered, the changes in conductivity are somewhat limited by the thermal mass of the snow itself.

While multiple bias sensitivity experiments were performed, this Section focuses on the combination of density and depth biases in CCSM; referred to hereafter as the "CCSM bias experiment". While the affect of depth biases alone was also considered, the result was similar to the combination of depth and density biases. Finally, the effect of the density bias only was also simulated. This model adjustment failed to produce a statistically significant response, so the discussion of the density only bias experiment is reserved for Appendix B.

The following series of equations outlines the simple calculation used to determine the experimental conductivity. Equation 4a is the bias corrected snow thermal transmittance, U_{insitu}. Equation 4b is the ratio between simulated snow cover and *in situ* validation, x. Equations 4c and 4d represent the calculation of new conductivity, $\frac{1}{x}k_{snow}$.

$$U_{insitu} = \frac{k_{snow}}{h_{insitu}} \quad (4a)$$

$$xh_{snow} = h_{insitu} \quad (4b)$$

$$U_{snow} = \frac{k_{snow}}{xh_{snow}} \quad (4c)$$

$$U_{snow} = \frac{\frac{1}{x}k_{snow}}{h_{snow}} \quad (4d)$$

To elaborate, the intent is to adjust the element of the total thermal transmittance due to the snow (see equation 1) to compensate for the biases in snow reported in Section 4a. Figure 11 reports the new conductivities used. Note that the higher conductivities in the CCSM bias experiment compensate for the excess snow depth, and will allow for more thermal transfer through the snow-ice column. In this way, the ice will experience the thermal effect of a thinner snow cover, correcting for the snow depth bias.

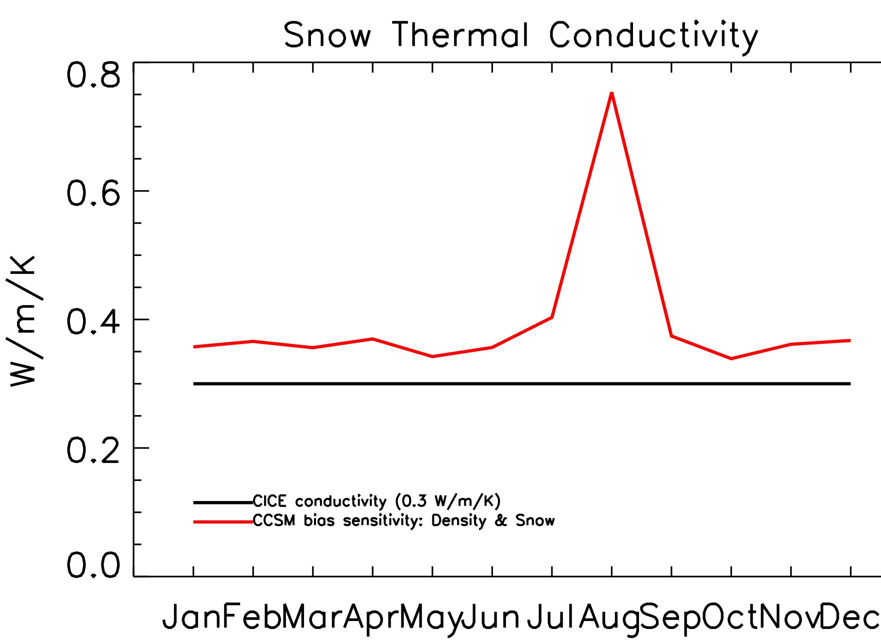

Figure 11. Snow conductivity adjustments: CCSM bias experiment.

III.4.c. CCSM Bias Sensitivity Simulation Results

An increase in thermal conductivity results in an increase in ice volume in the Arctic and corresponding increase in ice area. This is expected because a decrease in snow conductivity is expected to allow increased energy flux through the snow-ice column, triggering increased basal ice formation in the winter. This process is documented in the following analysis. Figure 12 provides a concise summary of experimental results, which are discussed in detail below. Qualitatively, this result

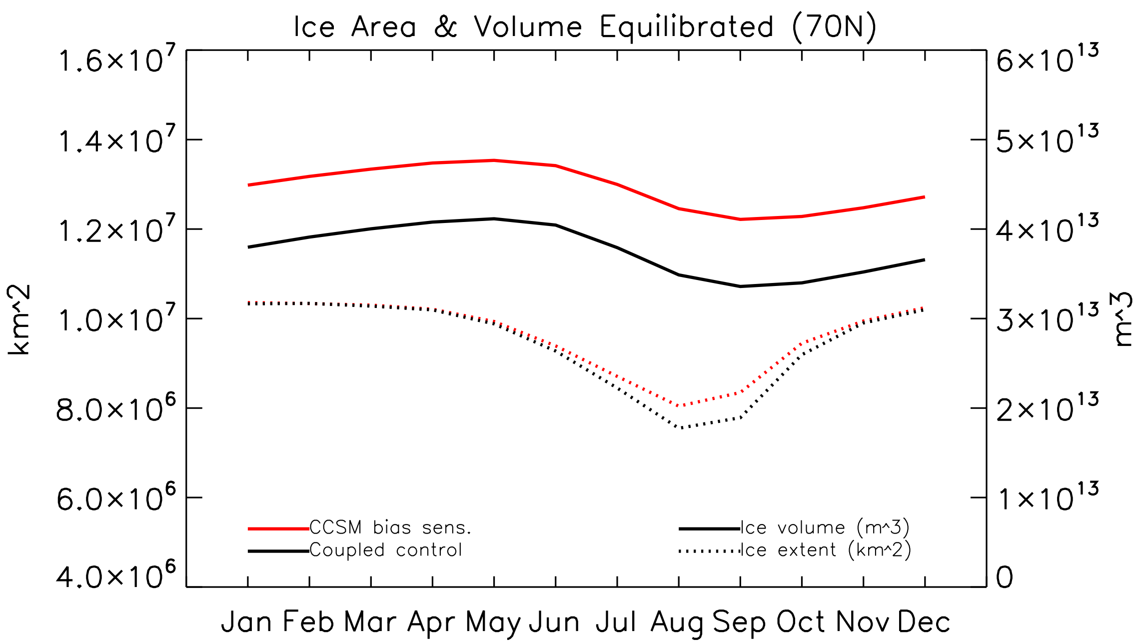

Figure 12. Arctic sea ice volume and extent for control run and CCSM bias experiment. Restricted to north of latitude 70N

suggests that the changes in winter ice growth exceed any changes in summer ice melt caused by our modifications to snow conductivity. In addition, the changes in ice conditions result in shifts in Arctic-wide temperature and cloud cover.

For purposes of clarity, this Section begins with a discussion of the changes to the ice state during the equilibrated period of the simulation; the equilibrated period is defined as the last 20 years of a 60-year simulation. While the definition of the equilibrated period is in part a result of the length of the simulation, and in turn the resources available, the standard deviation in the volume difference between experiment and control in the last 20 years of the simulation, defined as the equilibrated period, is 1.7×10^{12} m^3, which is lower than the 3.5×10^{12} m^3 standard deviation in volume difference for the first 40 years of the simulation, which is defined as the transient period of integration. Following the discussion of the equilibrated state, this paper moves to the beginning of the simulation, where the transient changes in the ice state triggered by our perturbations occur. While this period is more ill defined, it is defined here as the first 40 years of the 60-year simulation. This discussion leads naturally to an examination of the equilibrated effects of the ice change on the Arctic atmosphere and general climate, as well as the feedbacks between the atmosphere, ocean, and ice state.

The equilibrated CCSM bias experiment produces 19% more annual mean ice mass than the control and 7% more September ice area than control, both significant ($P<0.05$), see figure 12. This suggests more ice formation occurring due to the increased transfer of heat through the snow-ice column, as we will discuss shortly. However, as Fig 13 shows, by the equilibrated period of model integration the experimental snow depth has increased significantly relative to control, which offsets the perturbation

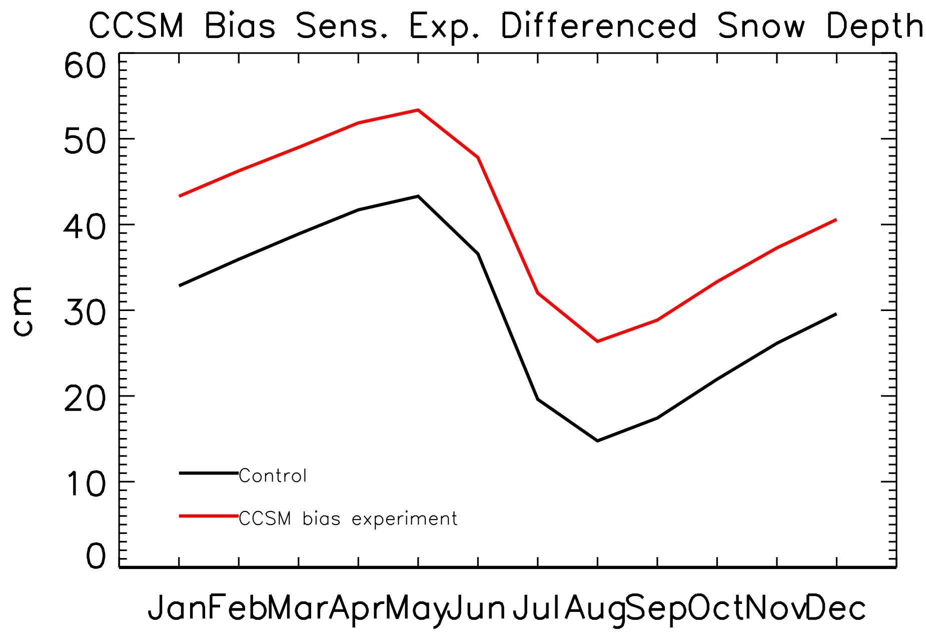

Figure 13. On ice snow depth in the Arctic Ocean during equilibrated period of integration (last 20 years of 60 year simulation).

introduced, and also inhibits conductive flux in the later period of model integration. Therefore, it is likely that other mechanisms conducive to ice growth are triggered by changes in the ice caused by the initial perturbation

Figure 14 reports the geographical patterns of change in ice thickness due to our snow conductivity modifications. Figure 14a shows the control simulation ice thickness,

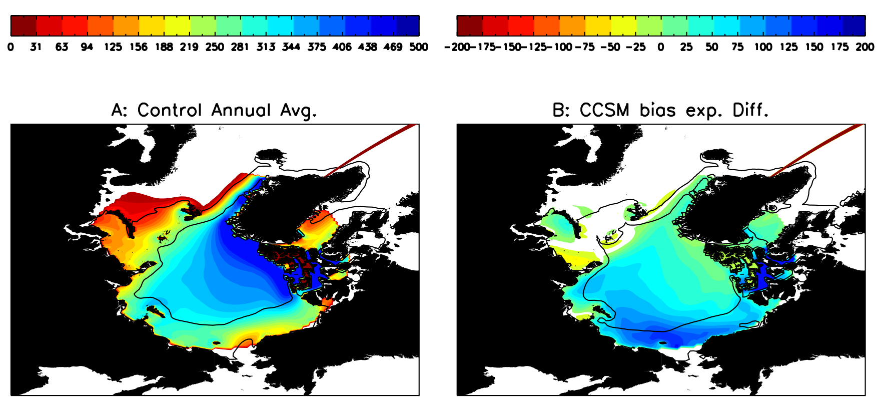

Figure 14. Panel A: Equilibrated ice thickness (depth given in cm by left bar) and 15% and 19% ice extent in September (given by solid black contours) for control run. Panels B: Difference in ice thickness between CCSM bias experiment and the control run (given in cm by right color bar) and 15% and 90% September ice extent (given by solid black contours).

with the pattern of thickest ice near the Canadian Archipelago being typical (Bourke and Garrett 1987). Figure 14b shows the difference between control and the CCSM bias experiment. The thickest ice near the Canadian Archipelago experiences less pronounced changes in ice growth, while the thinner ice along the marginal zone of the ice pack experiences the greatest thickening. This conforms to expectations from Equation 3. Due to the larger h_{ice} in the region of thick ice, the thermal characteristics of the snow has less impact on the total transfer of energy through the snow-ice column.

During the equilibration of the CCSM bias experiment (defined here as the first 20 years of simulation following initialization) there is a statistically significant ($P<0.05$) 7% increase in annual mean conductive heat flux at the top of the snow-ice surface (See Fig. 15a). This 0.5 W/m^2 increase in conductive flux is consistent with the increase in snow thermal conductivity. This change is comparable to the 1.1 W/m^2 change caused by the addition of black carbon and melt ponds to CICE (Holland et al 2011). In addition, note that in the later portion of the integration, this conductive flux in the experimental simulation is lower than in control. This is likely due to increased ice and snow thickness as seen in Figs. 12 and 13.

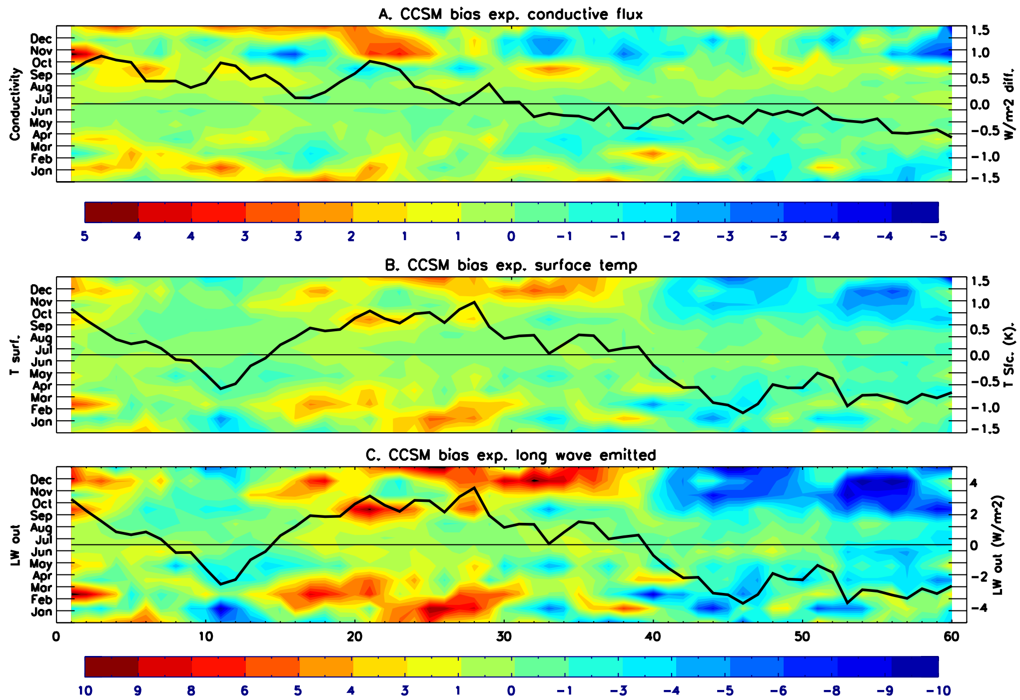

Figure 15. CCSM bias experiment surface energy budget terms relative to control as a function of integration year. A. Surface conductivity in W/m^2 given by the top color bar; positive values indicate greater flux to the surface. B. Surface temperature differences with respect to the control run K given by the top color bar. C. Long wave energy flux out in W/m^2 given by the bottom color bar. Colors are the smoothed monthly values and the solid lines indicate the annual mean.

These shifts in conductive heat flux have a significant impact on surface conditions for the CCSM bias experiment, which results in an annual mean increase of 0.25 K in surface temperature over the control simulation (See Fig. 15b), which in turn contributes to an annual mean increase in surface long wave flux from the surface of 0.8 W/m^2 (See Fig. 15c). Both of these increases are significant ($P<0.05$). We are able to outline a fairly complete picture of energy fluxes for the snow ice column for the CCSM bias simulation, whereby increased energy flux through the ice allows increased ice formation and an associated release of latent heat. This increased conductive flux more efficiently transfers the ice-ocean turbulent heat exchange, causing increased release of latent heat to maintain thermodynamic balance. This increased flux also raises the surface temperature and increases the blackbody radiation from the snow surface.

Figure 16 documents the annual mean difference in total Arctic Ocean ice volume when comparing the experimental simulations to the control simulation. By comparing the changes in volume to the cumulative volume changes due to the most pronounced terms in the ice mass balance budget we are able to gain insight into the processes controlling the ice.

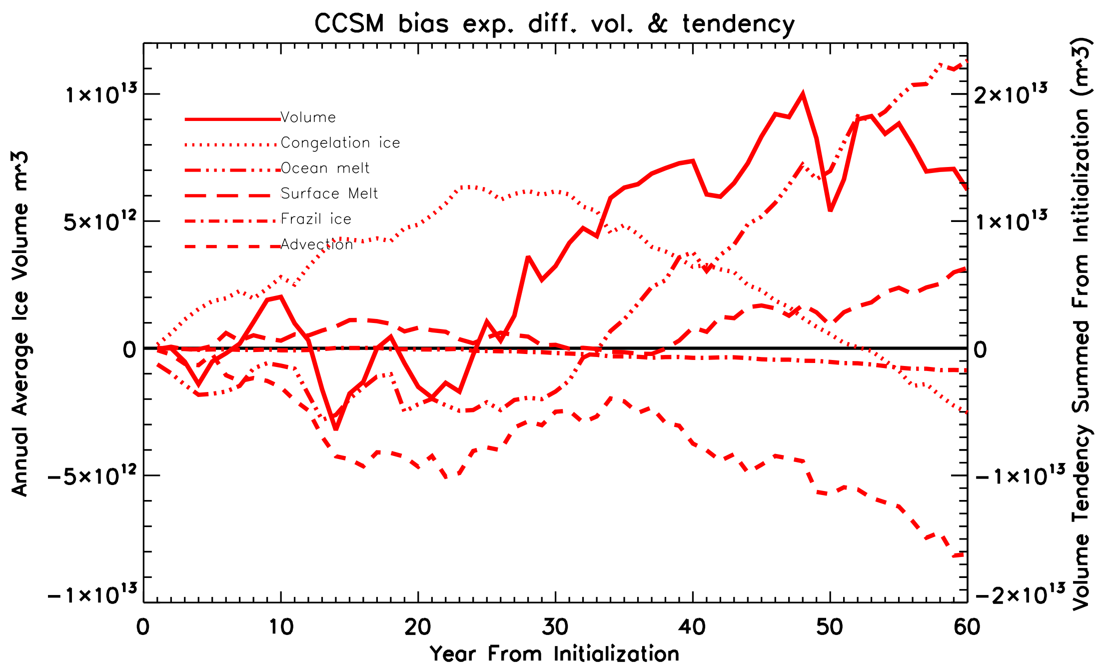

Figure 16. Difference in ice volume (solid line) and accumulated mass budget terms during simulation transient period (first 40 of 60 years) for CCSM bias experiment. Includes basal (congelation) ice growth, open water (frazil) ice growth, basal/lateral (Ocean) melt, surface melt, and loss to transport out of the Arctic (advection).

In Fig. 16, the primary effect of the modified snow conductivity in the CCSM-coupled bias experiment is the increase in congelation ice, which is ice formed at the base of the sea ice. The formation of congelation ice requires a negative imbalance in heat fluxes at the ocean ice interface. Stated more ore clearly, the conductive flux through the snow-ice column generally exceeds the flux from the ocean to the ice during the winter months. This imbalance causes the release of latent heat, and hence the formation of new ice at the ocean-ice interface. In addition, this increased ice production is offset by a negative feedback mechanism through the increased advection of ice mass from the Arctic Basin. This is fairly intuitive, as the ice becomes thicker, the advection of an equal area of ice results in more mass lost from our study area. However, near the end of the transient period of simulation (~1980), an increase in relative volume tendency due to ocean melt (basal and lateral melt) occurs. The increase of this element of the volume budget is indicative of the decreased transmission of energy from the ocean to either the base or margin of the ice pack. This is a result of increased ice area, whereby less open water is exposed, so less solar shortwave radiation is absorbed by the ocean to be retransmitted to the ice. This positive feedback has been termed the ice-ocean albedo feedback, and is expected to occur under any simulation where a perturbation resulted in an increase in ice area (Curry et al 1995).

Figure 17 shows the September ice extent difference between the CCSM bias sensitivity experiment and control. In Fig.17 it is apparent that the ice area is higher for

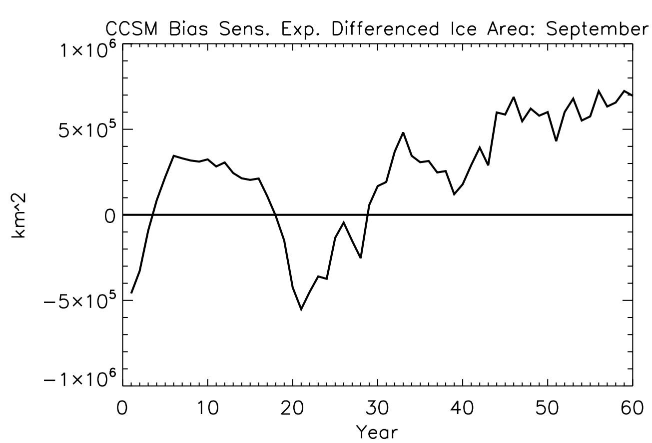

Figure 17. September ice area difference between CCSM bias sensitivity experiment and control, with a 5 year smoothing.

an early period of the model simulation, leading to the initially negative volume tendency due to ocean melt in the experimental configuration. However, around year 20 of the simulation the September ice area begins to trend upward, leading to a corresponding upward trend in cumulative ice volume tendency due to bottom and lateral melt, triggered by ocean heat.

Figure 18 complements Fig 16 and shows the annual mean fluxes of the longwave, ocean, and conductive flux terms. As with Fig. 16, Fig. 18 plots the difference with respect to the control run. Figure 18. Shows gradual decrease in the relative flux due to conduction at the snow-ice surface (dotted line). To clarify, a large negative value for the conductive flux at the ice surface indicates a large loss of energy due to

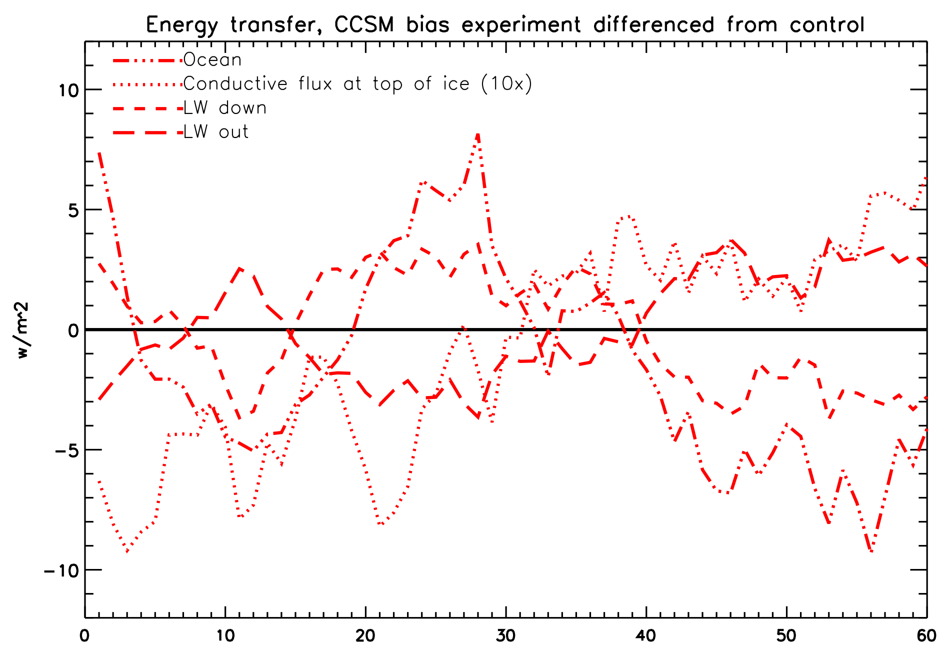

Figure 18. Annual difference in the energy transfer between experimental and CCSM bias sensitivity experiment as a function of year of integration. Terms are smoothed over a five-year average. Includes the long wave budget, conductive flux at the top of the ice (increased by a factor of 10 for clarity), and ocean heat flux from the SOM to the ice. Other flux terms have smaller differences from the control, and were not included for purposes of clarity. Positive values indicate more flux to the ice. In the case of conductivity, negative values indicate more energy transported from the basal ice forming region.

conduction through the ice. This increase in relative conductive flux is due to gradual thickening of the ice pack, reducing the effects of our initial perturbation, which increased the loss of heat through conduction from base to surface. Note that the conductive flux in Fig 18 has been increased by a factor of 10 for clarity. In Fig. 18, we also see the gradual decrease in relative ocean flux to the ice both in absolute terms and in the variability, which is a near mirror of the September ice extent in Fig 17. In addition the relative long wave flux out also gradually increases, indicating that the ice in this experiment is gaining less energy from the ocean while it radiates less heat to the atmosphere.

The flux differences during the last 20 years of the 60-year simulation are reported in Fig. 19; the initial perturbations to conductivity are fairly well equilibrated,

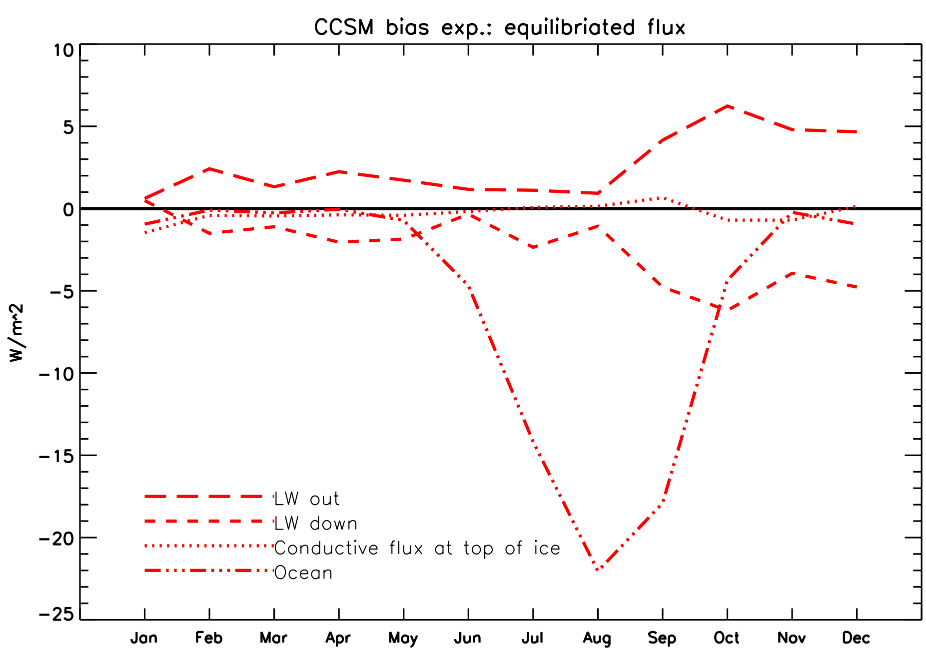

Figure 19. Monthly mean difference in energy transfer between experimental and control simulations during the equilibrated period (final 20 of 60 years) for CCSM bias sensitivity. As in Figure 10, positive anomalies indicated more flux to the ice.

with the differences between experimental and control simulations becoming more less variable, as with the total volume in Fig 16. In addition, due to reduced open water the flux in the summer ocean heat flux has dropped by as much as 20 W/m^2 (See Fig. 18). This results in an annual average 6 W/m^2 lower mean flux (statistically significant (<0.05)). As previously discussed, this is expected due to the perturbation inducing an ice-ocean albedo feedback. In addition to the ice-ocean albedo feedback, an autumn decrease in long wave flux from the atmosphere also occurs in the increased conductivity simulation (See Fig. 19). This results in an annual mean of 2 W/m^2 lower long wave absorbed by the ice, also statistically significant (P<0.05) Previous studies have shown decreases in autumn ice area lead to an increase in autumn cloud cover, and represents an additional expected positive ice area feedback (Schweiger et al 2008).

Figure 20 examines the effects the perturbation has on the Arctic atmosphere.

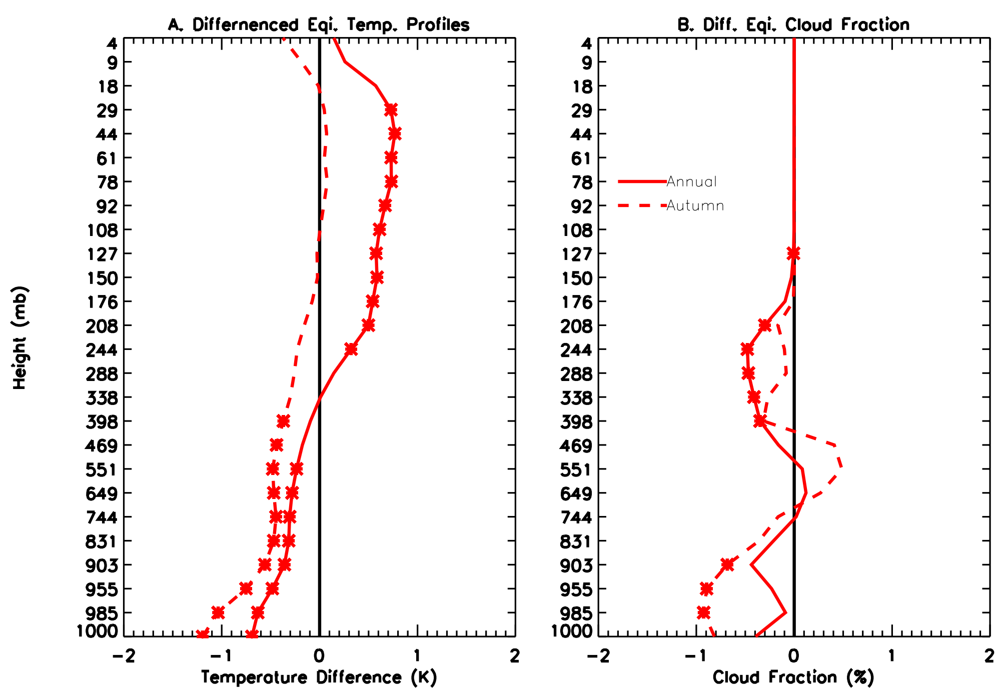

Figure 20. Differenced (experiment less control) annual and autumn (Sept-Nov) mean temperature and cloud fractions for the equilibrated period of the CCSM bias sensitivity (last 20 of 60 years) for 70N poleward.

While these effects are likely due in large part to the changes in the ice cover, they are representative of other processes, such as the changed ocean heat flux initiated by the perturbation. Figure 20a reports a ~1K drop in temperature near the surface in the CCSM bias sensitivity experiment. This drop is significant for the lower atmosphere both in the annual mean and autumn. The drop is more pronounced in the autumn. The initially high surface temperature should drop as the ice thickens and compensates thermally for the missing snow. To clarify, the initial perturbation reduces the thermal impedance through the snow-ice column, allowing for more conductive flux and an initial increase in temperature. If the ice were simply adjusting to the perturbation without feedbacks, the ice would thicken until the additional ice compensated for the thermally thinner snow cover. However, the decreased surface temperature in the equilibrated CCSM bias experiment indicates feedbacks have resulted in an enhanced effect beyond, but due to, the perturbation. In addition to the near surface effect, the upper atmosphere temperatures increase, which is not further diagnosed as it is beyond the scope of this study due to lack of direct interaction with the ice cover.

Figure 20b reports somewhat complex and generally not significant ($P<0.05$) reactions in cloud cover in our experimental simulation. In the CCSM bias experiment the annual mean is only significant in the upper atmosphere, where there is a drop in cloud fraction. In the lower atmosphere, there is a significant drop in the autumn cloud fraction. From Fig. 20, the down-welling long wave feedback observed in the CCSM bias sensitivity experiment is the result of both lower atmosphere decreases in both temperature and cloud cover.

In summary, an increase in snow conductivity results in significantly increased ice volume and area. In addition, as seen in Fig. 14, ice of different thicknesses reacts distinctly. We also stress the importance of oceanic and atmospheric response and induced feedbacks to our perturbations. These findings indicate that the ice state is sensitive to changes in snow conditions, in particular of the same magnitude as the biases identified in Section III.4.a.

III.5 CICE Reanalysis Driven Snow Depth Validation and Bias Sensitivity

III.5.a CICE-Reanalysis Validation

This Section describes the comparison of the CICE-Reanalysis simulation to the *in situ* measurements taken at the Russian drift stations. While the snow depths generated here will largely be a function of the reanalysis fields, this configuration is used to test the model, and as such biases in this configuration will affect these tests. Therefore, it is useful to assess whether this configuration is being supplied with accurate snow depths. In addition, the biases identified herein are of the opposite sign, and complement the sensitivity study in Section III.4. As with Section III.4.a, depth is compared as a function of season. The density validation in Section III.4.a is also valid here, as this default remains the same in both simulations. Additionally, the distribution of snow depths in the simulations and *in situ* data is discussed.

As with the CCSM model, the CICE-Reanalysis model produces significantly different snow thicknesses than the *in situ* measurements. However, the differences are not particularly similar between CCSM and CICE-Reanalysis. Figure 21 reports the general differences between CICE-Reanalysis and the *in situ* measurements. While not

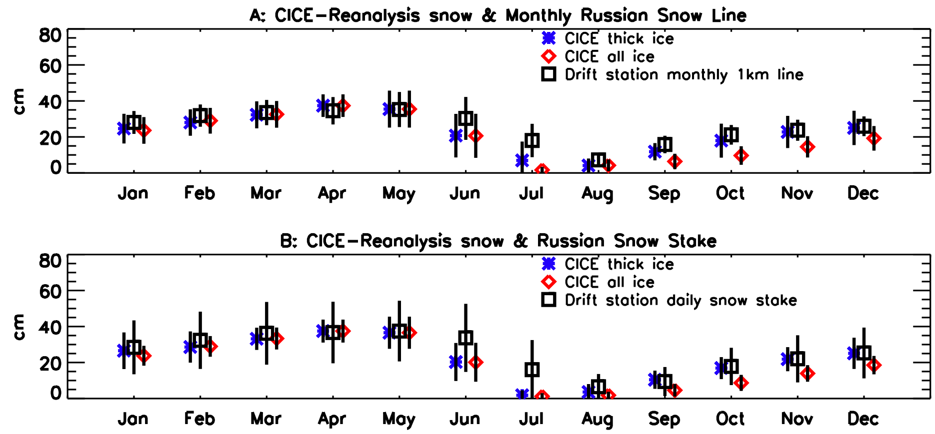

Figure 21. A&B: CICE-Reanalysis Arctic Ocean snow depths for the period 1954-1993 Validated against Russian drift station measurements. Black squares indicate the *in situ* values for the period, red diamonds indicate the snow depth overlaying the nearest ice of any thickness, and blue asterisks indicate the snow depth overlaying the nearest ice with greater than1.49m thickness.

as pronounced as the biases in the CCSM configuration, the CICE-Reanalysis configuration tends to have excessive springtime snow, with insufficient summer snow depth. Likely due to the low summer snow depth, the snow depth remains low in the autumn until the accumulation mitigates this initial deficiency.

Generally, the differences between CICE-Reanalysis snow depths (both all ice and thick ice) and *in situ* measurements are significant. The exceptions to this are the Russian snow-stake measurements and the CICE-Reanalysis and all ice snow for January, February, and November. This may be due to the small differences between these *in situ* and modeled snow depths resulting in lower significance. The thick ice snow depth differences are significant for all months. However, the differences between CICE-Reanalysis and the snow line measurements are not significant for several months, including the summer months (June, July, and August) in both cases. Again, this may be due to the lack of snow line measurements made in the summer.

In contrast to the CCSM ensemble, the CICE-Reanalysis integration tends to produce low biases in snow depth. In relation to the Russian drift station transects, low biases of 30% and 15% are observed for the all ice and thick ice snow depths. The greatest biases of 90% and 30% are simulated for the all ice and thick ice areas in July. Similar fractional biases occur for the snow stake *in situ* measurements, with significant thick ice snow depth biases, especially in July where a 90% low bias in snow depth occurs.

Next, Fig 22 returns to the geographical distribution of snow thickness biases. Examining the distribution confirms the results for the mean state. Namely, there is nearly no snow in the CICE-Reanalysis summer (June, July, August) with very little

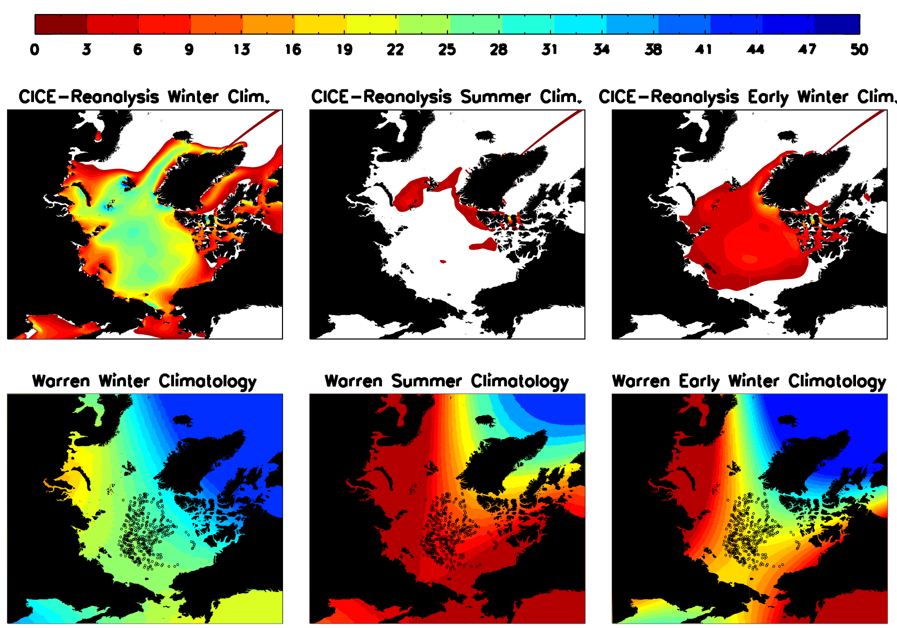

Figure 22. Geographical distribution of modeled snow depth and *in situ* measurements. As defined by the color bar, red corresponds to low snow depth and blue to high snow depth. From left to right: winter (Jan, Feb, March), summer (June, July, Aug), and freeze-up (Oct). The top row is the CICE-Reanalysis snow depth climatology in cm. The second row overlays the position of the Russian drift station locations over the snow depth climatology derived from the i*n situ* measurements taken at these stations (Warren et al 1999).

snow accumulated by October. By winter (January, February, March) the snow produced by CICE-Reanalysis appears to be a better match for the Russian station climatology (Warren et al 1999) than CCSM.

Figure 23 reports the distribution in snow thicknesses. The peak in the distribution of CICE-Reanalysis snow depths is at thicker depths than the *in situ* measurements. However, CICE-Reanalysis lacks the tail of very deep snow measured *in*

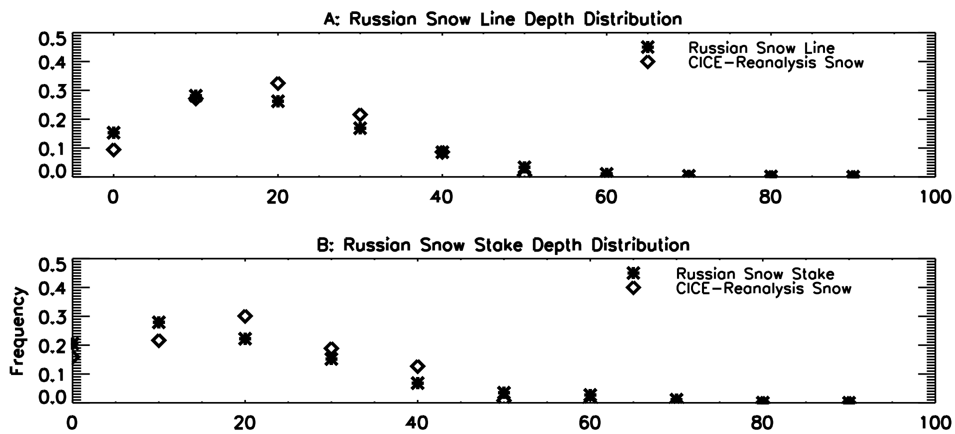

Figure 23. Histogram frequency of snow depth for CICE-Reanalysis model output and *in situ* observations. Panel A: Russian drift station transects. B: Russian drift station daily snow stake.

situ, and modeled by CCSM (Refer to Fig. 9.). As a tentative explanation, the lack of persistent snow cover in CICE-Reanalysis may result in lower maximum annual snow depths. CICE-Reanalysis utilizes the same snow density parameterization as CCSM, so no additional discussion of the density bias is provided here. In contrast to the previous validation, the combination of the snow thickness and snow density biases yield insufficient snow mass, as will be shown in Section III.5.b.

Overall, the CICE-Reanalysis simulation produces very low summer snow depths, with a slow accumulation to *in situ* values in the autumn months.

III.5.b. CICE-Reanalysis Bias Sensitivity Simulation Design

The design of the CICE-Reanalysis bias experiment closely follows the design of the CCSM bias experiment. Due to the low bias in snow depths, this experiment serves as a counterpoint to the CCSM bias experiment in Section III.4. CAM and CLM remain active, while POP is replaced with the SOM. As a result, the mean ice state will be different than the CICE-Reanalysis simulation. A 60-year integration is performed. However, the purpose of this simulation is to assess the effect of the biases in snow characteristics produced by CICE-Reanalysis. As in Section III.4.b, a modification is applied to the snow conductivity to impose a thermodynamic correction to the bias observed in CICE-Reanalysis snow depth and density. Please refer to Section III.4.b. for a more in depth discussion of this method. As in Section III.4.b., no modifications are made to albedo. This may have a larger effect in this bias sensitivity than that in Section III.4, due the near zero summer snow depths generated in CICE-Reanalysis. This could have a larger effect as the Delta-Eddington multiple scattering parameterization is most sensitive to snow depth changes when snow is thin. If this limitation were also corrected, it may result in higher albedos, lower melts, and hence greater summer ice survival.

Figure 24 reports the new conductivities implemented in the CICE-Reanalysis bias experiment. As this figure demonstrates, the modification of conductivity is of the opposite sign as the bias sensitivity experiment in Section 4, making this a complementary sensitivity experiment.

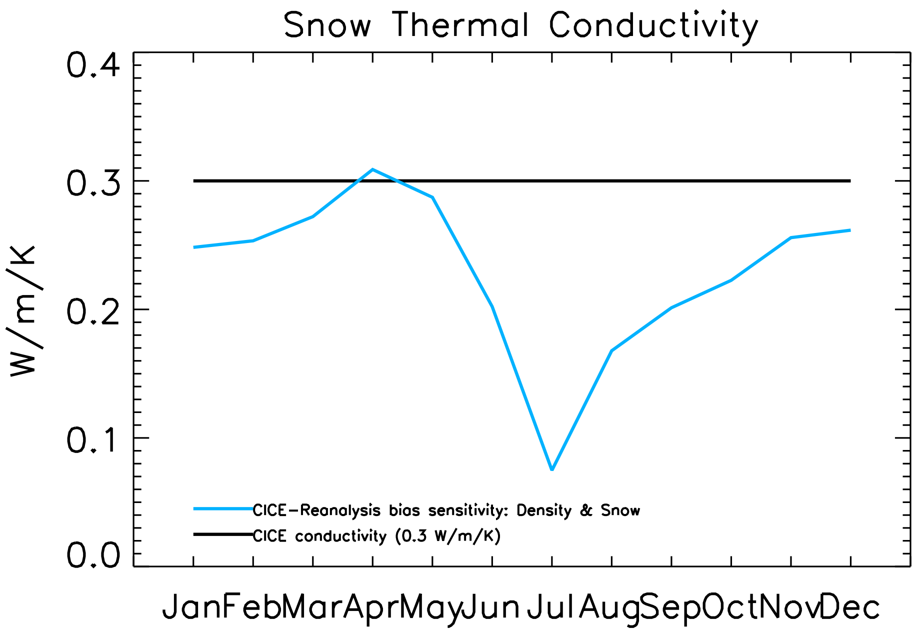

Figure 24. Snow conductivity adjustments for our CICE-Reanalysis bias experiment.

III.5.c. CICE-Reanalysis Bias Sensitivity Simulation Results

The CICE-Reanalysis bias experiment modifications to conductivity are of similar magnitude but opposite sign of those made in the CCSM bias sensitivity. However, the reductions in conductivity have a much less pronounced effect on the ice state. The changes in ice volume and extent are documented in Fig. 25.

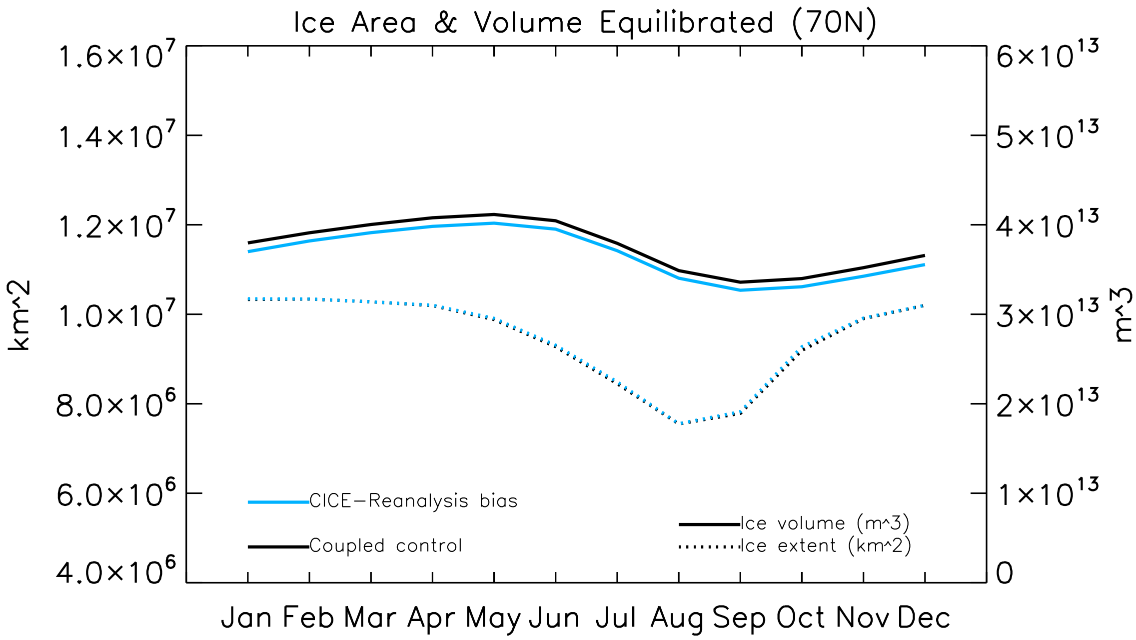

Figure 25. Arctic sea ice volume and extent for control run and CICE-Reanalysis bias experiment. Restricted to north of latitude 70N.

The reduction in conductivity in this experiment produces a 2% decrease in annual mean Arctic ice volume, significant to $P<0.05$. While much less than the 19% increase simulated under the increased snow conductivity in the CCSM bias sensitivity experiment, the sign of this difference is expected given our modifications to the snow thermodynamics. More specifically, the reduction in snow conductivity serves to impede the flow of energy from the basal ice-forming region to the surface of the snow. This reduction decreases the surface temperature and decreases the release of latent heat at the ice-ocean interface. As a result, the rate at which ice formation occurs will decrease.

The CICE-Reanalysis bias experiment produces a somewhat surprising result in ice area, whereby non-significant 1% increase in September ice area. This result suggests that while the ice mass balance of the Arctic Ocean is highly controlled by the ice growth implications of conductivity, there may be some unanticipated impact on summer melt as well, in this CICE-Reanalysis experiment at least. One potential explanation is delayed melt of the snow itself. In Fig. 26 it is apparent that the snow thickness in this experimental simulation also increases relative to control as in Section III.4. While this is circumstantial evidence of delayed snow melt, one possible explanation for this increase in snow depth is the slightly increased ice area and platform for snow accumulation. This presents a feedback mechanism, which is further explored in Chapter 4. Due to the lack of a significant response in the ice itself, we refrain from further diagnosis.

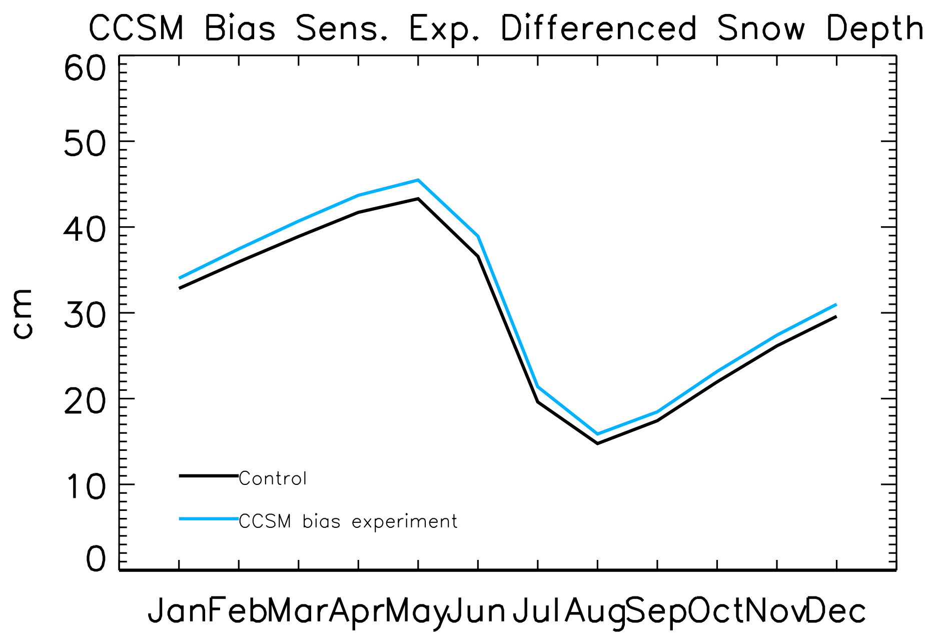

Figure 26. On ice snow depth in the Arctic Ocean during equilibrated period of integration (last 20 years of 60 year simulation).

In Fig. 27, the ice in the CICE-Reanalysis bias experiment is shown to thicken along the archipelago, and thins in the marginal zone and central Arctic. This response indicates the thicker ice seems less effected by changes in snow conductivity, as in Section III.4.c.

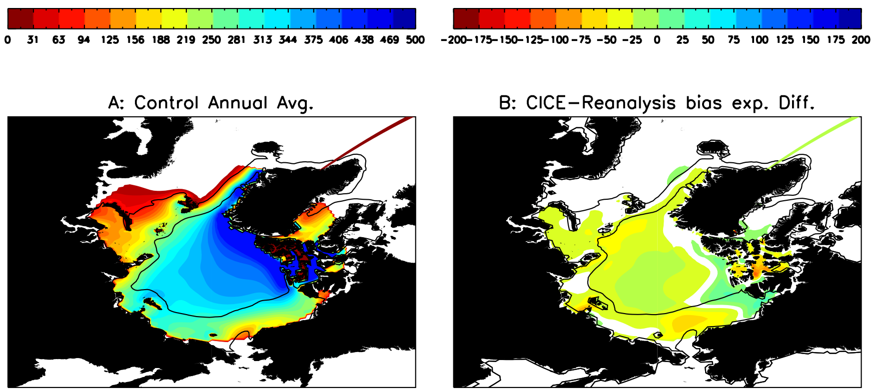

Figure 27. Panel A: Equilibrated ice thickness (depth given in cm by left bar) and 15% and 90% ice extent in September (given by solid black contours) for control run. Panels B: Difference in ice thickness between CICE-Reanalysis bias experiment and the control run (given in cm by right color bar) and 15% and 90% September ice extent (given by solid black contours).

During the equilibration of the CICE-Reanalysis bias simulation, defined as in Section III.4.c as the first 20 years of simulation, there is a statistically significant 3% decrease in conductive flux at the surface (Fig. 28a). This 0.4 W/m^2 reduction in

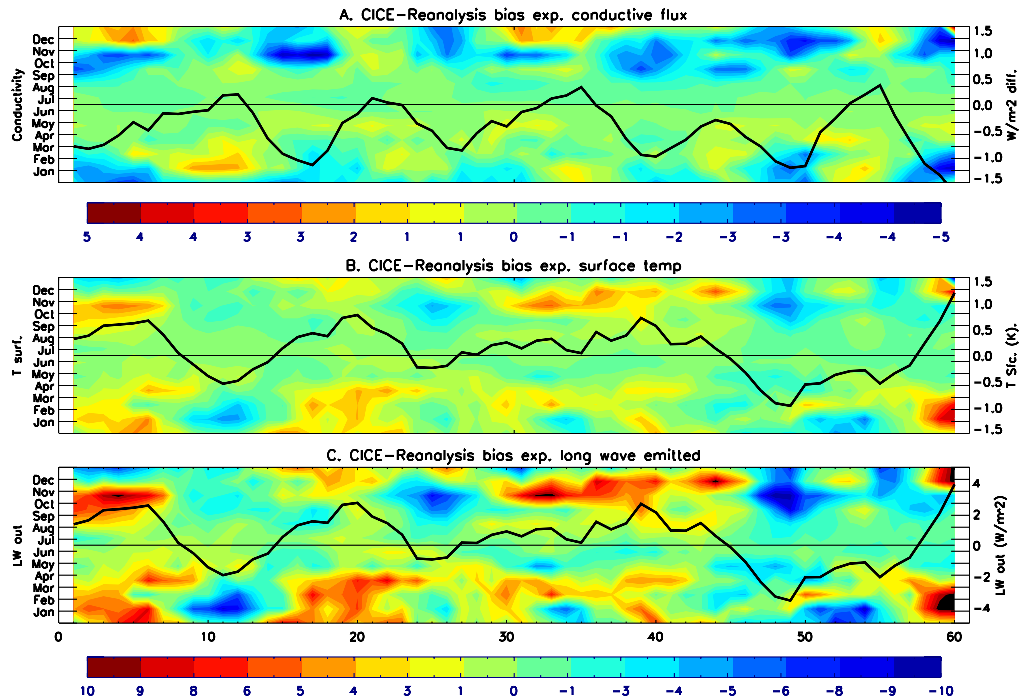

Figure 28. CICE-Reanalysis bias experiment surface energy budget terms relative to control as a function of integration year; positive vales indicate greater flux to the surface. A. Surface conductivity in W/m^2 given by the top color bar. B. Surface temperature differences with respect to the control run K given by the top color bar. C. Long wave energy flux out in W/m^2 given by the bottom color bar. Colors are the smoothed monthly values and the solid lines indicate the annual mean.

conductive flux implies a decrease in the amount of energy transferred from the basal ice forming region to the surface of the overlying snow. This is unsurprising given the decreased snow conductivity in this experiment. What is surprising, is the nearly significant (.05<P<.10) increase in surface temperature, and the increase in long wave energy out, which indicate additional terms of the surface energy budget are also playing a role (Fig.28b, Fig.28c) . However, individually these additional terms do not have significant responses.

Figure 29 relates the dominant role of decreased congelation ice formation in reducing the total ice volume. Continuing to Fig. 30, this is confirmed in the inter-annual mean energy budget figure, where the conductive flux at the ice surface is generally high, indicating a decrease in flux to the surface. While no one element of the surface energy budget explains well how this accounts for this imbalance, it is likely the sum of several terms in the energy budget is accountable.

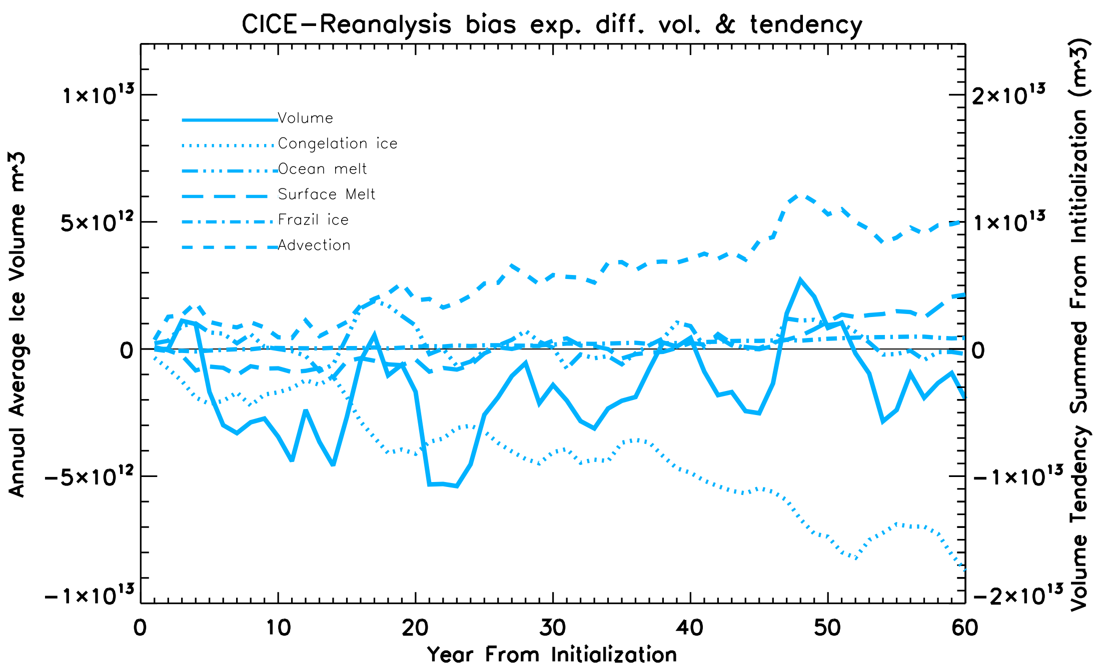

Figure 29. Difference in ice volume (solid line) and accumulated mass budget terms as a function of year of simulation for CICE-Reanalysis bias experiment. Includes basal (congelation) ice growth, open water (frazil) ice growth, basal/lateral (ocean) melt, surface melt, and loss to transport out of the Arctic (advection).

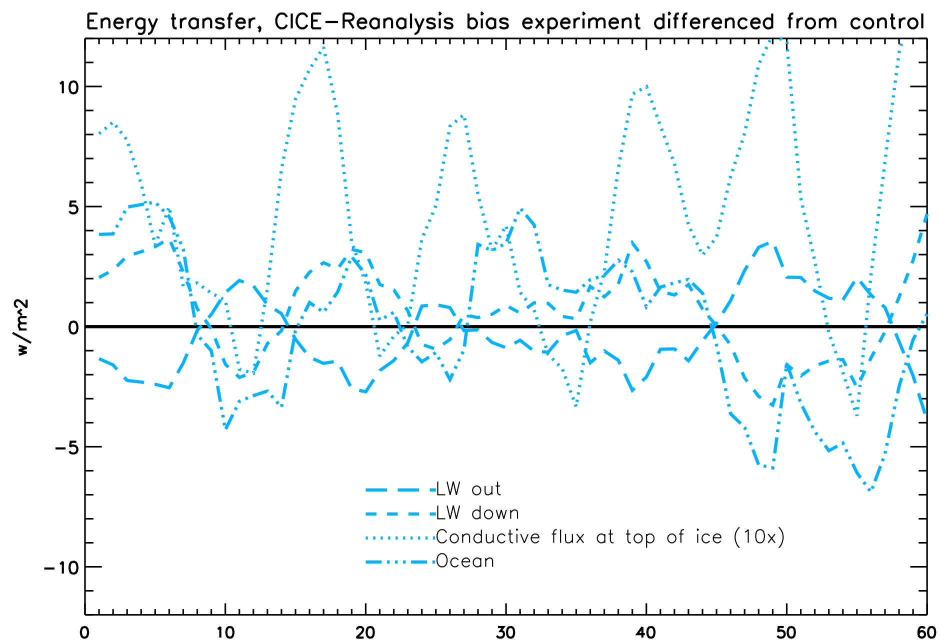

Figure 30. Annual difference in energy transfer between experimental and CICE-Reanalysis bias sensitivity experiment as a function of year of integration. Terms are smoothed over a five-year average. Includes the long wave budget, conductive flux at the top of the ice (increased by a factor of 10 for clarity), and ocean heat flux from the SOM to the ice. Other flux terms have smaller differences from the control, and were not included for purposes of clarity. Positive values indicate more flux to the ice. In the case of conductivity, negative values indicate more energy transported from the basal ice forming region.

Turning now to Fig. 31 the ice is well equilibrated, with the conductive flux similar to the control simulation. There is, however, a similar drop in ocean flux to the ice. At 3 W/m^2, this drop is half the size of the drop in the CCSM, but is also statistically significant (P<0.05). With no significant change in ice area, it is difficult to attribute this response to any specific mechanism.

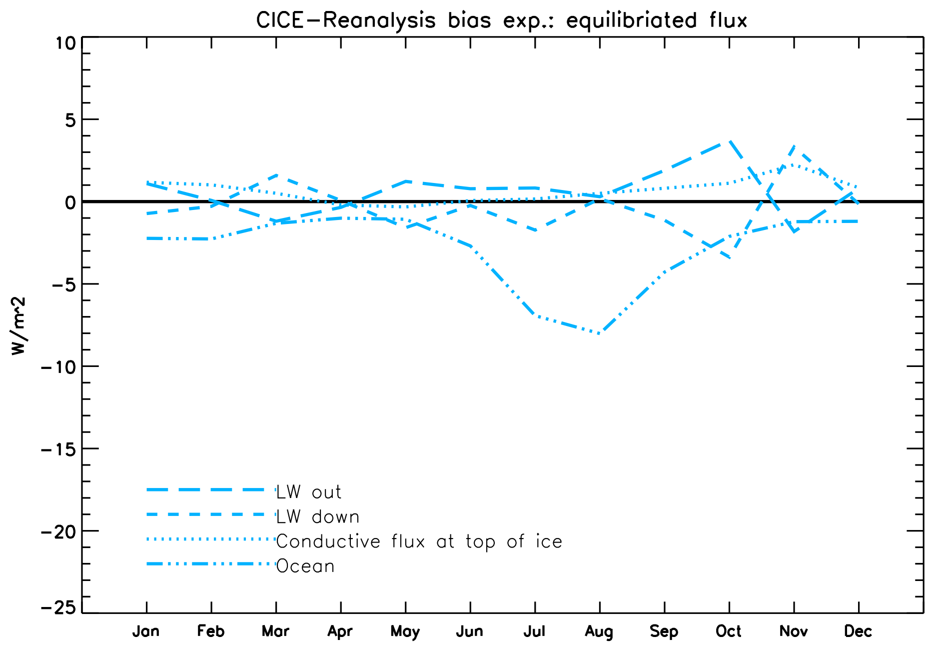

Figure 31. Monthly mean difference in energy transfer between experimental and control simulations during equilibrated period (final 20 of 60 years) for CICE-Reanalysis bias sensitivity. As in Fig 22, positive anomalies indicate more flux to the ice.

Finally, returning once more to the effects of the modification on the Arctic climate in Fig 32, there are generally small and non-significant (P<0.05) changes to atmospheric temperature and cloud cover.

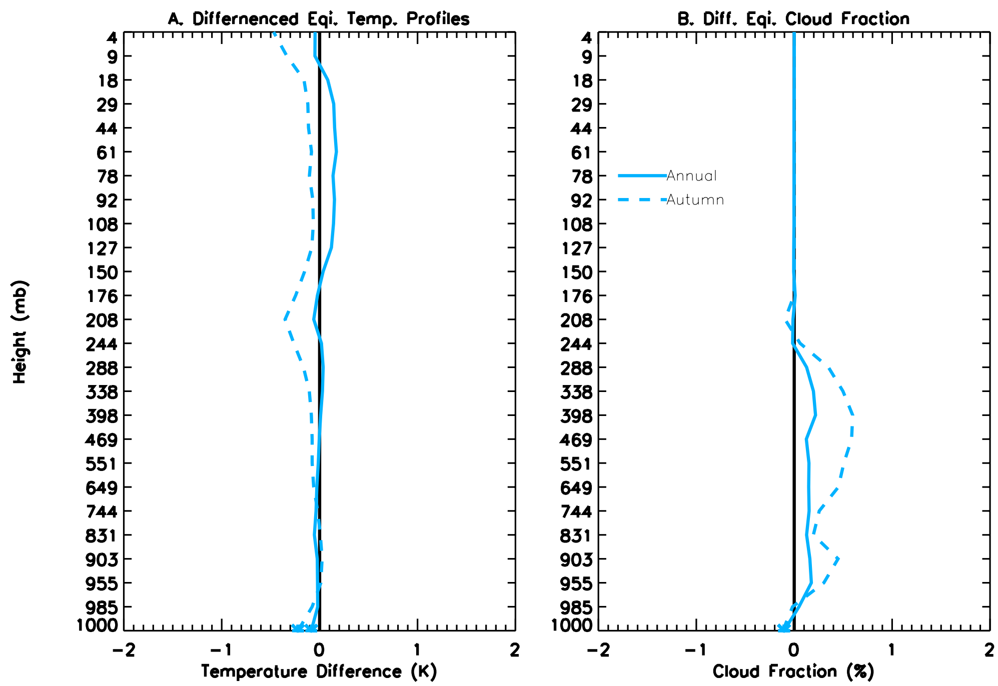

Figure 32. Differenced annual and autumn (Oct.-Nov.) mean temperature and cloud fractions for the equilibrated period of the CICE-Reanalysis bias sensitivity (last 20 of 60 years). Atmospheric layers with significant differences are denoted with asterisks.

Nevertheless, these findings indicate that the increase in snow depth, recreated here with a decrease in snow conductivity, leads to a decrease in basal ice formation, and a corresponding drop in ice volume. However, we reiterate that the inclusion of albedo may have resulted in additional modifications due to the increased albedo that would result from additional summertime snow. The inclusion of this would potentially limit the summer melt, resulting in increased ice.

III.6 Conclusion

This study has validated the model simulated on ice snow depth and density in the Arctic Ocean, and investigated the impacts of snow depth bias on thermal conduction and in turn the ice state in coupled simulations. The biases identified were dependent on model configuration, but a fully coupled ensemble simulation consistently produced excessive snow depth. In addition, the current parameterization in CICE lacks a seasonal density evolution, resulting in excessive autumn and early winter snow densities. We summarize the results of our validation in Table 8.

	Russian Drift Station Validation Results
CICE coupled (ensemble)	-CICE produces ~40% annual mean snow depth excess over thick ice. -During the summer months, this excess can exceed 150%
CICE uncoupled (stand-alone)	-CICE produces ~15% annual mean depth deficit over thick ice. -During summer/early fall, the deficit in snow depth is ~75%

Table 8. Key validation findings from comparison of CCSM and CICE-Reanalysis snow depth to *in situ* measurements of snow depth. See the text for evaluation of significance.

Following the identification of seasonally dependent snow depth biases, the sensitivity experiments modified the thermodynamic treatment of snow in CICE to compensate for the biases, as summarized in table 9. The examination of the sensitivity

Experiment	Parameter Modifications	Motivation
Control	- None, default CICE on ice snow conductivity of 0.3 W/m/K	Control simulation for direct comparison.
CCSM bias exp.: Snow & Density	-Seasonally evolving, generally higher conductivity - Red line in Fig 11. ~0.4 W/m/K	Sensitivity to biases in the coupled ensemble snow depth and density.
CICE-Reanalysis Bias: Snow & Density	- Seasonally evolving, generally lower conductivity. - Blue line in Fig. 24. ~0.2 W/m/k	Sensitivity of the ice cover to the biases found in the stand-alone depth and density of snow.

Table 9. Sensitivity experimental design and motivation.

of the ice state to these biases revealed that an increase in snow conductivity, used to compensate for excessive snow depth in our CCSM bias sensitivity experiment, results in an increase in winter basal ice growth. The effects of decreased conductivity, used to compensate for low snow depths used in the CICE-Reanalysis bias sensitivity experiment, generally have a less significant impact on the ice. Table 10 summarizes the response of the bias sensitivity experiments.

A	CCSM Bias: Snow & Density
Effect on ice	- Increased year round ice volume - Increased September ice area
Primary Mechanism	Increased snow conductivity ➔ enhanced basal ice growth
Observed Feedbacks	Neg: Increased ice thickness ➔ Increased volume lost to advection Pos: Increased ice area ➔ Decreased open water ➔ albedo feedback Pos: Increased ice area ➔ Reduced low level clouds in autumn, reduced low level temperatures ➔ Reduces long wave flux to ice

B	CICE-Reanalysis Bias: Snow & Density
Effect on ice	- Decreased year round ice volume (non-significant) - Increased September ice area
Primary Mechanism	Decreased snow conductivity ➔ inhibited basal ice growth
Observed Feedbacks	Neg: Reduced ice thickness ➔ decreased volume lost to advection

Table 10. Sensitivity experiment divergence from control run including: the observed changes in the ice, the primary controlling mechanism, and feedbacks observed to affect the state of the ice pack. A: CCSM snow depth and density bias correction, B: CICE-uncoupled snow depth and density bias.

As with the simplified snow depth sensitivity experiments in Chapter 2, an asymmetric response to changes in snow characteristics occurs. In Chapter 2, when snow was thinned the ice responded consistently, while thickening the snow triggered diverse and often minor responses. In Section III.4, an effective thinning of the snow triggered a stronger and expected response while the effective thickening of snow in Section III.5 triggered a smaller and somewhat unanticipated response. Rather than clarify the diverse responses to changes in snow depth previously identified in different modeling environments, this asymmetric response in the CCSM environment contributes to the lack of a consistent response. Taken together, these results and previous findings indicate the need for continued investigation of the role of snow cover on the Arctic sea ice.

If the response to the bias adjustments were uniform, it would be tempting to regard the snow conductivity as another tuning parameter. However, ice does not react uniformly to changes in snow conductivity. Specifically, thicker ice is less sensitive to changes in snow characteristics. This indicates that the response of the ice to snow characteristics is a complex system, and cannot simply be treated as a one-dimensional tuning parameter. In addition, the enhanced ice area resulting from an increase in conductivity leads to positive feedbacks in the form of the ice-ocean feedback and ice area – autumn cloud cover feedback.

These findings suggest that an improved understanding and treatment of the on ice snow cover would enhance the ability of CICE to generate an ice state consistent with observations. In particular, the complex relation of ice thickness and snow thickness is important in light of observations indicating changes in ice age and characteristics currently occurring in the Arctic.

We anticipate future investigations into the validity of the on ice snow cover would include a study assessing the degree to which snow redistributes among ice categories, and how this redistribution would affect the ice characteristics. The ideal *in situ* data set for such investigation would include coincident measurements of snow and ice thickness across the Arctic. In addition, such a dataset would have a high sampling rate following precipitation events, to allow for accurate parameterization of the speed of snow redistribution. Such a study would make use of more sophisticated local snow distribution models, such as SnowModel (Liston and Elder 2006) to create a new set of parameters to simplify the redistribution of snow over the sea ice. The parameterizations produced would need careful treatment to ensure mass and energy balance, and would introduce non-linear changes to conductive heat flux due to introducing ice thickness as a controlling variable with regards to snow thickness. A set of more in depth simulations investigating the importance of this process would confirm the need for a more detailed treatment of snow in future versions of CICE to better reflect the physical system. To reiterate, the preceding study used a spatially uniform conductivity modification. This approach would be inappropriate if proposed future work identified significant snow redistribution processes at play on the Arctic sea ice. The differing response of ice as a function ice thickness to changes in snow thickness implies that a spatially varying correction may not wash out in the mean.

A more in depth correction biases in other snow characteristics may also be warranted if this avenue of research were pursued. For example, including the changes in snow mass that result from correcting depth biases would increase the effect on the model by increasing thermal diffusivity. Similarly, introducing the direct effect of snow density and seasonal metamorphosis on snow thermal conductivity may have a pronounced effect.

One potential avenue to formally correcting the snow depth bias would be to immediately transfer an appropriate fraction of any precipitation to the ocean. However, this unseasonal freshwater flux to the ocean could conceivably alter the ocean stratification in undesirable ways. This possibility highlights the need to make minimal changes to the model where possible to avoid undesirable effects. Therefore, in future studies it would be more straightforward to make modifications to the snow characteristics, as in this study.

In general, we find that the snow characteristics currently produced by CCSM do not reproduce *in situ* measurements well. More importantly, the state of the sea ice has a complex reaction to correction of the thermal snow properties associated with these biases, which indicates the need for a more physical treatment of snow.

Chapter 4

IV. Projected 21st Century Decline of Snow on the Arctic Sea Ice: Causes and Implications

Abstract: Simulations using the Community Climate System Model (CCSM4) project a persistent decline of snow depth on sea ice in the Arctic Ocean. CCSM4 simulations project that the snow cover will decrease throughout the 21st century, with snow-free summer ice conditions occurring prior to the ice-free conditions projected for the 21st century. While increasing atmospheric temperature plays a role, the primary mechanism controlling snow depth is the decrease in snow accumulation due to reduced autumn ice cover. The loss of snow cover presents two potential feedback mechanisms via reduced ice albedo and increased thermal conduction through the snow–ice column. While the albedo decrease represents a positive feedback for ice loss, the role of the increased conductive heat flux results in a negative feedback of similar magnitude via increased rates of autumn and winter ice growth. Both of these processes represent a potential 10 Wm^{-2} increase in flux to the surface, indicating the need for a full understanding of the magnitude of both feedback mechanisms in any general circulation model.

IV.1 Introduction

Climate change in the Arctic has been observed in several elements of the Earth system (ACIA 2005). Most relevant to this study is the continuing decrease in ice area as the remaining ice becomes progressively younger (Stroeve et al 2007, Maslanik et al 2011). The loss is especially pronounced for the period 2007-2010, during which the four lowest recorded summer ice extent minima occurred (Perovich et al 2010). The Arctic is considered a bellwether for global climate change, with the highest sensitivity to climatic change of any region (IPCC 2007). As the observed changes in the Arctic reflect larger projected global changes for the 21st century, modeling and other communities need to understand the important processes in the Arctic region, including the potential for feedback, both positive and negative.

Of particular interest to this study is the change in precipitation in the Arctic region. A 7 % increase in Arctic river discharge has been observed from 1936-1999 (Peterson et al 2002). This increase in runoff is primarily due to increases in precipitation, which are linked to sea surface temperatures and sea-ice boundary conditions, as well as anthropogenic climate change (Kattsov and Walsh, 1999; Wu et al 2005). Despite increases in runoff and precipitation, observations on the Arctic land surface indicate snow cover has been decreasing (Brown et al 2010). Past trends in precipitation are expected to continue into the 21st century (Cassano et al 2007), with increased precipitation over the Arctic Ocean resulting in part from decreased ice area (Higgins and Cassano, 2009; Finnis et al 2007). A recent publication using the same model ensemble as this study found a 50%-70% increase in precipitation over the 21st century during the autumn months of October and November (Vavrus et al 2011).

During the ice growth season, snow cover serves to delay the growth of ice due to its low thermal conductivity (Sturm et al 2002), (Massom et al 2001). On freshwater ice, this effect is observed to create ice thickness gradients anti-correlated with observed snow thickness gradients (Sturm and Liston 2003). While snow cover reduces winter ice growth, the presence of snow in the summer serves to increase the surface albedo, reducing absorbed short wave radiation (Perovich 1998). In addition to radiative and thermodynamic impacts of "on-ice" snow cover, there are implications for the large fauna native to the Arctic ice. In particular, projected decreases in on-ice snow cover in previous versions of CCSM are implicated in decreased habitat with sufficient snow depth for the formation of sub-nivean lairs, with implications both for ringed seals and their primary predators, polar bears (Kelly and Bitz 2010)

Previous versions of the Community Climate System Model (CCSM) have been used in climate change studies, especially the Coupled Model Intercomparison Project (CMIP3), in which CCSM3 participated. In a more recent assessment of CCSM4, the model was found to simulate the general climate and Arctic state in the 20th Century reasonably well (Gent et al 2011, de Boer et al, 2012; Jahn et al., 2012).

In addition to these model performance surveys, a recent publication reported the 21st century response of the Arctic region in CCSM4 (Vavrus et al 2012). In this recent report, the authors outlined the general decline of snow pack on the ice, and indicated the likely causes as well as potential effects on the ice pack. This study is intended to more thoroughly explain the changes in the Arctic climate leading to decreasing snow cover on the Arctic ice. In addition, an effort is made to better demonstrate the importance of changing snow depth on ice thermal and radiative processes.

This paper focuses on the projected changes in on-ice snow cover under the strongest greenhouse forcing scenario as outlined by the Representative Concentration Pathways (RCPs) included in the current Coupled Model Intercomparison Project (CMIP5). This high-end forcing, RCP8.5, is defined by the 8.5 W/m^2 radiative forcing anomaly at the end of the 21st century. This change in radiative forcing is controlled primarily by an atmospheric CO2 concentration in excess of 900 ppm by the end of the 21st century (Moss et al. 2008). This study makes use of the strongest greenhouse gasforcing scenario for two reasons. First, this allows for consistent comparison to the projected changes in the Arctic climate and ice state described in Vavrus et al. Second, using the strongest anthropogenic forcing scenario provides the most significant change in the Arctic, allowing for ease of comparison between the late 20th century and the projected 21st century changes.

Section IV.2 more thoroughly describes CCSM4, and discusses the performance of CCSM4 in producing an accurate Arctic climate. Section IV.3 reports the changes in Arctic on-ice snow depth projected for the 21st century. Section IV.4 discusses the changes in the Arctic climate controlling snow cover. Section IV.5 demonstrates the implications of the 21st century snow cover with regards to feedback with the ice cover itself, including estimation of the magnitude of potential feedbacks. Finally, Section IV.6 offers concluding thoughts on the importance of accurate prediction of snow cover above the Arctic sea ice.

IV.2 Model Description and Performance

This study makes use of an ensemble of 21st century simulations generated using CCSM4. CCSM4 includes improvements to all component models of the CCSM3 configuration. The land model utilized by CCSM4 is the Community Land Model (CLM). Recent improvements to CLM are discussed in Lawrence et al 2010. The ocean model component is the Parallel Ocean Program version 2 (POP2) and is discussed in depth in Danabasoglu et al (2011). The atmospheric component model is the Community Atmosphere Model, version 4 (CAM4). CAM4 makes use of the Lin-Rood finite volume dynamical core (Lin, 2004) with 1degree resolution and 26 vertical levels. CCSM4 improvements include a 'freeze-dry' parameterization introduced to better describe low-level Arctic clouds (Vavrus and Waliser, 2008). In addition, this version of CAM includes improvements to the deep convection treatment (Richter and Rasch, 2008; Neale et al., 2008). CCSM4 uses the Community Ice CodE (CICE4.0) to simulate sea ice. CICE has been updated to include a shortwave energy transfer scheme with a melt pond parameterization and surface aerosol treatment (Hunke and Lipscomb 2010). Recent improvements to CICE are discussed in Holland et al (2011).

An in depth discussion of CCSM4's 20th century performance in the Arctic is available in two recent publications, with deBoer et al (2012) discussing the atmospheric simulation, and Jahn et al (2012) discussing the ice conditions. By way of summary, these authors find CCSM4 to capture the majority of sea ice characteristics, including concentration, extent, thickness, and ice age. Also important, the observed trend of decreasing September ice extent falls within the range of CCSM4 ensemble members. A caveat to the accurate performance of CCSM4 is the weak Beaufort gyre produced by CCSM4 (Barry 1989). When compared to the ERA40, the surface temperatures are too cold, on the order of 1-2K. The Sea Level Pressure (SLP) produced by CCSM4 is also too low. While during the spring and autumn the Beaufort high is under-simulated, other features such as the Siberian high are reasonably well represented. In addition, cloud cover is too low, especially in the winter months. However, the radiative energy budget is compensated in the form of excessive liquid water in clouds, resulting in increased long wave energy flux to the surface. Especially important for this study is the generation of excess precipitation on the order of 100% in the high latitudes. This excess in precipitation results in corresponding excesses in snow depth on the Arctic sea ice, see Chapter 3.

Due to the 21st century emphasis of this study, we summarize the basin wide changes projected for the 21st century as reported in Vavrus et al (2012). In the RCP8.5 simulations, the majority of the Arctic above 70N remains ice covered until around 2040 when the mean ice pack decreases to an annual mean of about 30% by the end of the century. In CCSM4, ice-free summer conditions (defined here as less than 10^6 km^2 ice area) occur around 2070. Figure 33, reproduced from Vavrus et al (2012), documents the 21st century evolution of the annual mean Arctic ice cover. In addition to changes in ice

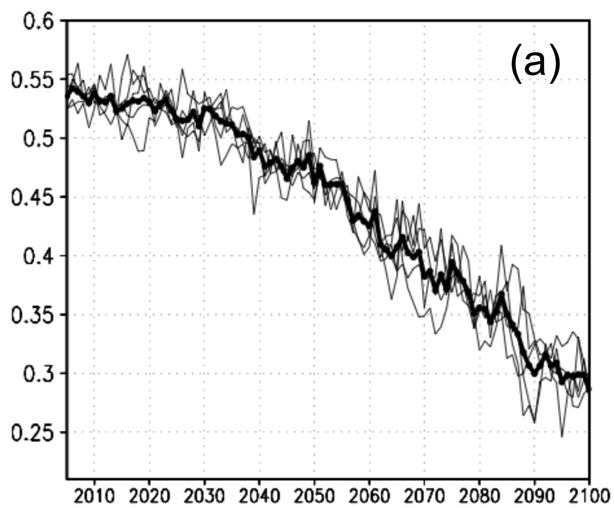

Figure 33. Time series of annual mean Arctic average ice concentration (fraction of ocean area 70N poleward covered with ice) as simulated in each ensemble member (thin lines) and the ensemble mean (thick line). (Plot reproduced from Vavrus et al 2011).

cover, an increase in annual mean near surface temperatures of 8K occurs from 2005-2100, with the largest changes occurring in the late autumn and winter months. Total annual mean cloud cover also increases on the order of 25%, with the increases primarily occurring in low cloud cover. This triggers a corresponding increase in total yearly precipitation of 25%-35%, which is of particular importance to this study.

IV.3 21st Century Simulated Changes to Snow Cover

Over the 21st century, the CCSM4 ensemble simulations project significant decreases in the depth and mass of snow cover on the Arctic sea ice. Figure 34a reports the changes in annual mean snow depth over the course of the 21st century. In particular, the late 20th century (1980-2000) annual mean depth of 17-23 cm decreases to 12-15 cm mid-century (2030-2050) and to 5-7 cm by late century (2080-2100). These significant ($P<0.05$) changes represent a 32% and 69% decrease, respectively. Figure 34b reports the basin wide nature of the 21st century thinning of the Arctic on-ice snow cover. Figure 34b includes contours of ice concentration, the fraction of a model grid cell with ice cover.

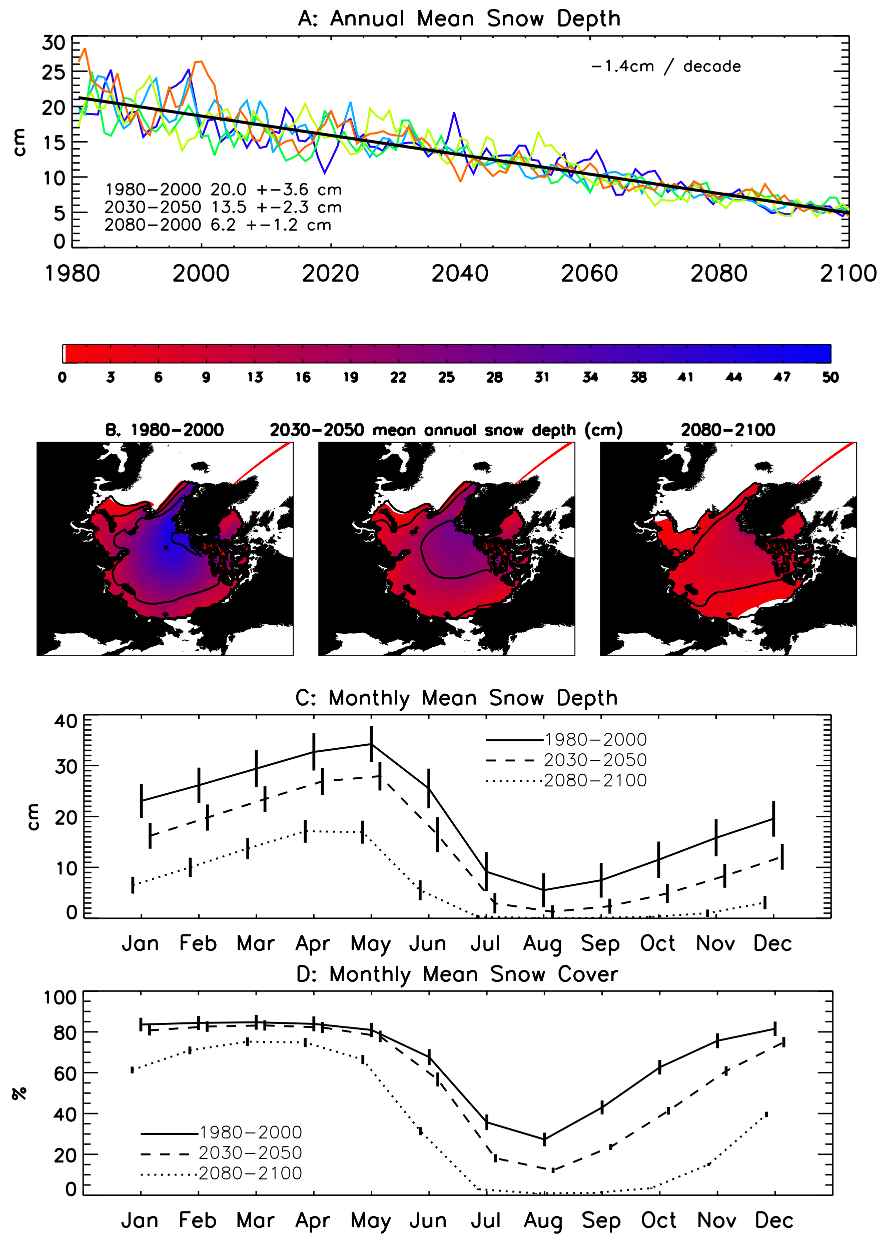

Figure 34. Late 20th century hindcast and projected 21st century changes in the Arctic Ocean snow cover. Panel A: Annual mean snow depths for the period 1980-2100 for each ensemble member (thin colored lines) and the 1980-2000 trend (thick black line). Panel B: Annual mean snow depth in cm (given by the color bar) for 1980-2000, 2030-2050, and 2080-2100). Solid contours indicate the annual mean 90%, 50%, and 15% ice concentrations (no 90% contour exists for the period 2080-2100). Panel C: Monthly mean on-ice snow depth where ice exceeds 15% concentration for 1980-2000 (solid line) 2030-2050 (dashed line) and 2080-2100 (dotted line). Panel D: Monthly mean on-ice snow cover where ice exceeds 15% concentration for 1980-2000 (solid line) 2030-2050 (dashed line) and 2080-2100 (dotted line).

Figure 34c and Fig. 34d demonstrate the seasonal changes in snow depth and cover. Figure 34c shows that pronounced snow depth loss occurs in most months by mid 21st century, and year round by late 21st century. Note that prior to the near complete disappearance of the underlying sea ice there is still some summer ice cover surviving by mid-century (Vavrus et al 2012). However, by mid-century, the majority of snow cover is melted during the summer months. This is made clear in Fig. 34d, which documents that the nearly snow free summer conditions occur by mid-century, when the change in annual mean snow cover has only dropped 14% ($P<0.05$). By late 21st century, the annual mean fraction of snow covered ice has dropped by 45% since the late 20th century. Note that the changes in snow cover are pronounced in the summer and early autumn, when the ice is still exposed to incoming short wave radiation, and the higher albedo of snow may serve to reduce the short wave energy absorbed by the ice. This drop in snow cover and corresponding drop in ice surface albdeo is a potential positive feedback mechanism to continued ice loss, which is discussed later in this study. To bring context to these changes, it is important to note that the simulated 20th century summer snow depths are nearly twice the observed snow depths, see Chapter 3.

Figure 35 reports the distribution of annual mean snow depth, defined as the probability of a grid cell above 70N with greater than 15% ice area having snow of a given thickness. Figure 35 shows the shift from thick snow pack with a high variability

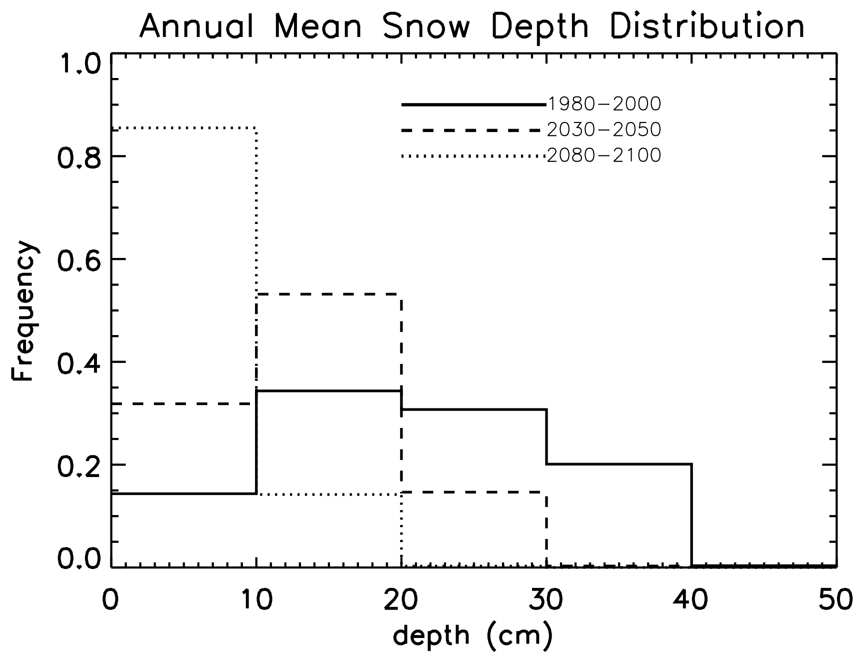

Figure 35. Annual mean snow depth distribution (cm) for 1980-2000 (solid line), 2030-2050 (dashed line) and 2080-2100 (dotted line).

during the late 20th century to a progressively thinning snow pack over the 21st century. The restriction to 15% ice fraction results in slightly deeper snow than in Figure 34a. During the late 20th century ice is overlain by 26+-12cm of snow. By mid century this decreases to 17+-7cm, and drops to 9+-4cm by late century.

The discussion to this point has centered on snow depth, CCSM4 projects corresponding decreases to the maximum annual snow mass on the Arctic sea ice, shown in Fig. 36a. This significant ($P<0.05$) decrease in total snow mass persists throughout the 21st century, from 11-13 x 10^{14} kg in the late 20th century to 8-10 x 10^{14} kg mid 21st century, with maximum masses of 5-7 x 10^{14} kg by late 21st century.

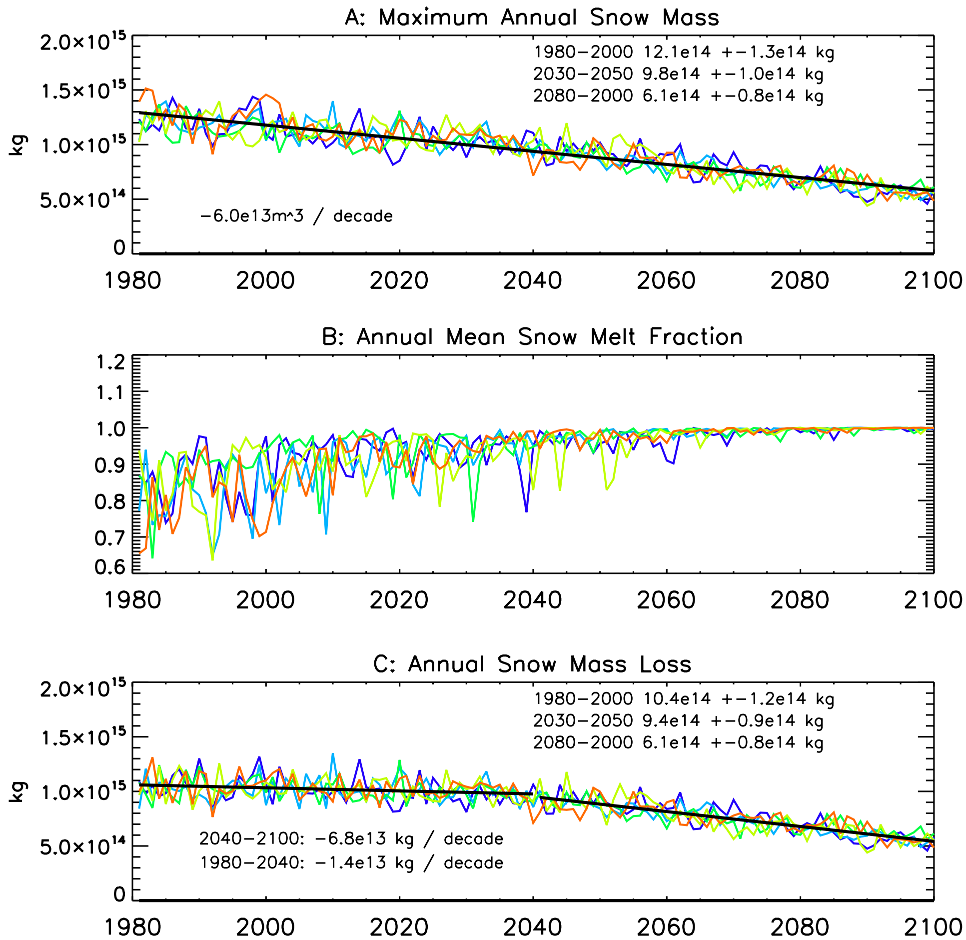

Figure 36. Panel A: Maximum total snow mass over the Arctic sea ice. Thin colored lines indicate individual ensemble members, solid lines indicate inter-ensemble trend for the period 1980-2100. Panel B: Fraction of on-ice snow which is lost during melt season for all ensemble members. Panel C: Mass of snow lost in each ensemble member (thin lines). Thick lines indicate linear fits for the period 1980-2040 and the period 2040-2100. Mid-century delineates the change from persistent on-ice snow cover to complete snowmelt.

Figure 36b reports the fraction of the annual maximum snow mass lost by the end of the melt season. During the period 1980-2000 approximately 15% of the snow mass survives the summer melt. This can be compared to the climatology of Warren at al (1999), which reported that some snow does survive the summer months. However, note that the Warren climatology used mid- to late 20th century snow measurements located on thicker ice floes. Even so, the 20th century on ice snow depths produced by CCSM are generally much too high in the summer, see Chapter 3. Regardless of the initial validity, the fraction of snow surviving the summer decreases through the 21st century, with complete summer snow melt becoming regular by mid-century and the norm by the late 21st century. The changes in melt fraction from early 20th to mid 21st and late 21st century are both significant ($P<0.05$). Note that while the definition of 'ice free' conditions allows for some nominal ice cover in the Arctic, this is a completely snow free state by late 21st century.

The final panel, Fig. 36c, reports the difference between the annual maximum snow mass and the annual minimum snow mass. This is equivalent to the amount of snow mass lost to melt or other processes, neglecting additional accumulation and concurrent loss. In the hindcast period, 9-12x10^{14} kg of the maximum snow is melted. The overlap between the range of snow mass lost and maximum snow mass indicates the occasional snow free summer as seen in Fig. 36b, but most summers experience some snow surviving throughout the melt season during this time period. By mid-century, persistent snow cover has become anomalous, with 8-10x10^{14} kg lost annually. This continues into late century, when all or the vast majority of the 5-7 x 10^{14} kg of snow is lost. Both the mid- and late 21st century decreases in lost snow are significant to $P<0.05$. Due to the switch from persistent snow cover to entirely snow-free ice around mid-century, the trend in annual snow loss is better represented by two fits (See Fig. 36c). The first trend of -1.4 x 10^{13} kg per decade matches the period during which some snow persists throughout the melt season (1980-2040). During this period, there is 0.76 correlation between the maximum annual snow mass and the annual snow mass loss in a given ensemble member. Once the snowpack becomes entirely seasonal (2040-2100), the annual mass of snow lost decreases at -6.8 x 10^{13} kg per decade, which corresponds well to the decadal decrease in the maximum annual snow mass -6.0 x 10^{13} kg for the period 1980-2100. This corresponding decrease is confirmed by a 0.99 correlation between maximum annual snow mass and annual snow mass melt during the period 2040-2100. This confirms that by mid-century in the majority of summers all of the snow is lost from the ice. The almost perfect correlation occurs because the entirety of the snow mass is lost, making these two values the same for any given year.

In general, the snow cover on the Arctic sea ice decreases throughout the 21st century. Completely snow-free ice cover commences before the onset of near ice-free conditions.

IV.4 Causal Mechanisms for Changes to 21st Century Snow Cover

While the direct effects of a warming Arctic climate, such as increased surface temperatures, play a role on the decrease in Arctic on-ice snow, the reduced ice cover through the year is the dominant mechanism by which the snow depth decreases. As a result of decreasing ice cover, in particular during the autumn months, there is a reduction in the amount of snow that can be accumulated. This occurs despite projected increases in total Arctic precipitation.

First, Fig. 37a demonstrates that the total mass of snow precipitated annually poleward of 70N does not increase appreciably. Instead, the increase in total precipitation projected to occur over the 21st century is dominated by an increase in rain

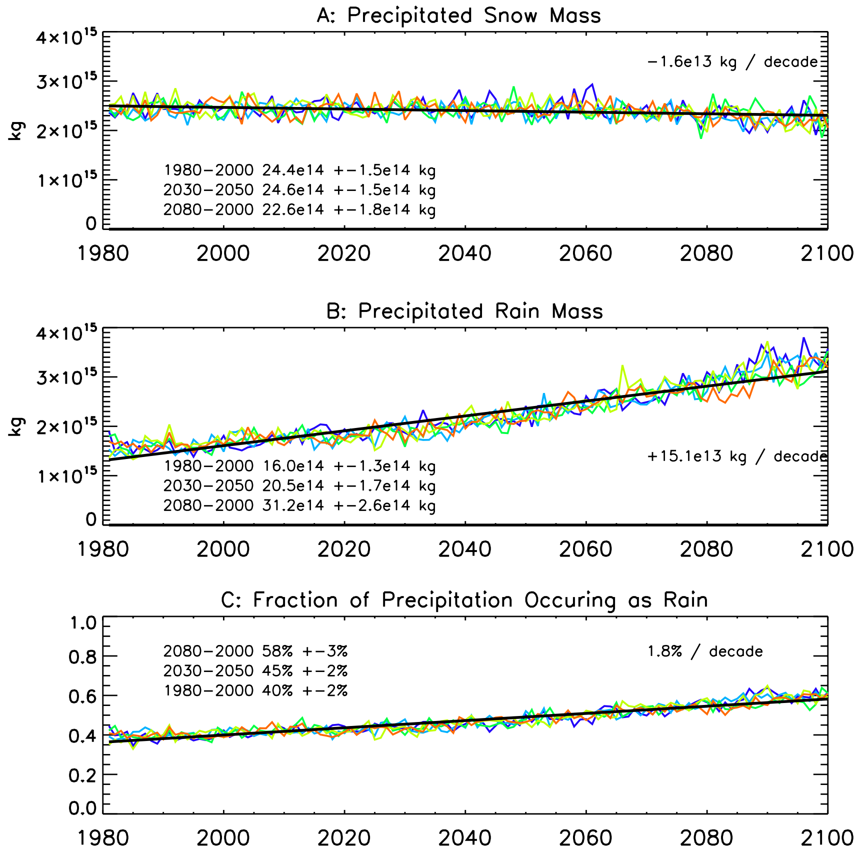

Figure 37. Panel A: Total annual snow mass precipitated. Thin colored lines indicate individual ensemble members, solid lines indicate inter-ensemble trend for the period 1980-2100. Panel B: Total annual mass precipitated as rain. Thin colored lines indicate individual ensemble members, solid lines indicate inter-ensemble trend for the period 1980-2100. Panel C: Fraction of total precipitation occurring as rain. Thin colored lines indicate individual ensemble members, solid lines indicate inter-ensemble trend for the period 1980-2100.

fall, which nearly doubles from 16.0×10^{14} kg +- 1.3×10^{14} kg to 31.2×10^{14} kg +- 2.6×10^{14} kg from the late 20th century to late 21st century, see Fig. 37b. Both the mid- and late 21st total annual precipitation as rain are statistically different from the total annual precipitation as rain in the late 20th century ($P<0.05$). As a result, the ratio of rain to snow nearly reverses, with snow accounting for 60% of the precipitated mass in the late 20th century, but only 42% by late 21st century (also significant to $P<0.05$).

However, due to the seasonal pattern in ice cover, the ice does not experience the same precipitation as the Arctic Ocean where ice is absent. Figure 38 reports the precipitation accumulated by the ice cover. Note that rain 'accumulated' on the ice is immediately transferred to the ocean. As such this definition of accumulation is more accurately described as impacting the surface, but the term accumulation is used for simplicity and consistency. Both the snow and rain mass accumulated decrease significantly over the course of the 21st century from 18.0×10^{14} kg +-1.3×10^{14} kg to

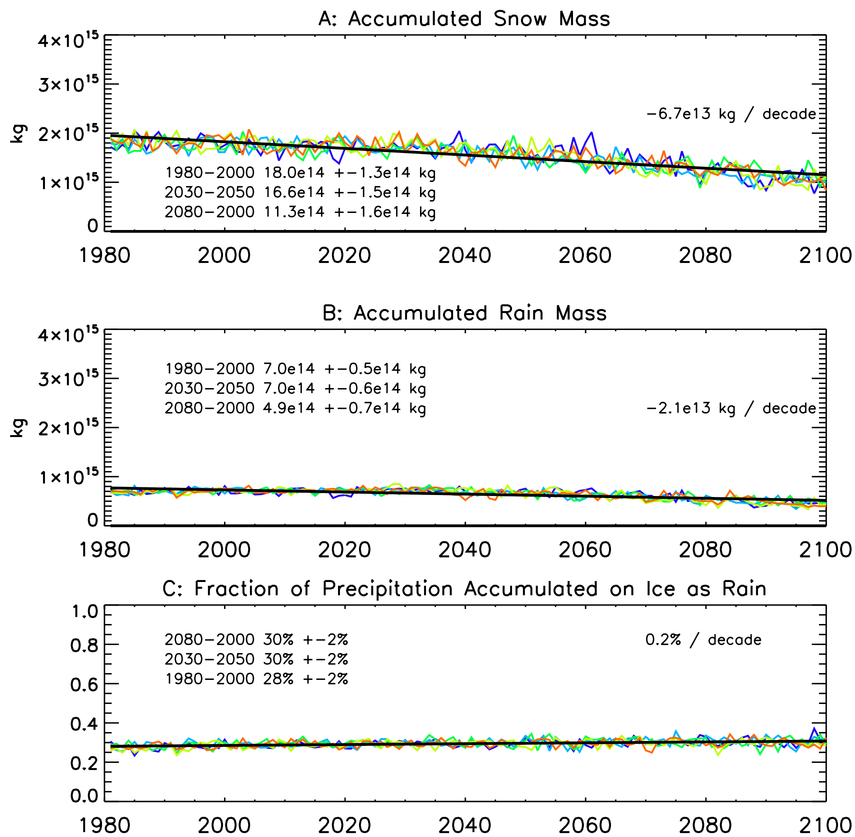

Figure 38. Panel A: Total annual snow mass accumulated on the ice cover. Thin colored lines indicate individual ensemble members, solid lines indicate inter-ensemble trend for the period 1980-2100. Panel B: Total annual mass of rain accumulated on the ice cover. Thin colored lines indicate individual ensemble members, solid lines indicate inter-ensemble trend for the period 1980-2100. Panel C: Fraction of total accumulated precipitation occurring as rain. Thin colored lines indicate individual ensemble members, solid lines indicate inter-ensemble trend for the period 1980-2100.

$11.3x10^{14}$ kg +-$1.6x10^{14}$ kg for snow and $7.0x10^{14}$ kg +-$0.5x10^{14}$ kg to $4.9x10^{14}$ kg +-$0.7x10^{14}$ kg for rain (see Fig. 38a and Fig. 38b). The fraction of on-ice precipitation occurring as rain does increase significantly over the 21st century, but only by 2% of the total, see Fig. 38c.

Figures 39 and 40 clarify the mechanism responsible for the decreasing accumulation of rain and snow on the ice despite increased total precipitation. In Fig.39a and Fig. 40a, the decreasing fraction of total precipitation accumulated (both rain and snow) is clearly dominated by the summer and early autumn months. For example, in Fig. 40a the snowfall in the month of October between the late 20th and mid-21st century periods is similar. However, there is significantly ($P<0.05$) less snow accumulated by mid-century. In Figs. 39b and 40b, the causal mechanism is more clearly outlined by comparing the fraction of precipitated snow that accumulates on the ice with the total ice area in the Arctic. Because some of the ice present in the late 20th century is 'missing' by mid 21st century, the precipitation lands in the ocean and does not accumulate. This is unsurprising considering decreased ice area leads to increased precipitation (Higgins and Cassano 2009), so the months when the greatest increases in precipitation are projected over the 21st century (Vavrus et al 2011) are the same months with exceptionally low ice cover.

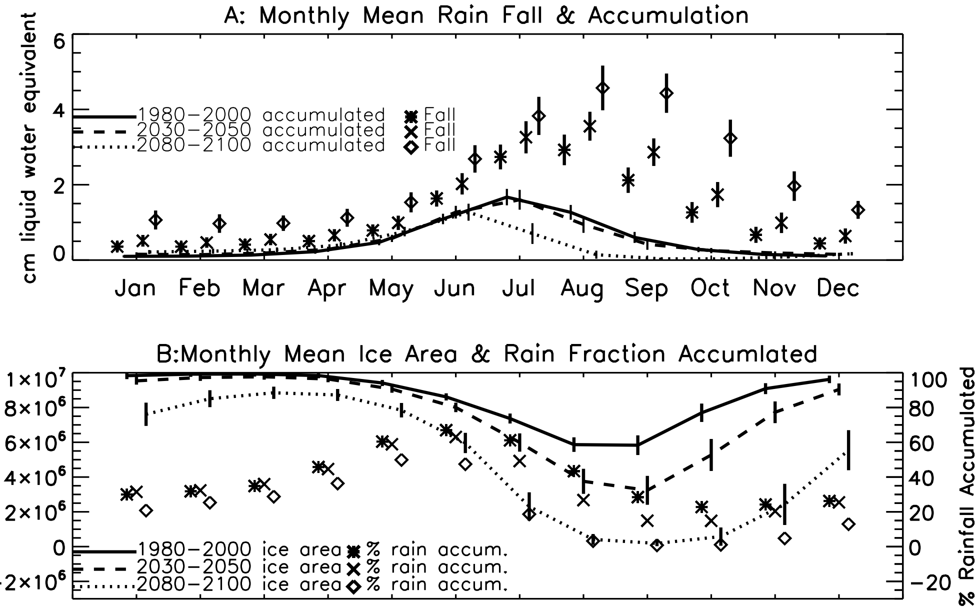

Figure 39. Panel A: Monthly mean rainfall and on-ice accumulation rates for the periods 1980-2000 (asterisk and solid lines), 2030-2050 (crosses and dashed lines) and 2080-2100 (diamond and dotted lines). Panel B: Monthly mean ice area poleward of 70N (lines) and fraction of the precipitated rainfall accumulated on the ice cover (symbols) for three time periods.

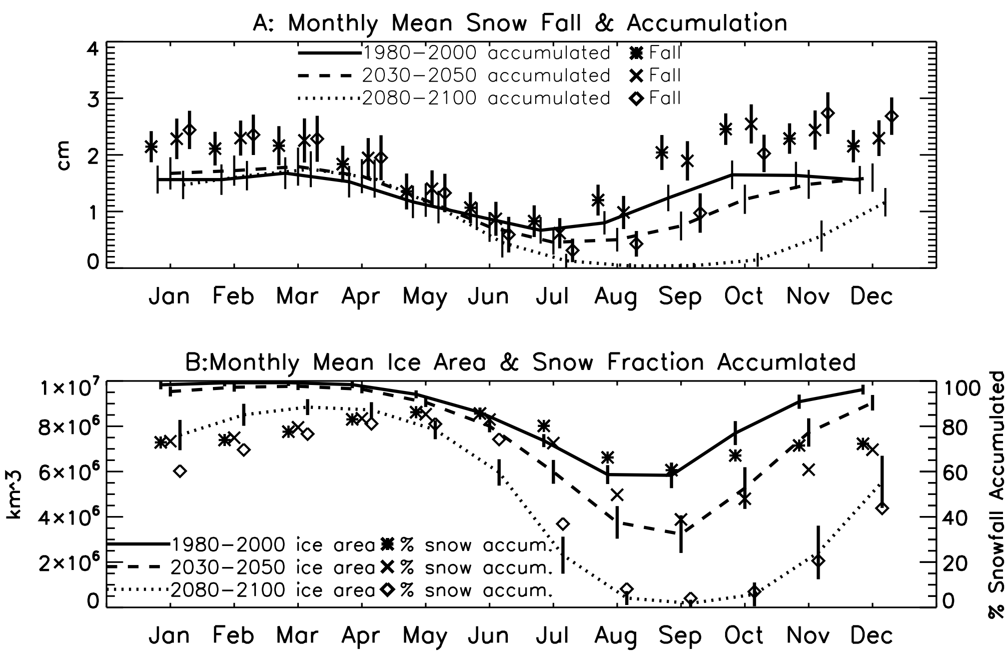

Figure 40. Panel A: Monthly mean liquid water equivalent snowfall and on-ice accumulation rates for the periods 1980-2000 (asterisk and solid lines), 2030-2050 (crosses and dashed lines) and 2080-2100 (diamond and dotted lines). Panel B: Monthly mean ice area poleward of 70N (lines) and fraction of the precipitated snowfall (liquid water equivalent) accumulated on the ice cover (symbols) for three time periods.

This 'missing ice' effect becomes pronounced by late century, when there is usually no ice during the early autumn. While a repartitioning of precipitation from solid to liquid phase does occur, see Fig. 37c, the entire or nearly entire absence of ice cover during the months when rain occurs makes this largely irrelevant, see Fig. 38c and Fig. 39. However, as the precipitation transitions back to snow in the autumn, the ice is still absent, and after it forms lacks the snow cover currently accumulated during this period.

Figure 41 reproduces Fig. 38a in combination with two ratios to document the relative role of accumulated on-ice snow throughout the simulation period. Figure 41b reports the ratio between total snow accumulated per annum and the annual maximum

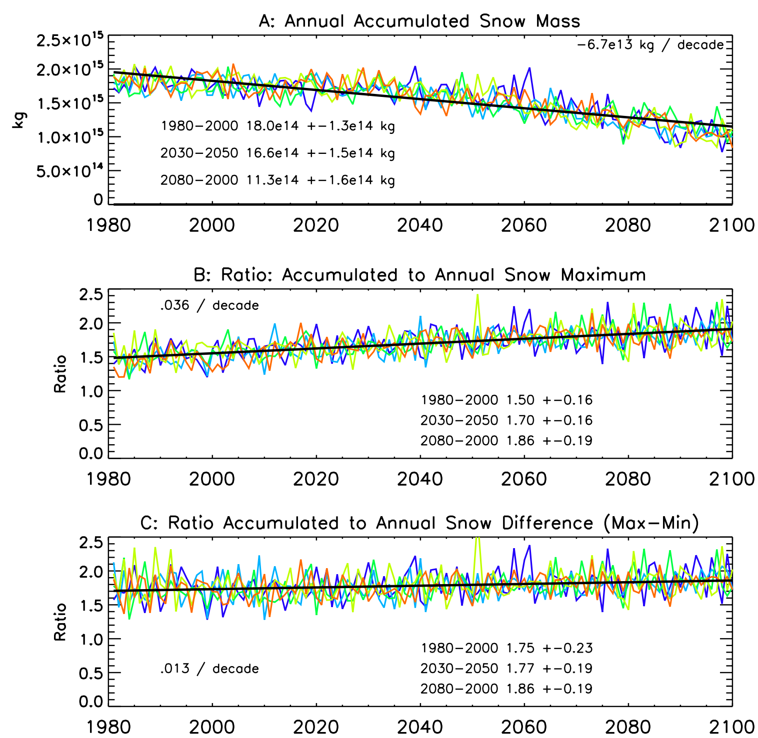

Figure 41. Panel A: Annual snow mass (kg) accumulated in all ensemble members (colored lines) and the linear trend for the period 1980-2000 (solid black line). Panel B: Ratio of snow mass accumulated to annual snow maximum. Panel C: The ratio of snow mass accumulated on the ice to the intra-annual increase in snow depth (fall/winter snow pack).

snow depth. This ratio increases from 1.50 +- 0.16 to 1.86 +- 0.19 from late 20th to late 21st century. This significant increase is unsurprising considering the annual cycle in snow depth changes from one in which some snow persists in late 20th century to a cycle in which all of the snow accumulated is lost by the end of the melt season, effectively resetting the snow budget each year. The ratio between the snow accumulated per annum and the difference between the annual maximum snow volume and annual minimum snow volume also increases significantly from 1.50 +-0.23 to 1.86 +-0.19. While this change is significant, the change in this ratio by mid 21st century reported in Fig. 41b is not. The increase in this ratio indicates more loss occurring during accumulation, making it more difficult for the accumulation to 'stick', effectively requiring 24% more accumulation to achieve a given snow depth. This is smaller than the 37% decrease in accumulation from late 20th century to late 21st century.

While changes in precipitation and accumulation play a role in determining the snow depth on the Arctic ice, the annual loss of snow to melt and other processes also play an important role. There are four mechanisms in CCSM that act as sinks for snow mass. The most obvious is loss to melt. In CICE when the ice is deformed due to stress, 50% of the snow on the ice is transported to the ocean, making deformation (of ice) the second sink. Another physical mechanism to snow loss occurs when the mass of the snow cover exceeds the buoyant force produced by the density difference between the sea ice and the underlying ocean. When this occurs the ice surface is flooded, and snow is quickly converted into ice until hydrostatic equilibrium is restored. The final sink is the advection of ice from the study region. When ice cover is transported south of 70N, it is no longer in the region considered the Arctic Ocean for purposes of this study, and as such any on-ice snow is lost. Potentially, advection of ice into the study region presents a source, rather than a sink, of snow mass to the Arctic Ocean. However, the total mass lost or gained via ice advection and the mass loss to snow to ice conversion were generally found to be nominal relative to the other sinks. While these are included in the following figure, the discussion will be limited primarily to snow melt and snow loss due to ice deformation.

Figure 42 reiterates the repartitioning of precipitation and documents the changes in precipitation sinks over the 21st century. As previously documented, the increase in precipitation over the 21st century occurs as rain, while an increasing fraction of the snowfall is lost to the ocean. As Fig 42 shows, the accumulated snow accounts for 44% of the precipitation in late 20th century, but only 21% by late 21st. This means that the snow available for loss drops from 18.0x10^{14} kg +-1.3x10^{14} kg to 11.3x10^{14} kg +-1.6x10^{14} kg. As a result, the absolute values of the sinks generally decrease. For

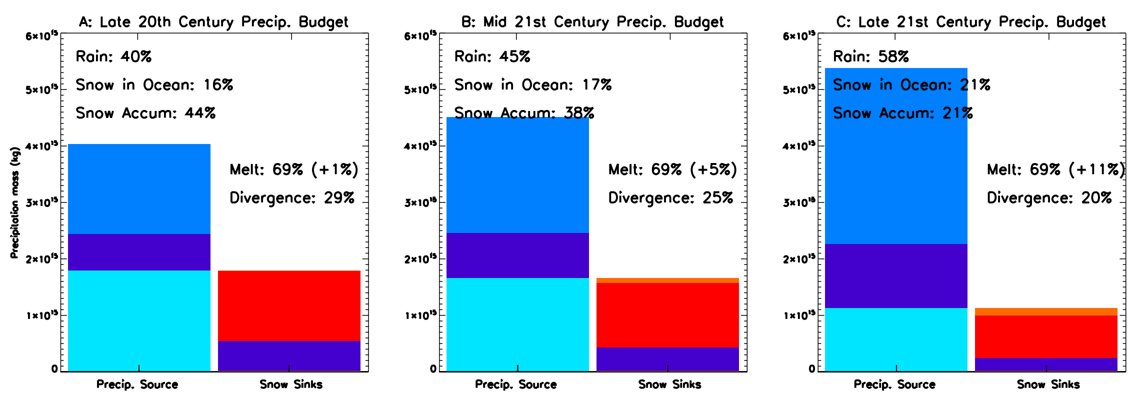

Figure 42. Comparison of precipitation partitioning and sinks. Panel A is late 20th century (1980-2000), panel B is mid 21st century (2030-2050), and panel C is late 21st century (2080-2100). At left is the precipitation partitioning. Lightest blue is accumulated snow, darkest blue is snow lost to the ocean. Middle blue is rain. At right are the sinks of snow after accumulation. Dark blue is lost to the ocean through ice deformation. Dark red and orange are the loss to melt, see text for the distinction. Loss to advection and snow to ice conversion are included but are not visible.

example, on the left side of figures 42a-c the mass of snow lost to melt drops from 12.4×10^{14} kg +-1.1×10^{14} kg in late 20th century to 7.6×10^{14} kg +-1.0×10^{14} kg in late 21st century. However, this remains a relatively consistent 69% of the accumulated snow. Divergence also decreases in absolute terms, from 5.3×10^{14} kg +-0.7×10^{14} kg in late 20th century to 2.3×10^{14} kg +-0.4×10^{14} kg in late 21st century but also decreases relative to the accumulated snow mass, from 29% to 20%. While advection and snow to ice conversion are both present in these figures, together they account for less than 1% of the snow mass lost and are not further discussed.

However, these terms lead to a shortfall, where the total snow mass lost is less than the snow accumulated, despite complete summer snow loss by late century. This is due to the method used to calculate these values. More specifically, while CCSM is capable of outputting daily history files, the ensemble of simulations used would generate a prohibitively large output in this configuration; as such, monthly history files are used. This monthly averaging results in a snow melt bias.

To understand the source of the bias, consider the following simplified scenario: at the beginning of June there a grid cell of $1km^2$ is completely covered (100%) with ice and uniform 10cm snow. All of the snow is melted in the first two weeks and then 50% of the ice is melted in the following two weeks. The mass of snow lost to melt is a function of: the thickness of snow melted, Δh_{snow}, the average area of ice present, $\overline{a_{ice}}$, and the density of snow, ρ_{snow} as in equation 5. Δh_{snow} is be 10cm, ρ_{snow} is defined as

$$m_{snow} = \frac{\rho_{snow} \Delta h_{snow}}{\overline{a_{ice}}} \qquad (5)$$

330kg/m^3. Physically, this was lost over 1.0 km^2, however due to the monthly mean nature of $\overline{a_{ice}}$, the value used will be somewhat lower, .875 km^2. As a result, the mass of snowmelt calculated from monthly means is 2.9x10^{7}kg, while the amount actually lost is 3.3x10^{7}kg. As a result the mass of snow lost to melt would be underestimated by 13%.

In general snowmelt occurs prior to the loss of the ice, especially where surface ice melt is considered. As such, the lost snow thickness is loaded more heavily towards the beginning of a given month when the highest ice area in that month occurs. While errors can occur in other sinks of snow mass due to monthly averaging, the mechanism at play in the summer months preferentially causes low biases in the snow mass lost to melt. In other times of the year, this error is less likely to favor underestimation of a sink, and as such will not generate systemic biases. For this reason, we assign the missing budget term to melt. In Fig. 42 this is shown by the orange bar, and is added to melt in parentheses. The increase in this effect over the 21st century is intuitive; thin ice in this warm climate is more likely to loose snow cover early in a given month followed by pronounced reductions in ice area, increasing the role of this effect. Earlier in the model period, the ice takes longer to melt after the snow is removed. As such, the missing budget term increases from 1% in late 20th century to 11% in late 21st century, see orange bar in Fig 42.

When this term is added to the melt mass, the fraction of snow lost to melt increases from 70% in late 20th century to 80% in late 21st century. After this correction, snowmelt becomes a stronger sink for snow mass than the other sinks, especially deformation. While the physical characteristics of the ice change in such a way that it would be unwise to assume the rate of ice deformation is unchanged, the processes effecting snow melt are more direct, and trigger a clear enhancement in melt.

With regards to the physical and thermodynamic mechanisms controlling snow depth on the Arctic sea ice, the snow mass budget indicates that the loss in ice area in the early autumn results in snowfall events 'missing' the ice. As this occurs, the total mass melted actually decreases, while the ratio of annual snow mass melted to annual snow mass maximum increases. A corresponding increase in the ratio between annual snow mass accumulated and annual maximum snow mass also occurs, indicating the snow cover is generally more easily lost. Indeed, by late century, all of the snow is lost from one season before the accumulation occurs in the next. The amount of snow accumulated decreases due to a lack of autumn ice cover, resulting in reduced snow depth and mass. Due to the decreasing snow mass available, the impact of sinks to snow mass decreases. However, the fraction of the accumulated snow lost to melt does increase relative to other sinks to snow mass.

Potentially, the enhanced relative snow melt would result in earlier snow-free conditions, which would contribute to the potential feedback mechanisms discussed next in Section 5. Figure 43 explores this effect. When considering the snow depth melted in the basin-wide average, the annual maximum snow depth generally occurs in May, although the maximum shifts to April in some years by late 21st century. During the late 20th and mid-21st century, 0.0-0.1 cm of snow are lost in May, but by late 21st 0.0-0.9 cm of snow are lost, a significant change. This leads to a higher loss of snow depth by June, with the 6.2-11.2 cm loss in late 20th century increasing significantly to 9.0-14.0 cm by mid 21st century and 9.8-13.8cm by late 21st century. However, by July, the cumulative

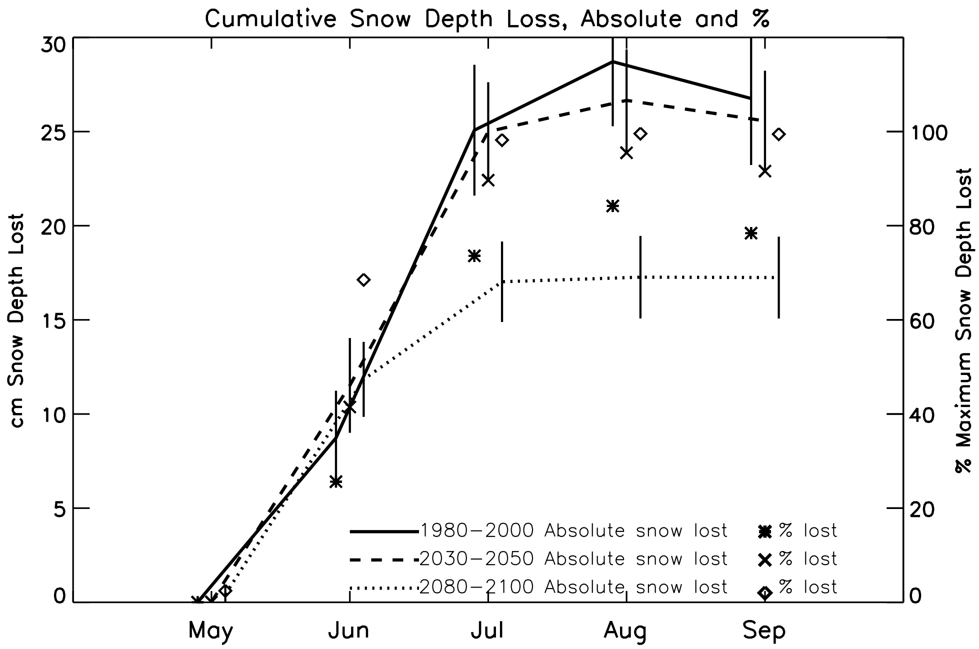

Figure 43. Seasonal spring and summer snow loss patterns for late 20th century, mid-21st century and late 21st century. Lines indicate absolute loss in basin wide mean depth lost, symbols indicate fraction of total basin wide mean snow depth lost.

annual snow loss of 21.6-28.6 cm in late 20th century is significantly greater than the 15.1-19.5 cm loss by late 21st century. This occurs because during the latter part of the 21st century all of the snow is lost by July (see Fig. 43). While the snow is lost more quickly in the spring and summer, this effect merely enhances the effect of the lower initial snow depth. The combination of these effects results in early low snow cover conditions on an annual scale, and indeed causes completely snow free summer conditions by late 21st century earlier than minimum snow depth is reached in late 20th century melt season. As such, shifting summer albedos offer a potential feedback mechanism with regards to ice conditions and snow cover. In the next Section, we investigate the strength of this feedback.

Overall, the snow mass budget and seasonal pattern of snow loss indicate that while melt does increase relative to available snow mass, this is secondary to the lower annual snow mass accumulation.

IV.5 Implications of Changes in 21st Century Snow Cover

As mentioned previously, snow cover plays competing thermodynamic and radiative roles in the winter and in the summer. In the winter, the decreased snow thickness projected for the 21st century has been found to result in increased conductive flux through the sea ice, in turn yielding increased basal ice growth (Powell et al 2005). In the summer, the decreased snow coverage will lead to decreased albedo, due to the higher albedo of snow relative to ice. This should lead to increased short wave radiation absorption and, in turn, surface melt. These effects compete regardless of the time period over which CCSM4 simulations are run. The strengths of these effects are important and warrant investigation in the CCSM environment; however, such an investigation is beyond the scope of this study.

Instead, this study will assess the relative strength of the changes in these feedback mechanisms. Ideally, this investigation would manipulate CICE to simulate the radiative and thermodynamic contributions of late 20th century snow on the ice state throughout the 21st century. Due to resource constraints, this investigation will instead make use of an analytic solution to a statistical model, described below. This solution is restricted to ice thicker than 25 cm to avoid the lower albedo of thin ice and the very high conductive flux through thin ice.

First, consider the effects of snow on the albedo of the ice surface, and hence absorbed short wave radiation. Snow generally has a higher albedo than the underlying ice cover. Both of these albedos are described with the Delta-Eddington albedo parameterization in CICE. In addition, the surface albedo can be decreased by the presence of melt ponds and entrained aerosols. Because of this, a simple model of albedo as a function of snow cover does not exist. As a result, we make use of a multiple linear regression to determine the role of snow cover in determining absorbed short wave radiation. More specifically, the regression determines the dependence of short wave absorbed by the ice surface as a function of surface characteristics and downwelling short wave radiation. Equation 3 describes the equation used in this regression. $SW_{absorbed}$ is the short wave radiation absorbed by the ice surface, SW_{down} is the downwelling short wave radiation before interacting with the ice surface, f_{snow} is the fraction of the ice

$$SW_{absorbed} = c_{swdn} SW_{down} + c_{snow} SW_{down} f_{snow} + c_{pond} SW_{down} f_{pond} + c_{melt} SW_{down} f_{melt} \tag{6}$$

surface covered with snow, f_{pond} is the fraction of the ice surface overlain with melt ponds, and f_{melt} is the fraction of the ice surface experiencing melt. The c terms are the constants produced by the regression. The pond fraction and snow cover fraction are both reported in the CICE model output, the fraction of melting ice was defined as the ice area with a monthly average temperature greater than -3 degrees C. This regression was performed separately for each ensemble member, month, and year, with individual grid cells representing data points.

Table 11 presents the regression coefficients for melting snow and melt ponds alongside the broadband albedo values from the current Delta-Eddington alongside the

	DE Overcast (ΔIce)	DE Clear (ΔIce)	June Coefficient
Bare Ice (Cold)	0.647 (N/A)	0.610 (N/A)	(N/A)
Melting Snow	0.726 (-.08)	0.640 (-.03)	-0.02 to -0.10
Melt Pond	0.192 (.46)	0.156 (.45)	0.18 to 0.44

Table 11. Comparison of Delta Eddington albedo values (Briegleb and Light 2007) and regression coefficients for bare ice, melting snow, and melt ponds for the month of June.

broadband albedo values from the current Delta-Eddington absorption parameterization (Briegleb and Light 2007). Table 11 uses albedo values calculated for a solar zenith value of 60 degrees under the Delta Eddington Parameterization, so the coefficients compared are from the month of June, across all ensemble members. In turn, the Delta-Eddington snow albedo most applicable is the melting snow value. Note that because of the term $c_{swdn}SW_{down}$, the coefficients derived by the regression in equation 6 are actually representative of the difference in albedo between the surface type in question and bare ice. For example, when the Delta-Eddington melting snow albedo is differenced from the bare ice clear sky albedo, the result is between -0.08 and -0.03 depending on cloud conditions. This compares favorably to the -0.06+-.04 coefficient for snow cover produced by the preceding regression. While the regression coefficient for melt ponds is not quite as good of a match to the Delta-Eddington albedo, the following calculations make use only of the snow coefficient, so this regression is found to perform adequately for these purposes. The pond albedo is omitted from the Delta-Eddington documentation, so a direct comparison is omitted here as well.

Next, for each month the change in short wave flux absorbed was calculated using Equation 7. Equation 7 uses c_{snow}, the coefficient calculated using the regression of

$$\Delta SW_{absorbed} = c_{snow} f_{snow} SW_{down} - c_{snow} f_{snow(1980-2000)} SW_{down} \qquad (7)$$

Equation 6. SW_{down} is the monthly mean downwelling short wave radiation for each grid cell. f_{snow} is the basin-wide average current snow cover fraction and $f_{snow(1980-2000)}$ is the average snow cover fraction for the period 1980-2000. The change in short wave absorption due to changing snow fraction, $\Delta SW_{absorbed}$, for each month was then averaged over the sea ice poleward of 70N. The annual mean change in short wave absorbed per unit ice area due to changes in snow cover is plotted in Fig. 44a. Tests regarding the significance of changes were then performed on these annual mean changes in short wave radiation flux absorbed, with each year and ensemble member providing a sample.

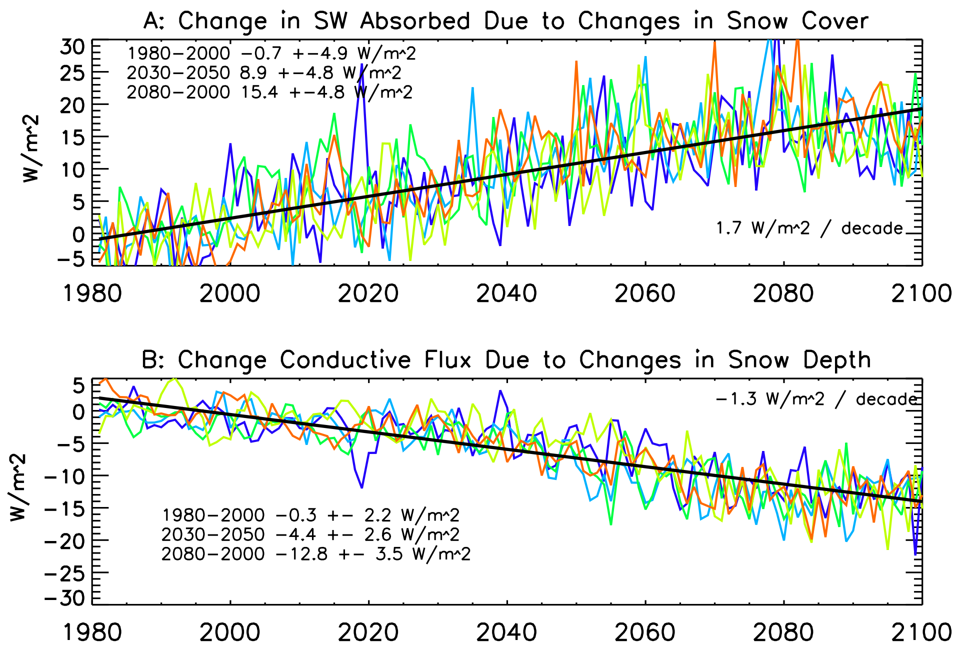

Figure 44. Estimated changes in energy budget due in snow characteristics using statistical/analytical models, see Section 5 for a discussion of the methods used. Panel A: Change in short wave radiation absorption due to reduced snow cover, in comparison to the period 1980-2000 snow cover. Panel B: Change in conductive flux to the ice surface due to reduced snow depth, in comparison to the snow depth for the period 1980-2000.

The mean for the period 1980-2000 does not diverge significantly from zero, indicating the model used is reacting appropriately during the period when $f_{snow(1980\text{-}2000)}$ was determined. Large changes in absorbed short wave radiation occur over the 21st century. By mid-century, the annual average short wave absorption has increased by a mean of 8.9 Wm^{-2}, reaching 15.4 Wm^{-2} by late 21st century. This corresponds to an approximately 4^{0} C increase in annual mean temperature. These changes are significant, and imply large changes in the surface energy budget due to decreased albedo as a result of shrinking summer snow fraction.

Next, the changes in conductive flux due to the decreased snow depth are considered. In CICE, snow has a fixed thermal conductivity of 0.3 W/m/K. The thermal conductivity of ice is not defined, but a value of 2.0 W/m/K is used as a reasonable mean as this value has been used when this term was fixed in other ice thermodynamic models (Thorndike 1992), and is close to the value defined for fully fresh ice in CICE (Hunke and Lipscomb 2010). Equation 8 defines the conductive flux. ΔT is the temperature difference between the snow/ice surface and the ocean, defined as -1.8 deg C. h is the thickness of ice and snow, k is the thermal conductivity of ice and snow, defined as 2.0W/m/k and 0.3 W/m/k, respectively.

$$F_{conduct} = \frac{\Delta T}{\frac{h_{ice}}{k_{ice}} + \frac{h_{snow}}{k_{snow}}} \tag{8}$$

While CICE does output the conductive flux, it is not possible to manipulate this term directly as a function of snow depth to determine the magnitude of the conductive flux feedback. Instead, we make use of the analytical model in Equation 9 to determine the changes in conductive flux due to changes in snow depth. The two quantities

$$\Delta F_{conduct} = \frac{\Delta T}{\frac{h_{ice}}{k_{ice}} + \frac{h_{snow}}{k_{snow}}} - \frac{\Delta T}{\frac{h_{ice}}{k_{ice}} + \frac{h_{snow(1980-2000)}}{k_{snow}}} \tag{9}$$

subtracted on the right side of Equation 9 are identical with the exception of h_{snow} and $h_{snow(1980\text{-}2000)}$, which are the current snow depth and the mean snow depth for the month under consideration during the period 1980-2000. Equation 9 can be used to calculate the conductive flux under current and historic snow depths. The difference can be taken as the magnitude of the feedback mechanism. This requires a value for the late 20th century snow depths; determined as a function of ice thickness using a simple linear regression. For consistency in snow depth estimates, this is performed for each year, month, and ensemble member. A simple linear fit is applied with snow depth being the dependent variable and ice thickness the independent variable. The late 20th century ensembles are then averaged for comparison to the 21st century. For consistency, the current year snow depth is also determined using a linear fit of the same design as the late 20th century fit.

This calculation should be regarded as a lower bound on the effect of the snow depth change on conductive flux through the snow-ice column. Stated more clearly, this method neglects the loss of snow on thick ice, which generally has thicker snow cover, see Chapter 3, and does not exist in the late 21st century. Due to this, the total snow mass being applied to simulated late 20th century ice conditions is potentially lower than the snow mass that actually existed during the late 20th century. However, this method allows the comparison of snow conditions on a given ice thickness, and still shows significant changes in the energy budget. Regardless, Equation 9 can be re-expressed as Equation 10, which is then used to calculate changes in the conductive flux, reported in

$$\Delta F_{conduct} = \frac{\Delta T}{\frac{h_{ice}}{k_{ice}} + \frac{f_{snow}(h_{ice})}{k_{snow}}} - \frac{\Delta T}{\frac{h_{ice}}{k_{ice}} + \frac{f_{snow(1980-2000)}(h_{ice})}{k_{snow}}} \qquad (10)$$

Fig. 44b. To reiterate, Equation 10 has replaced f_{snow} and $f_{snow(1980\text{-}2000)}$ with the functions $f_{snow}(h_{ice})$ and $f_{snow(1980\text{-}2000)}(h_{ice})$, which are now both functions of the current ice thickness, h_{ice}, although each function is characteristic of the current and 1980-2000 time period, respectively.

As with the short wave radiation absorption, the monthly change determined by Equation 10 is averaged over the ice area and year, creating an annual mean change in conductive flux through the snow ice column per unit area. Also similar to the short wave radiation absorption model, the mean change for the period 1980-2000 is not statistically different from zero, see Fig. 44b. As with the short wave absorption, the change by mid- and late 21st century is both large and significant. By mid 21st century, the ice looses an additional 4.4 Wm^{-2} to conductive flux through the snow-ice column, reaching 12.8 Wm^{-2} by late 21st century. This increase represents an approximately 3.3^{0} C increase in annual mean temperature.

The competing feedback mechanisms due to conductive flux and shortwave radiation absorption are potentially powerful, with the models used indicating feedback magnitudes in excess of 10 Wm^{-2} or 3^{0} C by late 21st century. These estimates exceed the global average 8.5 Wm^{-2} flux increase due to anthropogenic greenhouse gas forcing in this ensemble. Note that this value is determined prior to any feedback processes. While the models do indicate that the positive feedback due to albedo is stronger than the negative feedback due to conductive flux, these estimates should be regarded with skepticism. The two models used are both statistical/analytical and restrict the ice to a minimum thickness. In the case of the conductive flux, the model assesses the impact on the conductive flux of snow depth changes on a given ice thickness. The impact could potentially be very different if, instead, the changes in total snow mass were considered. Nonetheless, the basic setup of the model used for conductive flux is similar to the full treatment in CCSM and other models. Similarly, the regression coefficient produced for the short wave absorption statistical model is within the range of albedo values generated in CCSM.

Despite these limitations, it is clear the energy budget feedback due to increased short wave radiation absorption as a result of decreased snow cover and increased conductive flux through the ice due to decreased snow depth are both of large magnitude. The details and magnitude of these competing mechanisms should be carefully considered.

IV.6 Conclusion

The snow cover on the Arctic Sea ice thins and decreases in total mass significantly throughout the 21st century under the RCP 8.5 climate scenario as simulated by CCSM4. Under this strong greenhouse gas scenario, the ice itself becomes nearly absent in summer by late 21st century. The near complete loss of ice cover is preceded by decreased snow cover which results in completely snow free summer ice conditions decades prior to the nearly ice free summer conditions occurring in the CCSM ensemble. This loss has implications for the ice energy budget, as documented by this study.

The snow cover decreases from an average annual depth of 17-23 cm from 1980-2000 to 5-7cm annual average from 2080-2100. This loss is basin-wide, and is accompanied by decreased ice area covered by snow. This occurs despite projected 21st century increases in precipitation both in this ensemble and other simulations. In fact, the ice receives much less precipitation. While a repartitioning from snow to rain is projected in the 21st century ensemble, less rain falls directly on the ice as well. This is due to reduced summer and autumn ice pack throughout the 21st century, when the majority of rain, and much of the snow occur. This study finds the lack of autumn snow accumulation due to missing ice is a dominant causal factor in the decreased snow on the Arctic ice in the 21st century.

Due to decreased accumulation, the amount of snow melted actually decreases in absolute terms, but does increase relative to the mass of snow on the ice, indicating higher annual turnover in snow cover. Moreover, the lower snow accumulation and enhanced melt result in snow free conditions by mid-summer in the late 21st century, which is expected to increase surface albedo and contribute to a positive feedback mechanism for ice loss.

The statistical/analytical model used in this study finds the magnitude of the increased short wave radiation absorption as a result of decreased snow cover to be nearly twice the anthropogenic energy increase prescribed in the RCP 8.5 scenario. However, this positive feedback appears heavily mitigated by a competing feedback mechanism, whereby decreased snow depth allows for enhanced wintertime conduction of energy through the ice, increasing basal ice growth. The lower bound for this negative feedback mechanism is less than the positive feedback caused by a decreased albedo, but still exceeds the anthropogenic global average signal in this scenario. The relative strengths of these feedback mechanisms are uncertain due to assumptions of the analytic models and restrictions imposed on the statistical determination of the relationship between the energy budget and the independent variables (snow cover fraction and snow depth). Nonetheless, the absolute strength of these feedbacks indicates a need to better understand these competing mechanisms.

In addition, the strength of these feedback mechanisms may change due to the recently identified 20th century biases in snow depth, see Chapter 3. If these biases were absent, the snow free summer state may not be a future condition, but a present one. In this case, the increased short wave radiation absorption would still occur due to an earlier snow free state. Additional work on the effect of changes in 21st century on-ice snow cover in CCSM 4 would benefit from making use of daily output of ice conditions, including snow depth and cover would allow for more precise diagnosis of the changing timing of snow melt.

In addition, the focus of this study has been on the effect of changing precipitation on the ice cover. However, the amount and timing of freshwater flux to the ocean will also change. As a first effect, the overall increase in precipitation may freshen the arctic ocean, which has recently been observed (Morrison et al 2012). Second, because the autumn snowfall is lost to the ocean, the timing of freshwater flux may shift from the spring melt to the autumn. Overall, the increase in freshwater flux may serve to strengthen the halocline and thermal stratification of the ocean. This would have additional implications for the ice state. Another avenue for future work with relevance to the ice state is an investigation of the changes in the Arctic upper ocean in the 21st century.

Finally, the negative feedback mechanisms observed in CCSM4 due to changes in snow depth and the associated increase in conductive flux represents an important element to ice treatment in all ice models. While hindcast simulations are also sensitive to snow characteristics, see Chapter 3, inter-model hindcast snow variability is potentially compensated by other model differences. However, the timing and strength of both feedback mechanisms between ice area and snow could contribute to the variability between different models for projected 21st century ice conditions. For example, if the timing of significant snow thinning is earlier in a GCM, the negative feedback identified in this study would trigger more quickly, presumably forestalling additional ice loss. Of course, due to the strength of these feedback mechanisms, correctly assessing both the negative feedback due to conductivity and the positive feedback due to albedo is crucial to accurately projecting 21st century ice conditions. While biases in these feedback mechanisms may be mutually correcting in the hindcast simulations, this may not be the case in projections. In addition, while both the negative and positive mechanisms are present in most ice models used as part of GCMs, the relative strengths identified here are not necessarily the same in other model environments. As such, the intermodel implications of these feedback mechanisms are potentially important to understanding variability in projections of Arctic climate.

Chapter 5

V. Conclusion

Snow cover overlying the Arctic Ocean sea ice is an integral element of the Arctic climate system. Due to its low density, low thermal conductivity, and high albedo, snow has a complicated relation to the ice cover itself as it hinders both winter growth and summer melt of the ice. As such, the snow cover presents an integral element of the sea ice system with significant impacts on the ice state and Arctic climate, both in hindcast simulations and 21st century projections. The uncertainties associated with the snow on sea ice represent a source of uncertainty in climate models.

This collection of studies has endeavored to use the CCSM model environment to increase community understanding of the role of snow cover in modulating Arctic ice conditions while demonstrating the importance of snow cover for the Arctic sea ice and Arctic climate. In so doing, additional avenues have presented themselves for future investigation.

While each chapter stands as a separate study, together these investigations illuminate the role of snow on the Arctic Ocean sea ice. For clarity, short summaries of each chapter are provided. Chapter 2 demonstrated the sensitivity of the ice to snow depth. A 50% decrease in snow depth triggered a 10-20% decrease in ice area and volume, depending on initial conditions and atmosphere atmospheric forcing. An increase in snow depth generally did not greatly affect the ice, but when applied to thinner ice, as is expected in to occur in the 21st century, increased snow depth triggered pronounced increases in ice area and volume.

Chapter 3 identified a 20-30% bias of excessive snow depth in a CCSM hindcast ensemble. In addition, Chapter 3 found that the excessive snow depth results in decreased wintertime ice growth. Without considering the effect of snow cover fraction on albedo and short wave absorption by the surface, correction for this bias led to atmospheric and oceanic interactions resulting in a 20% increase in ice volume.

Finally, Chapter 4 projected dramatic decreases to snow depth over the course of the 21st century. These decreases were found to be due in large part to the decreasing autumn ice cover. The decrease in snow was found to result in enhanced wintertime conductive flux, and presumably ice formation, as in Chapter 3. However, this effect was dominated by enhanced summertime short wave absorption.

In concert, these studies have confirmed and elucidated a pair of feedback mechanisms between the ice cover and snow overlain upon the ice. As the 21st century progresses, the ice cover declines; this is especially pronounced in the summer and autumn months. Although the total precipitation increases, much of this increase occurs in the form of rain. This rain generally does not fall on the ice, but neither does the snow, which fails to accumulate on the ice cover. Rather, the absence of autumn ice cover results in the snow falling directly into the ocean. Due to this, accumulated snow cover on the ice decreases. As the winter progresses, this decreased snow cover results in an increase in basal ice growth due to enhanced thermal conductivity through the ice. This process presents a negative feedback mechanism to further ice loss. However, once the melt season initiates in the spring, the reduced snow cover is rapidly melted. In the following months, the ice is exposed to an increased flux of absorbed short wave radiation, resulting in enhanced melt. This enhanced melt due to lost snow cover contributes to the continued decline of the summertime ice pack, reinforcing both feedback mechanisms. However, if the enhanced conductive flux and basal growth dominates, the increased growth would serve to arrest continued degradation of the ice pack.

Chapter 3 showed that changes in conductive flux through the snow-ice column have a dramatic effect on the ice cover. However, the nearly 20% increase in ice volume was due in large part to feedback mechanisms with other components of the Arctic climate. The initial perturbation in snow thermal conductivity only contributed an annual 0.5 W/m^2 change to the energy budget of the ice. However, as the model adjusted, the ocean and atmosphere feedback mechanisms produced a total 8 W/m^2 change in the energy budget of the ice. Were the albedo affect of a snow cover fraction bias correction included in Chapter 3, it seems likely these feedback mechanisms would not have initiated, and potentially would have reinforced the effect of decreased snow cover on the short wave absorption, rather than the effect of decreased snow depth on the conductive flux.

This is what occurred in both Chapters 2 and 4, where reductions in snow triggered a decrease in sea ice area and volume. Chapters 2 and 4 did not separately introduce the conductive and shortwave radiation absorption effects of snow on the ice energy budget as in Chapter 3. In both of these investigations, a decrease in snow was linked to a decrease in ice. In Chapter 2, this decrease was of the order 10-20% in both volume and area. In Chapter 4, the changing mean climate did not allow a direct attribution of the ice decline to changes in snow, but the increased short wave absorption due to decreased snow cover fraction was estimated at 15.4 Wm^{-2} by late 21st century, with the enhanced conductive flux through the ice lagging at 12.8 Wm^{-2}. In light of the more modest change in conductive flux in Chapter 3, these estimates may seem high, but the changes in snow depth over the 21st century are more profound than the biases in the 20th century, a 70% decline in comparison to a 20-30% excess. Regardless of the potential overestimation of the absolute value of the albedo and conductive flux effects of decreased snow, the increase in shortwave radiation absorption is greater in relation to the increase in conductive flux. The positive feedback mechanism due to declining snow cover and enhanced shortwave absorption dominates the negative feedback mechanism due to enhanced conductive flux and basal ice growth. As a result, the net effect of the interaction between declining ice cover and declining snow cover produces a positive feedback mechanism to continued warming of the Arctic.

This conclusion increases the significance of the high snow depth bias identified in 20th century snow depth. Again, due to the nature of the *in situ* measurements used, Chapter 3 quantified only the effects of the bias on conductive flux. If the snow cover fraction were also validated, and the sensitivity to any biases tested, it is likely that the enhanced short wave absorption would dominate as seen in Chapters 2 and 4. Regardless of this limitation, were the excessive snow depths in the 20th century not present in the model environment, the feedback mechanisms identified in Chapter 4 would occur earlier and more strongly in the 21st century. As a result, decreases in ice cover would occur more rapidly, potentially bringing model results more in line with observations.

This dissertation has suggested that the albedo of snow dominates the conductive flux in terms of the energy budget. As such, one important avenue of future investigation would be the validation of snow cover fraction. Given the availability of appropriate observations, similar techniques as those employed in Chapter 3 could be applied to both the validation and study of sensitivity to biases in snow cover. The study would be predicated on the hypothesis that the snow cover fraction in CCSM is too high, and that the correction of this bias would produce an equal or greater effect than the depth bias identified in Chapter 3.

While Chapter 3 and the accompanying appendix assessed the sensitivity of ice cover to the density bias identified in Chapter 3, the modification to snow thermal conductivity was a function of the decreased snow depth due to excessive density. However, as mentioned in Chapter 3, the snow density directly affects the thermal conductivity of snow. An experiment could easily be designed which would include a seasonal evolution in thermal conductivity of snow designed to correspond to the observed seasonal density evolution. Due to the lower conductivity of low-density snow, this would likely result in decreased autumn ice growth and an overall decrease in ice volume. If appropriate, such a parameterization would be a fairly simple addition to the CICE treatment of snow.

Finally, as mentioned in Chapter 3, ice of different thickness responds differently to changes in snow depth. Thus redistribution of snow on the ice may have a measurable effect on the ice state in CCSM. Given the necessary resources, the ideal method of investigating this would include a field component, a process modeling component, and finally the introduction and testing of a new parameterization to CICE. More specifically, the field component would measure both the temporal and spatial variability of snow depth. This measurement would include spatial variability as a function of ice roughness and thickness, and would also assess the rate at which snow redistributes after deposition events. A model of snow distribution and evolution such as SnowModel could be adapted for the ice environment to serve as a transitional tool to test the ability of redistribution parameterizations to reproduce observations from the direct measurements. Using the results of field observations and process modeling, a sub-grid scale redistribution of snow parameterization would be developed and tested in the CCSM and CICE reanalysis environments. If the ice state were found to be sensitive to this parameterization, inclusion of this improvement would hopefully be considered for future versions of CICE. The addition of such a parameterization would be intended to improve fidelity of the response of ice cover to snow regardless of total snow accumulated or ice conditions; this would in turn improve confidence in 21st century projections of the ice state.

In summary, the timing of snowfall and characteristics of the snow cover has profound and diverse impacts on the Arctic ice thickness and extent. There are two primary, opposing mechanisms of interaction between the snow and ice. While increased snow depth inhibits wintertime basal ice growth, the increased survival of the snow cover during the summer months results in lower absorbed shortwave radiation, delaying the summertime melt. The relative strengths of these feedback mechanisms represent an uncertainty in current climate models which could be reduced through more detailed treatment of the snow cover on the sea ice. Increasing the consistency with which models reproduce the measured snow cover, depth, and thermal characteristics throughout the seasonal evolution of this element of the sea ice will increase the fidelity with which these models simulate the Arctic sea ice and in turn the Arctic climate.

References

Alexander, M., U. Bhatt, J. E. Walsh, M. Timlin, J. Miller, and J. Scott (2004), The atmospheric response to realistic Arctic sea ice anomalies in an AGCM during winter, *J. Climate, 17(5),* 890–905.

Arctic Climate Impact Assessment (2005), Impacts of a Warming Arctic: Arctic Climate Impact Assessment, 144 pp., Cambridge Univ. Press, New York.

Arctic Climatology Project. (2000), *Environmental working group Arctic meteorology and climate atlas*, Edited by F. Fetterer and V. Radionov. Boulder, CO: National Snow and Ice Data Center. CD-ROM

Arrigo, K.R., G. vanDijken, S. Pabi, (2008), Impact of a shrinking Arctic ice cover on marine primary production, *Geophys. Research Lett.,* 35, L19603.

Arzel, O., T. Fichefet, and H. Goosse (2006), Sea ice evolution over the 20th and 21st centuries as simulated by current AOGCMs*, Ocean Modell.,* 12, 401 – 415.

Bailey, D. C. Hannay, M, Holland, R. Neale, NCAR (2012) Slab Ocean Model Forcing, NCAR, 10 April 2012, < http://www.cesm.ucar.edu/models/ccsm4.0/data8/SOM.pdf>

Barry, R.G. (1989) The present climate of the Arctic Ocean and possible past and future states. In: Herman, Y., ed. The Arctic seas—Climatology, oceanography, geology, and biology. New York: Van Nostrand Reinhold Company.

Bitz, C.M., K.M. Shell, P.R. Gent, D.A. Bailey, G. Danabasoglu, K.C. Armour, M.M. Holland, and J.T. Kiehl (2012), Climate Sensitivity of the Community Climate System Model Version 4, *J. Climate,* doi:10.1175/JCLI-D-11-00290.1 *In press*

Bitz, C.M., and W.H. Lipscomb, (1999), An energy-conserving thermodynamic model of sea ice, *J. Geophys. Res.,* 104(15), 669-15,677

Bourke, R.H., R.P. Garret, (1987), Sea ice thickness distribution in the Arctic Ocean. *Cold Regions Sci. & Tech. Vol13(3) pg 259-280*

Briegleb, B.P., B. Light (2007), A Delta-Eddington Multiple Scattering Parameterization for Solar Radiation in the Sea Ice Component of the Community Climate System Model, Ncar Tech. Note NCAR/TN-472+STR 100pp.

Briegleb, B.P., C.M. Bitz, E.C. Hunke, W. H. Lipscomb, M.M. Holland, J.L. Schramm, R.E. Mortiz (2004), Scientific Description of the sea ice component in the Community Climate System Model, Version Three, NCAR Tech. Note NCAR/TN-463+STR, 70 pp.

Briegleb, B.P., G. Danabasoglu, W.G. Large (2010), An Overflow Parameterization for the Ocean Component of the Community Climate System Model NCAR Tech, Note NCAR/TN-???+STR, 72 pp. *Draft*

Brown, R., C. Derksen, and L. Wang (2010), A multi-dataset analysis of variability and change in Arctic spring snow cover extent, 1967-2008. *Journal of Geophysical Research.* 115, doi:10.1029/2010JD013975

Brown, R.D. and P. Cote (1992), Interannual variability of landfast ice thickness in the Canadian High Arctic, 1950-8, *Arctic*, 45(3), 273-284

Cassano, J.J., P. Uotila, A.H. Lynch, and E.N. Cassano (2007), Predicted changes in synoptic forcing of net precipitation in large arctic river basins during the 21st Century, *J. Geophys. Res-Biogeosciences, 112*, G04S49.

Cheng, B., Z. Zhang, T. Vihma, M. Johansson, L. Bian, Z. Li, and H. Wu (2008), Model experiments on snow and ice thermodynamics in the Arctic Ocean with CHINARE 2003 data, *J. Geophys. Res.*, *113*, C09020, doi:10.1029/2007JC004654.

Comiso, Josefino C. (2012), Large Decadal Decline of the Arctic Multiyear Ice Cover. *J. Climate*, 25, 1176–1193. doi: http://dx.doi.org/10.1175/JCLI-D-11-00113.1

Curry, J.A., J. Schramm and E. E. Ebert (1995), On the sea ice albedo climate feedback mechanism, *J. Climate,* 8, 240-247.

Danabasoglu, G., S. Bates, B. P. Briegleb, S. R. Jayne, M. Jochum, W. G. Large, S. Peacock, S. G. Yeager (2011), The CCSM4 ocean component. *J. Climate,* in review

Danabasoglu, G., W. G. Large, and B. P. Briegleb (2010), Climate impacts of parameterized Nordic Sea overflows, *J. Geophys. Res.*, *115*, C11005, doi:10.1029/2010JC006243.

Danabasoglu, G. and P. Gent, 2009: Equilibrium Climate Sensitivity: Is It Accurate to Use a Slab Ocean Model? *Journal of Climate*, 22

de Boer, G., W. Chapman, J. Kay, B. Medeiros, M. D. Shupe, S. Vavrus, and J. Walsh (2011), A characterization of the present-day Arctic atmosphere in CCSM4. *J. Climate,* Vol. 25, Iss. 8, pp. 2676–2695

Drobot, Sheldon, James Maslanik, Ute Christina Herzfeld, Charles Fowler, Wanli Wu, (2006) Uncertainty in Temperature and Precipitation Datasets over Terrestrial Regions of the Western Arctic. *Earth Interact.*, **10**, 1–17

Drobot, S. D., J. A. Maslanik, B. A. Blazey, C. Fowler, W. Emery, J. Francis, X. Wang, J. Key (Unpublished 2009), A Comparison of Six Arctic Temperature Data Sets.

Ebert, E.E. and J. A. Curry (1993), An intermediate one-dimensional thermodynamic sea ice model for investigating ice-atmosphere interactions, *J. Geophys. Res.,* 98, C6, 10,085-10,109.

Eicken, H., R. Gradinger, A. Graves, A. Mahoney, I. Rigor (2005), Sediment transport by sea ice in the Chukchi and Beaufort Seas: Increasing importance due to changing ice conditions?, *Deep-Sea Res. Part II,* 52, 3281-3302

Fichefet, T., B. Tartinville, and H. Goosse (2000), Sensitivity of the Antarctic sea ice to the thermal conductivity of snow. *Geophys. Res. Lett., 27*(3), 401– 404.

Fichefet, T., M. A. Morales Maqueda (1999), Modeling the influence of snow accumulation and snow-ice formation on the seasonal cycle of the Antarctic sea-ice cover, *Clim. Dyn., 15,* 251– 268

Fichefet, T., and M. A. M. Maqueda (1997), Sensitivity of a global sea ice model to the treatment of ice thermodynamics and dynamics, *J. Geophys. Res.*, *102*(C6), 12,609–12,646

Finnis, J., M.M. Holland, M.C. Serreze, and J.J. Cassano (2007), Response of Northern hemisphere extratropical cyclone activity and associated precipitation to climate change, as represented by CCSM3, *J. Geophys. Res.*, 112, G04S42, doi:10.1029/2006JG000286

Ford, J. D. (2009), Vulnerability of Inuit food systems to food insecurity as a consequence of climate change: a case study from Igloolik, Nunavut, *Reg Environ Change, 9(2),* 83–100, doi:10.1007/s10113-008-0060-x.

Fowler, C., W. J. Emery, and J. Maslanik (2004), Satellite-derived evolution of Arctic sea ice age: October 1978 to March 2003, *IEEE Geosci. Remote Sens. Lett.,* 1(2), 71–74

Gent, P. R., G. Danabasoglu, L. J. Donner, M. M. Holland, E. C. Hunke, S. R. Jayne, D. M. Lawrence, R. B. Neale, P. J. Rasch, M. Vertenstein, P. H. Worley, Z.-L. Yang, and M. Zhang (2011), The Community Climate System Model Version 4, *J. Climate, In press (Early Online Release)*

Gerdes, R., C, Koberle (2007), Comparison of Arctic sea ice thickness variability in IPCC Climate of the 20th Century experiments and in ocean–sea ice hindcasts, *J. Geophys. Res.,* 112, C04S13.

Hibler, W.D., G.M. Flato (1992), Sea Ice Models. Climate System Models, Ed. K. E. Trenberth, pp.413-436 Cambridge University Press, New York

Higgins, M. E. and J.J. Cassano (2009), Impacts of reduced sea ice on winter Arctic atmospheric circulation, precipitation, and temperature, *J. Geophys. Res.,* 114, D16107, doi:10.1029/2009JD011884

Holland, D.M, Mysak, L.A., D.K. Manak, J.M. Oberhuber (1993), Sensitivity Study of a Dynamic Thermodynamic Sea Ice Model, *J. Geophys. Res.* 98(2), 2561-2586

Holland, M.M., David A. Bailey, Bruce P. Briegleb, Bonnie Light, Elizabeth Hunke (2011), Improved sea ice shortwave radiation physics in CCSM4: The impact of melt ponds and aerosols on Arctic sea ice. *Journal of Climate (Early online release)*

Holland, M.M, J. Finnis, A.P. Barret, M. C. Serreze (2007), Projected Changes in Arctic Ocean Freshwater Budgets. *J. Geophys Res.,* 112, G04S55

Holland, M. M., C. M. Bitz, E. C. Hunke, W. H. Lipscomb, and J. L. Schramm (2006a), Influence of the sea ice thickness distribution on polar climate in CCSM3, *J. Climate, 19(11),* 2398–2414.

Holland, M.M., C.M. Bitz and B. Tremblay (2006b), Future abrupt reductions in the summer Actic sea ice. *Geophys. Res. Lett.,* 33, L23503, doi:10.1029/2006GL028024, 2006

Hunke, E. C., and W. H. Lipscomb (2010), CICE: the Los Alamos Sea Ice Model, Documentation and Software User's Manual Version 4.1. T-3 Fluid Dynamics Group, Los Alamos National Laboratory, Tech. Rep. LA-CC-06-012

Hunke, E. C., and W. H. Lipscomb (2004), CICE: the Los Alamos Sea Ice Model, Documentation and Software User's Manual. T-3 Fluid Dynamics Group, Los Alamos National Laboratory, Tech. Rep. LA-CC-98-16 v.3.1

Hunke, E.C. and J. K. Dukowicz (2002), The Elastic-Viscous-Plastic sea ice dynamics model in general orthogonal curvilinear coordinates on a sphere—Effect of metric terms. *Mon. Wea. Rev.,* 130:1848– 1865

IPCC, 2007: Climate Change (2007), Synthesis Report. Contribution of Working Groups I, II and III to the Fourth Assessment Report of the Intergovernmental Panel on Climate Change [Core Writing Team, Pachauri, R.K and Reisinger, A. (eds.)]. IPCC, Geneva, Switzerland, 104 pp

Jahn, A., M. M. Holland, K. Sterling, J. E. Kay, J. A. Maslanik, C. M. Bitz, D. A. Bailey, J. Stroeve, E. C. Hunke, W. H. Lipscomb, D. Pollak, 2011: Late 20th century simulation of Arctic sea-ice and ocean properties in the CCSM4. *J. Climate, In Review,* Vol. 25, Iss. 5, pp. 1431–1452

Johannessen, O.M., L. Bengtsson, M.W. Miles, S.I. Kuzmina, V. Semenov, G.V. Alekseev, A.P. Nagurny, V.F. Zakharov, L.P. Bobylev, L.H.Pettersson, K.Hasselmann, H.P. Cattle (2004), Arctic Climate Change – Observed and Modeled

Temperature and Sea Ice. *Tellus, Dynamic meteorology and oceanography, Series A*: 56(4), pp. 328-341

Jones, B. M., C. D. Arp, M. T. Jorgenson, K. M. Hinkel, J. A. Schmutz, and P. L. Flint (2009), Increase in the rate and uniformity of coastline erosion in Arctic Alaska, *Geophys. Res. Lett.*, 36, L03503, doi:10.1029/2008GL036205.

Kalnay and coauthors (1996) The NCEP/NCAR 40-year reanalysis project,,*Bull. Amer. Meteor. Soc.*, 77, 437-470, 1996.

Kattsov, V. M, J.E. Walsh, W.L. Chapman, V.A. Govorkova, T.V. Pavlova, X. Zhang (2007), Simulation and Projection of Arctic Freshwater Budget Components by the IPCC AR4 Global Climate Models, *J. Hydrometeorology*, 8, 571-589

Kattsow, V. M, J.E. Walsh (1999), Twentieth-Century Trends of Arctic Precipitation from Observational Data and a Climate Model Simulation, *J. of Climate,* 13, 1362-1370

Kelly, B.P., C.M. Bitz, (2010), The ringed seal's last refuge and the importance of snow cover, Abstract C43E-0590 Poster presented at 2010 Fall Meeting, AGU, San Francisco, Calif. 13-17 Dec.

Large, W. G., and S. G. Yeager (2009), The Global Climatology of an Interannually Varying Air-Sea Flux Data Set. *Clim. Dyn.*, 33, 341-364, doi:10.1007/s00382-008-0441-3.

Large, W.G., S.G. Yeager (2004), Diurnal to Decadal Global Forcing For Ocean and Sea-Ice Models: The Data Sets and Flux Climatologies. NCAR Tech. Note NCAR/TN-460+STR 105pp.

Lawrence, D.M., K.W. Oleson, M.G. Flanner, P.E. Thornton, S.C. Swenson, P.J. Lawrence, X. Zeng, Z.-L. Yang, S. Levis, K. Sakaguchi, G.B. Bonan, and A.G. Slater (2011), Parameterization improvements and functional and structural advances in version 4 of the Community Land Model. *J. Adv. Model. Earth Sys.*, **3**, DOI: 10.1029/2011MS000045

Lawrence, D. M., A. G. Slater, R. A. Tomas, M. M. Holland, and C. Deser (2008), Accelerated Arctic land warming and permafrost degradation during rapid sea ice loss, *Geophys. Res. Lett.*, *35*, L11506, doi:10.1029/2008GL033985

Lecomte, O., T. Fichefet, M. Vancoppenolle, and M. Nicolaus (2011). A new snow thermodynamic scheme for large-scale sea-ice models. *Annals of Glaciology*, 52(57):337-346,

Ledley, T.S. (1991), snow on sea ice: competing effects in shaping climate, *J. Geophys. Res.,* 96, 17,195-17,208.

Lin, S.J. (2004), A “Wertically Lagrangian” finite-volume dynamical core for global models. *Mon. Wea. Rev.* 132:2293-2307.

Lipscomb, W.H. and E. C. Hunke (2004), Modeling sea ice transport using incremental remapping. *Mon. Wea. Rev.,* 132:1341–1354.

Lipscomb, W.H. (2001), Remapping the thickness distribution in sea ice models. *J. Geophys. Res.–Oceans,* 106(13):989–14,000

Liston, G. E., and K. Elder (2006), A distributed snow-evolution modeling system (SnowModel). *J. Hydrometeorology*, 7, 1259-1276.

Maksym, T. and T. Markus (2008), Antarctic sea ice thickness and snow-to-ice conversion from atmospheric reanalysis and passive microwave snow depth. *J. Geophys. Res*., 113, C02S12, doi:10.1029/2006JC004085.

Mars, J. C., and D. W. Houseknecht (2007), Quantitative remote sensing study indicates doubling of coastal erosion rate in past 50 yr along a segment of the Arctic coast of Alaska, *Geology,* 35(7), 583-586

Maslanik, J., J. Stroeve, C. Fowler, and W. Emery (2011), Distribution and trends in Arctic sea ice age through spring 2011, *Geophys. Res. Lett.*, *38*, L13502, doi:10.1029/2011GL047735.

Maslanik, J.A., C. Fowler, J. Stroeve, S. Drobit, J. Zwally, D. Yi and W. Emery (2007), A younger, thinner Arctic ice cover: Increased potential for rapid, extensive sea-ice loss, *Geophys. Res. Lett.,* 34, L24501, doi:10.1029/2007GL032043.

Massom, R. A., H. Eicken, C. Haas, M. O. Jeffries, M. R. Drinkwater, M. Sturm, A. P. Worby, X. Wu, V. I. Lytle, S. Ushio, K. Morris, P. A. Reid, S. Warren, & I. Allison (2001), Snow on Antarctic sea ice, *Reviews of Geophysics*, 39(3):413-445

Mauritzen, C., and S. Häkkinen (1997), Influence of sea ice on the thermohaline circulation in the Arctic-North Atlantic Ocean, *Geophys. Res. Lett.*, *24*(24), 3257–3260, doi:10.1029/97GL03192

Maykut, G. A., and N. Untersteiner (1971), Some results from a time dependent, thermodynamic model of sea ice, *J. Geophys. Res.,* 76(6), 1550-1575

McPhee, M. G., T. P. Stanton, J. H. Morison, and D. G. Martinson (1998), Freshening of the upper ocean in the Arctic: Is perennial ice disappearing?, *Geophys. Res. Lett.,* 25(10), 1729 – 1732.

Meehl, G. A., J. M. Arblaster, and C. Tebaldi (2005), Understanding future patterns of increased precipitation intensity in climate model simulations, *Geophys. Res. Lett.,* 32, L18719, doi:10.1029/2005GL023680.

Meier, W. N., J. Stroeve, and F. Fetterer (2007), Whither Arctic sea ice? A clear signal of decline regionally, seasonally, and extending beyond the satellite record. *Annals of Glaciology,* 46:428-434

Morison, J., R. Kwok, C. Peralta-Ferriz, I. Rigor, R. Andersen, M. Steele, 2012. Changinge Arctic Freshwater Pathways. *Nature*, 481:66:70

Moss R. and coauthors, 2008. Towards New Scenarios for Analysis of Emissions, Climate Change, Impacts, and Response Strategies. Intergovernmental Panel on Climate Change, Geneva, 132 pp.

Neale, R. B., J. Richter, S. Park, P. H. Lauritzen, S. J. Vavrus, P. J. Rasch, and M. Zhang (2011), The mean climate of the Community Atmosphere Model (CAM4) in forced SST and fully coupled experiments. *J. Climate, In preparation*

Neale, R. B., J. H. Richter and M. Jochum, (2008), The impact of convection on ENSO: From a delayed oscillator to a series of events. *J. Climate,* 21, 5904-5924

Nghiem, S. V., I. G. Rigor, D. K. Perovich, P. Clemente-Colón, J. W. Weatherly, and G. Neumann (2007), Rapid reduction of Arctic perennial sea ice, *Geophys. Res. Lett.*, *34*, L19504

Oleson, K. W., D. M. Lawrence, G. B. Bonan, M. G. Flanner,E. Kluzek, P. J. Lawrence, S. Levis, S. C. Swenson, P. E.Thornton, A. Dai, M. Decker, R. DIckinson, J. Feddema, C. L. Heald, F. Hoffman, J. F. Lamarque, N. Mahowald, G.-Y. Niu, T. Qian, J. Randerson, S. Running, K. Sakaguchi, A. Slater, R. Stockli, A. Wang, Z.-L. Yang, X. Zeng, and X. Zeng (2010), Technical description of version 4.0 of the Community Land Model. NCAR Tech. Note NCAR/TN-478+STR, 257

Overpeck, J.T. (2004), Arctic System on trajectory to New, Seasonally Ice-Free State, *EOS*, 86(34):309-316

Parkinson, C.L., D.J. Cavalieri, P. Gloersen, H.J. Zwally and J.C. Comiso (1999), Arctic sea ice extents, areas, and trends, 1978–1996. *J. Geophys. Res.,* 104:20,837–20,856.

Peltier, W. R., G. Vettoretti, and M. Stastna (2006), Atlantic meridional overturning and climate response to Arctic Ocean freshening, *Geophys. Res. Lett.*, *33*, L06713, doi:10.1029/2005GL025251

Perovich, D., W. Meier, J. Maslanik, and J. Richter-Menge (2011), Arctic Report Card: Update for 2011 (Sea ice cover) [http://www.arctic.noaa.gov/reportcard/seaice.html]

Perovich, D., W. Meier, J. Maslanik, and J. Richter-Menge (2010), Arctic Report Card: Update for 2010 (Sea ice cover) [http://www.arctic.noaa.gov/report10/seaice.html]

Perovich, D.K., J.A. Richter-Menge, B. Elder, K. Claffey, and C. Polashenski (2009), Observing and understanding climate change: Monitoring the mass balance, motion, and thickness of Arctic sea ice, http://IMB.crrel.usace.army.mil

Perovich, D.K. (1998), Optical properties of sea ice, *Physics of Ice-Covered Seas,* Vol 1, (Ed. M. Lepparanta), pp195-230, University of Helsinki Press, Helsinki, Finland.

Peterson , B.J., R.M. Holmes, J.W. McClelland, C.J Vorosmarty, R.B. Lammers, A.I. Shiklomanow, I.A. Shiklomanow, and S. Rahmnsrorf, (2002), Increasing river discharge to the Arctic Ocean. *Science*, 298, 2171-2173.

Pfirman, S., W. Haxby, H. Eicken, M. Jeffries, D Bauch (2004), Drifting Arctic Sea Ice Archives Changes in Ocean Surface Conditions, *Geophys. Res. Lett. 31*, L19401

Porter, D.F., J.J. Cassano, and M.C. Serreze (2012), Atmospheric response to reduced Arctic sea ice cover in the WRF model. *J. Geophys. Res., In Review*

Powell, D C., T. Markus, A Stossel (2005), Effects of snow depth forcing on Southern Ocean sea ice simulations. *J. Geophys. Res., 110,* C06001

Richter, J. H., and P. J. Rasch (2008), Effects of Convective Momentum Transport on the Atmospheric Circulation in the Community Atmosphere Model, Version 3. *J. Climate,* 21, 1487–1499

Rigor, I., R. Colony, and S. Martin (2000), Variations in surface air temperature observations in the Arctic, 1979 – 1997*, J. Clim.,* 13, 896 – 914.

Rossow, W.B., and Y-C. Zhang (1995), Calculation of surface and top-of-atmosphere radiative fluxes from physical quantities based on ISCCP datasets, Part II: Validation and first results. *J. Geophys. Res*., 100, 1167-1197

Saloranta, T. M. (2000), Modeling the evolution of snow, snow ice and ice in the Baltic Sea. *Tellus*, 52A, 93-108.

Schweiger, A. J., R. W. Lindsay, S. Vavrus, and J. A. Francis (2008), Relationships between Arctic Sea Ice and Clouds during Autumn, *J. Climate*, 21(18), 4799– 4810, doi:10.1175/2008JCLI2156.1.

Screen, J. A., I. Simmonds, and K. Keay (2011), Dramatic interannual changes of perennial Arctic sea ice linked to abnormal summer storm activity, *J. Geophys. Res.*, 116, D15105, doi:10.1029/2011JD015847

Screen, J. A., and I. Simmonds (2010), Increasing fall-winter energy loss from the Arctic Ocean and its role in Arctic temperature amplification, *Geophys. Res. Lett.,* 37(16), doi:10.1029/2010GL044136.

Serreze, M., C. Hurst (2000), Representation of Mean Arctic Precipitation from NCEP-NCAR and ERA reanalyzes, *J. of Climate,* 13, 182-201

Serreze, M. C., M. M. Holland, and J. Stroeve (2007), Perspectives on the Arctic's shrinking sea-ice cover. *Science,* 315(5818): 1533-1536

Smith, R., P. Jones, B. Briegleb, F. Bryan, G. Danabasoglu, J. Dennis, J. Dukowicz, C. Eden, B. Fox-Kemper, P. Gent, M. Hecht, S. Jayne, M. Jochum, W. Large, K. Lindsay, M. Maltrud, N. Norton, S. Peacock, M. Vertenstein, and S. Yeager (2010), The Parallel Ocean Program (POP) Reference Manual: Ocean Component of the Community Climate System Model (CCSM). LAUR-10-01853

Smith, R,, Legler DM, Verzone KV (2001) Quantifying uncertainties in NCEP reanalyses using high-quality research vessel observations. *J Clim* 14:4062–4072

Stroeve, J. C., M. C. Serreze, M. M. Holland, J. E. Kay, J. Maslanik, and A. P. Barrett (2011), The Arctic's rapidly shrinking sea ice cover: A research synthesis. *Climatic Change*, doi:10.1007/s10584-011-0101-1

Stroeve, J., M. Serreze, S. Drobot, S. Gearhead, M. Holland, J. Maslanik, W. Meier, and T. Scambos (2008), Arctic Sea Ice Extent Plummets in 2007 *EOS,* 89(2)

Stroeve, J., M.M. Holland, W. Meier, T. Scambos, and M. Serreze (2007), Arctic sea ice decline: Faster than forecast, *Geophys. Res. Lett.,* 34, L09501, doi:10.1029/2007GL029703.

Sturm, M., and G.E. Liston (2003), The snow cover on lakes of the Arctic Coastal Plain of Alaska, *J. of Glaciology*, 49 (166), 370-380.

Sturm, M., D.K. Perovich, J. Holmgren (2002), Thermal conductivity and heat transfer through the snow and ice of the Beaufort Sea. *Journal of Geophysical Research-Oceans*, 107, doi:10.1029/2000JC000409

Sturm, M., K. Morris, R. Massom, (1998), The winter snow cover of the West Antarctic pack ice: its spatial and temporal variability. Antarctic Sea Ice Physical Processes, Interactions and Variability, ed M.O. Jeffries, pp. 1-18. American Geophysical Union, Washington, DC.

Sturm, M., Holmgren, J., König, M., and K. Morris (1997) The thermal conductivity of seasonal snow. *Journal of Glaciology*, 43 (143), 26-41.

Thorndike, A. S. (1992), A toy model linking atmosphere thermal radiation and sea ice growth, *J. Geophys. Res.,* 97(C6), 9401 – 9410.

Thorndike, A.S., D. A. Rothrock, G. A. Maykut, and R. Colony (1975), The thickness distribution of sea ice. *J. Geophys. Res.,* 80:4501–4513

Untersteiner, N. (1964), Calculations of temperature regime and heat budget of sea ice in the central Arctic, *J. Geophys. Res.,* 69, 4755-4766

Vavrus, S.J., M.M. Holland, A. Jahn, D.A. Bailey, and B.A. Blazey (2011), 21st-Century Arctic climate change in CCSM4. *J. Climate*, *Submitted,* Vol. 25, Iss. 8, pp. 2696–2710

Vavrus, S., and D. Waliser, (2008), An improved parameterization for simulating Arctic cloud amount in the CCSM3 climate model, *J. Climate,* 21**,** 5673-5687

Warren, S. G. , I . G. Rigor, V. F. Radinov, N. N. Bryazgi n, Y. I . Aleksandrov, and R. Colony (1999), Snow depth on Arctic ice, *J. Clim.,* 9, 1814 – 1829

Wu, X. W. F. Budd, V. I. Lytle, and R. A. Massom (1999), The effect of snow on Antarctic sea ice simulations in a coupled atmosphere-sea ice model, *Clim. Dyn,* 15,127-143

Yang, D. (1999), An improved precipitaction climatology for the Arctic Ocean, *Geophys. Res. Lett.,* 26, 1625-1628

Yeager, S. JAS Mean g3_5_19.11 (2009) http://www.cgd.ucar.edu/oce/yeager/ccsm_data/g3_5_19.11/ice/yrs1-116/line/line_avg_JAS_NH.png, Accessed 2 Fed 2009

Zhang, X., J. E. Walsh (2006), Toward a Seasonally Ice-Covered Arctic Ocean: Scenarios from the IPCC AR4 Model Simulations. *J. Clim.,* 19, 1730-1747

Zhang, Y., W. B. Rossow, A. A. Lacis, V. Oinas, and M. I. Mishchenko (2004), Calculation of radiative fluxes from the surface to top of atmosphere based on ISCCP and other global data sets: Refinements of the radiative transfer model and the input data, *J. Geophys. Res.*, *109*, D19105, doi:10.1029/2003JD004457

Zhang, J., D. Rothrock, and M. Steele (2000), Recent changes in Arctic sea ice: The interplay between ice dynamics and thermodynamics, *J. Clim.,* 13, 3099 – 3114.

Appendix A. Exclusion of IMB buoy in situ data

In addition to the validation of model produced snow depths against Russian drift station data, the study in Chapter 3 attempted to make use of contemporary ice mass balance buoys. However, as mentioned in Chapter 3, the location of many of these buoys makes matching the buoy location to appropriate ice populations difficult. This appendix reports the results of the validation of model snow depths against the buoy snow depths, and documents the motivation for eliminating this *in situ* data from the body of Chapter 3.

The Ice Mass Balance (IMB) buoys are managed by the Cold Regions Research and Engineering Laboratory (CRREL) (Perovich et al 2009). After calibration during deployment, these installations use an acoustic rangefinder to measure the height of the snow – ice surface and thereby derive snow depth. The IMB buoys provide no snow density measurements. These buoys have a very high data rate, so we analysis is limited to a once-daily measurement near 1200 UTM for purposes of this study.

Other than this restriction, the matching method described in Section III.4.a applies. Figure A1 reports the results of the comparison of the IMB buoys and the CCSM ensemble. Figure A2 reports the results of validating the CICE-Reanalysis against the buoys.

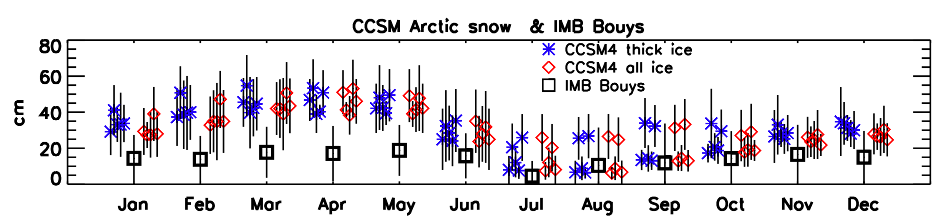

Figure A1. CCSM Arctic Ocean snow depths for the period 1993-2007 validated against IMB buoy measurements. Black squares indicate the *in situ* values for the period, red diamonds indicate the snow depth overlaying the nearest ice of any thickness, blue asterisks indicate the snow depth overlaying the nearest ice with greater than 1.49m thickness.

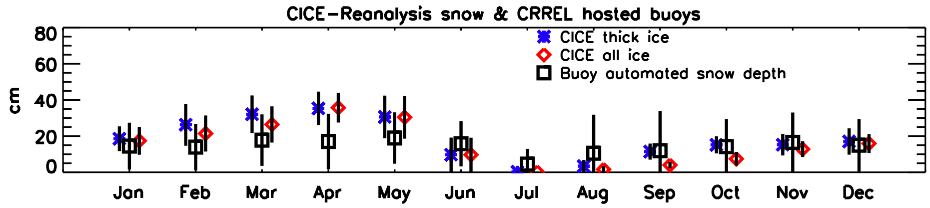

Figure A2. CICE-reanalysis Arctic Ocean snow depths for the Period 1993-2007 Validated against IMB buoys. Black squares indicate the *in situ* values for the period, red diamonds indicate the snow depth overlaying the nearest ice of any thickness, blue asterisks indicate the snow depth overlaying the nearest ice with greater than 1.49m thickness.

The differences between the IMB buoys and both the CCSM and CICE-Reanalysis models are significant for all months. The IMB buoy validation shows very large annual mean snow depth biases for the all ice and thick ice cells in CICE-coupled, 110% and 120% high, respectively. These biases tend to exceed 100% in the spring, while dropping closer to 50% in the summer.

The CCSM simulation produces a similar seasonal bias as CICE-Reanalysis when validated against the IMB buoys. However, the lower overall snow depths in CICE result in summer biases of 90% in July changing to excesses greater than 100% by April. These snow depth biases are similar in both the all ice and thick ice snow depth comparison

The comparison of the IMB buoys in Fig. A3 suggests the distribution of IMB buoys is potentially responsible for the odd behavior of the IMB validation. In particular, many of the IMB buoys are advected along the Eastern side of Greenland. When compared with CCSM in this area (see Fig. A3), very deep snowpack is produced by the model. However, the area of the CICE grid with ice is very small, which results in an ice edge with little ice or snow. As such, in some cases no nearby appropriate ice will be

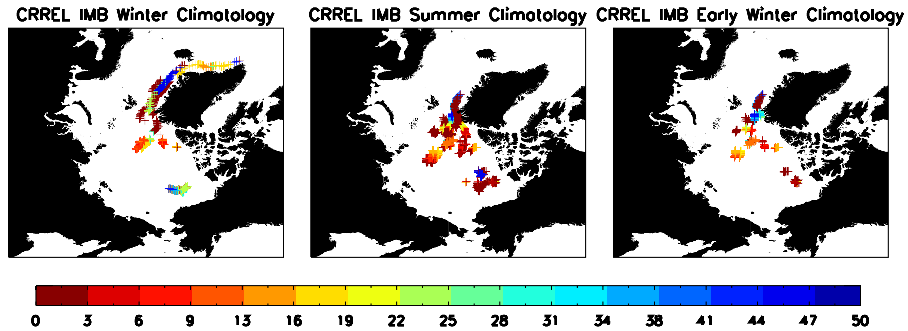

Figure A3. Geographical representation of IMB buoy data. The locations of the IMB buoys are color coded to indicate the depths reported by the buoy.

available in CICE, so distant ice will be matched. Conversely, CICE–Reanalysis has no snow here in the summer and fall. However, this area accumulated deeper snow pack over the winter in both CCSM and CICE-Reanalysis.

The mismatch between the models and the IMB buoys may be caused by difficulty in matching the advected buoys to appropriately proximate model cells. More specifically, if the model is currently advecting little ice through this corridor, the cells that match to a buoy in this region will be in a different geographic area. As a result, matched cells may be of different populations. In general, the dynamic nature of this region makes effective matching difficult.

Finally, Fig A4 presents a histogram of the frequency of snow depths modeled by CCSM and CICE-Reanalysis and observed *in situ* at the IMB buoys. The intra-ensemble

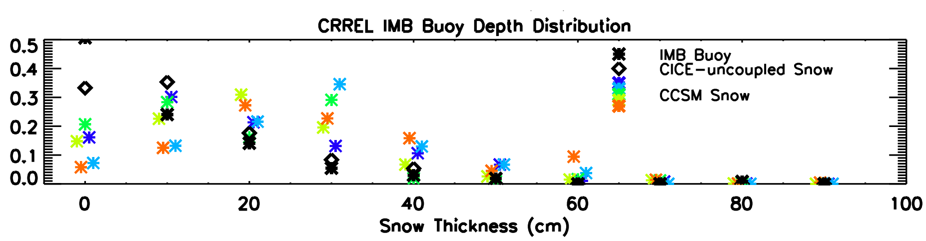

Figure A4. Histogram frequency of snow depth for model outputs and IMB *in situ* measurements.

variability in IMB matched location depths suggests a bimodal distribution. This apparent bimodal distribution is circumstantial confirmation of the mismatch of buoys due to rapid advection near the ice margin. As previously suggested this may create the unusual relation between the IMB buoys and the model output. As a result, the IMB buoys are eliminated from the body of Chapter 3.

The limitations to the buoy data used could be overcome with more careful matching to CICE grid cells. For example, eliminating IMB buoy data with no ice within a prescribed range would serve to eliminate the poor matching. Such an effort would also determine whether the unusual frequency distribution in the models when matched to the IMB is the result of poor matching, or a more interesting phenomenon in this region of the Arctic. However, the former case is suspected to be more likely, so the IMB buoys are eliminated from this study.

Appendix B. Density only simulations

In addition to the CCSM bias experiment and CICE-Reanalysis bias experiment, the effects of only the density bias reported in Fig. 10 are simulated. While this bias was incorporated into the CCSM bias and CICE-Reanalysis experiments, this appendix reports the results of a model simulation correcting for this bias independent of the snow depth biases. The discussion of this density only bias sensitivity experiment is relegated to this appendix due to the lack of a significant ($P<0.05$) response in the ice.

For the density bias correction, the same type of correction used in Chapter 3 is applied. Only the 'missing' snow depth due to the excessive autumn snow density reported in Fig 4 is corrected. The method applied is to change the snow conductivity to decrease the thermal conductivity as in equation 2. This adjustment results in the seasonally dependent conductivity in Fig. B1, where lower autumn

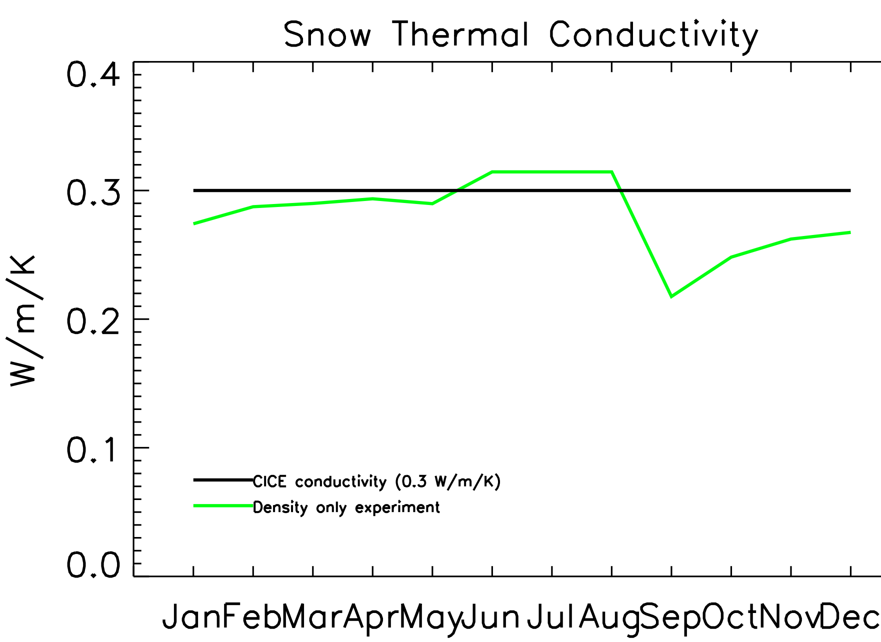

Figure B1. Snow conductivity adjustments for the density bias sensitivity experiment.

thermal conductivity compensates for the high density bias in same period, which would result in thicker snow if corrected directly. As in the body of this study, this neglects to account for changes to the snow conductivity due to direct changes in conductivity as a result of density (Sturm 2002).

Figure B2 reports the equilibrated (last 20 years of the 60 year simulation) ice extent and volume in the density only bias sensitivity experiment in comparison to the control simulation. Ice extent is 2% greater than control and the ice volume <1% less. However, neither of these differences is statistically significant.

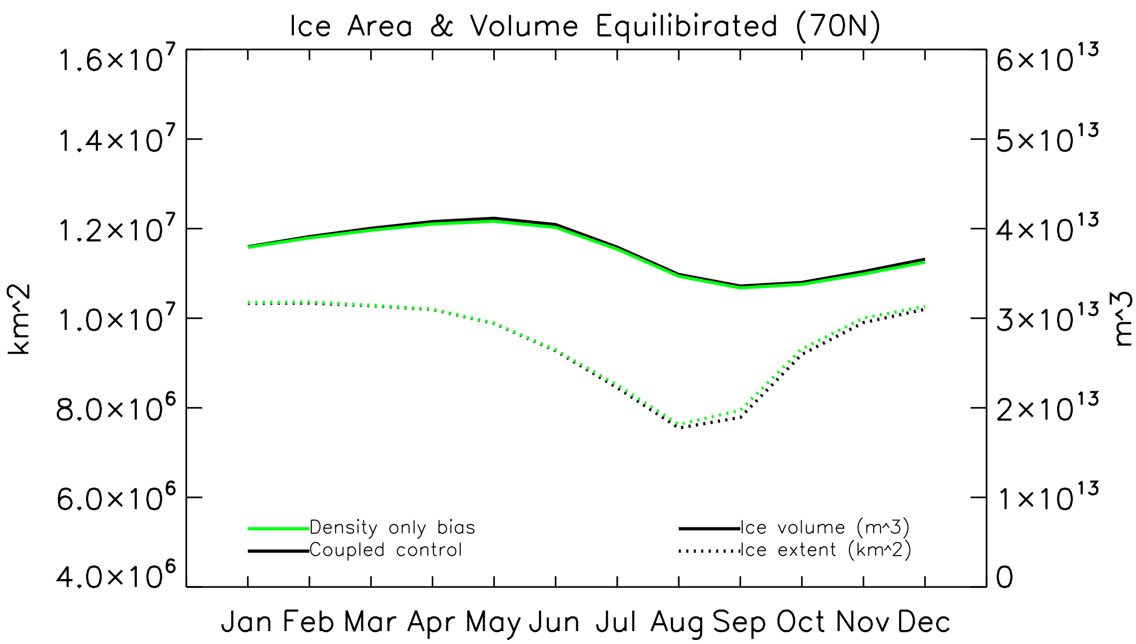

Figure B2. Arctic sea ice volume and extent for control run and density only bias sensitivity simulation. Restricted to north of latitude 70N.

While not of the same magnitude, the changes to conductivity applied in the density only bias sensitivity experiment are similar to those used in the CICE-Reanalysis bias sensitivity experiment, see Fig 23. As such, it is unsurprising the density bias sensitivity experiment has a similar but less significant response.

However Fig B3 reports that the geographical distribution of the ice response is quite different in the density bias sensitivity experiment. In the CICE-Reanalysis bias sensitivity experiment, thinning of the ice pack tended to occur in the central Arctic and marginal ice zone, with slight thickness increases in the thicker ice along the Canadian Archipelago. In this simulation, the thicker ice tends to thin relative to control, while the marginal regions are thicker. Due to the lack of significance in total volume between the density only simulation and control, it is possible this is simply variability. If only the autumn state were of import, the CICE-Reanalysis sensitivity experiment and density-only experiment would produce similar patterns, albeit of differing magnitude. The differing spatial patterns indicate the spring and summer conductivities play a (potentially non-significant) role.

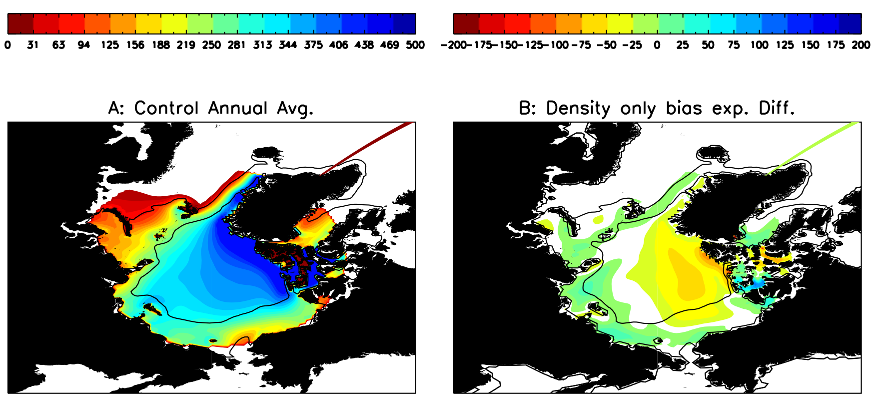

Figure B3. Panel A: Equilibrated ice thickness (depth given in cm by left bar) and 15% and 19% ice extent in September (given by solid black contours) for control run. Panels B: Difference in ice thickness between density only bias sensitivity experiment and the control run (given in cm by right color bar) and 15% and 90% September ice extent (given by solid black contours).

While an ensemble of bias sensitivity experiments could determine the significance of this divergence that beyond the scope of this study. Instead, this study concludes that this reaction alludes to a seasonal dependence on snow characteristics that is fairly complex. Rather than attempt to characterize in full the response of the ice to myriad variations in snow characteristics, we suggest future efforts would be better allocated to increasing the degree to which CICE snow reflects the physical system.